

Binary Microlensing Events from the MACHO Project

C. Alcock^{1,2}, R.A. Allsman³, D. Alves^{1,4}, T.S. Axelrod⁵, D. Baines⁶, A.C. Becker^{2,7},
D.P. Bennett^{1,2,8}, A. Bourke⁹, A. Brakel⁶, K.H. Cook¹, B. Crook⁶, A. Crouch⁹, J. Dan¹¹,
A.J. Drake⁵, P.C. Fragile⁸, K.C. Freeman⁵, A. Gal-Yam¹¹, M. Geha^{1,12}, J. Gray⁹, K. Griest^{2,10},
A. Gurtierrez⁶, A. Heller¹¹, J. Howard⁶, B.R. Johnson¹³, S. Kaspi¹¹, M. Keane¹⁴, O. Kovo¹¹,
C. Leach⁶, T. Leach⁶, E.M. Leibowitz¹¹, M.J. Lehner¹⁵, Y. Lipkin¹¹, D. Maoz¹¹, S.L. Marshall¹,
D. McDowell⁶, S. McKeown⁶, H. Mendelson¹¹, B. Messenger⁹, D. Minniti^{1,16}, C. Nelson^{1,17},
B.A. Peterson⁵, P. Popowski¹, E. Pozza⁶, P. Purcell⁶, M.R. Pratt^{2,18}, J. Quinn⁸, P.J. Quinn¹⁹,
S.H. Rhie⁸, A.W. Rodgers⁵, A. Salmon⁶, O. Shemer¹¹, P. Stetson²⁰, C.W. Stubbs^{2,7},
W. Sutherland²¹, S. Thomson⁹, A. Tomaney⁷, T. Vandehei^{2,10}, A. Walker¹⁴, K. Ward⁶,
G. Wyper⁶

(The MACHO/GMAN Collaboration)

¹Lawrence Livermore National Laboratory, Livermore, CA 94550

²Center for Particle Astrophysics, University of California, Berkeley, CA 94720

³Supercomputing Facility, Australian National University, Canberra, ACT 0200, Australia

⁴Space Telescope Science Institute, 3700 San Martin Drive, Baltimore, MD 21218

⁵Mt. Stromlo and Siding Spring Observatories, Australian National University, Weston, ACT 2611, Australia

⁶Reynolds Amateur Photometry Team, Canberra Astronomical Society, Canberra, ACT 0200, Australia

⁷Departments of Astronomy and Physics, University of Washington, Seattle, WA 98195

⁸Department of Physics, University of Notre Dame, Notre Dame, IN 46556

⁹Dept of Mathematics and Statistics, Monash University, Clayton, Victoria, 3168, Australia

¹⁰Department of Physics, University of California, San Diego, CA 92093

¹¹School of Physics & Astronomy and Wise Observatory, Tel-Aviv University, Tel-Aviv 69978, Israel

¹²Department of Physics, University of California, Davis, CA 92093

¹³Tate Laboratory of Physics, University of Minnesota, Minneapolis, MN 55455

¹⁴Cerro Tololo Interamerican Observatory, National Optical Astronomy Observatories.

¹⁵Department of Physics, University of Sheffield, Sheffield s3 7RH, UK

¹⁶Departamento de Astronomia, P. Universidad Católica, Casilla 104, Santiago 22, Chile

¹⁷Department of Physics, University of California, Berkeley, CA 92093

¹⁸Center for Space Research, MIT, Cambridge, MA 02139

¹⁹European Southern Observatory, Karl-Schwarzschild Str. 2, D-85748, Garching, Germany

²⁰National Research Council, 5071 West Saanich Road, RR 5, Victoria, BC V8X 4M6, Canada

²¹Department of Physics, University of Oxford, Oxford OX1 3RH, U.K.

ABSTRACT

We present the lightcurves of 21 gravitational microlensing events from the first six years of the MACHO Project gravitational microlensing survey which are likely examples of lensing by binary systems. These events were manually selected from a total sample of ~ 350 candidate microlensing events which were either detected by the MACHO Alert System or discovered through retrospective analyses of the MACHO database. At least 14 of these 21 events exhibit strong (caustic) features, and 4 of the events are well fit with lensing by large mass ratio (brown dwarf or planetary) systems, although these fits are not necessarily unique. The total binary event rate is roughly consistent with predictions based upon our knowledge of the properties of binary stars, but a precise comparison cannot be made without a determination of our binary lens event detection efficiency.

Towards the Galactic bulge, we find a ratio of caustic crossing to non-caustic crossing binary lensing events of 12:4, excluding one event for which we present 2 fits. This suggests significant incompleteness in our ability to detect and characterize non-caustic crossing binary lensing. The distribution of mass ratios, $N(q)$, for these binary lenses appears relatively flat. We are also able to reliably measure source-face crossing times in 4 of the bulge caustic crossing events, and recover from them a distribution of lens proper motions, masses, and distances consistent with a population of Galactic bulge lenses at a distance of 7 ± 1 kpc. This analysis yields 2 systems with companions of $\sim 0.05M_{\odot}$.

Subject headings: dark matter - gravitational lensing - stars: low-mass, brown dwarfs - binaries: general

1. Introduction

The search for gravitational microlensing has been very successful since first envisioned by Paczyński (1986). Several teams have reported observations of stellar brightenings that are consistent with the microlensing interpretation (Alcock et al. 1993; Aubourg et al. 1993; Paczyński et al. 1994; Alard et al. 1995). The total number of reported candidate events now exceeds 400. With second generation surveys now operating, we can expect a similar number of events in the coming years (Udalski, Kubiak, & Szymański 1997; Palanque-Delabrouille 1997).

By comparing the (efficiency-corrected) observed event rate with model predictions, microlensing surveys have ruled out a large class of dark matter candidates (Alcock et al. 1998c; Alcock et al. 1997b; Renault et al. 1997), and appear to have detected a previously unknown component of the Galactic-Magellanic Cloud system in lensing objects (Alcock et al. 1997b). The extensive microlensing databases have also allowed important constraints to be placed on Galactic structure (Alcock et al. 1998a; Paczyński & Stanek 1998; Alcock et al. 1998b; Alcock et al. 1997c; Zhao, Rich, & Spergel 1996; Stanek 1996; Stanek et al. 1994).

The gravitational lensing technique uses astronomical sources to backlight a foreground mass distribution. Lensing occurs due to the deflection of light rays by gravity, and most events are well described by the weak field, small angle limit of the gravitational scattering of photons. The equation describing the image positions in the lensing plane, for a single point lens, is

$$\vec{s} = \vec{i} - R_E^2 \frac{\vec{i} - \vec{x}}{(\vec{i} - \vec{x})^2}, \quad (1)$$

where \vec{s} , \vec{i} , and \vec{x} are the positions of the source, image, and lens, projected along the line of sight into the lens plane. R_E refers to the Einstein ring radius given by

$$R_E^2 \equiv 4GM \left(\frac{D_{ol}D_{ls}}{D_{ol} + D_{ls}} \right), \quad (2)$$

where D_{ol} is the distance to the lens, D_{ls} is the lens-source distance, M the mass of the lensing object, and G is the Newtonian gravitational constant. If we define the origin of the lens plane as the position of the lens ($\vec{x} = 0$), then it is obvious from Eqn. 1 that $\vec{i} \parallel \vec{s}$. This symmetry provides two images during a lensing event. (There is actually a third image of negligible magnification that can be found if we give the lens a finite extent, or if we depart from the weak field approximation.)

The magnification of an image is given by the inverse of the determinant of the lens mapping from image to source (Eqn. 1), evaluated at the position of the image. The sum of the two image magnifications, which, if the images are unresolved, is the observed magnification of the source, is

$$A(t) = \frac{u^2 + 2}{u\sqrt{u^2 + 4}}, \quad (3)$$

$$\begin{aligned} \text{where } u(t) &= \sqrt{u_{\min}^2 + (2(t - t_0)/\hat{t})^2} \\ \text{and } \hat{t} &= 2R_E/v_{\perp}. \end{aligned}$$

The lens passes closest to the source at an impact parameter (scaled by R_E) of u_{\min} , at the time t_0 . The variable \hat{t} represents the time it takes the lens to cross its own Einstein diameter (a function of M and D_{ol}/D_{os}), given its unknown transverse velocity v_{\perp} . This simple form of the event “lightcurve” is based on point–source and point–lens approximations, and an assumption of uniform linear motion between observer, source and lens. As a practical consideration, one must also model additional (unlensed) light which contributes to the source object’s baseline brightness, and modifies the observed shape of the lightcurve. This may come from unresolved neighboring stars, or possibly from the lens itself. We therefore include a blending parameter for each passband, f , which represents the fraction of the photometered object’s flux which was lensed.

2. Binary Microlensing

Binary lensing is described by the generalization of Eqn. 1 to the case of two deflectors:

$$\vec{s} = \vec{i} - R_E^2 \left(\epsilon_1 \frac{\vec{i} - \vec{x}_1}{(\vec{i} - \vec{x}_1)^2} + \epsilon_2 \frac{\vec{i} - \vec{x}_2}{(\vec{i} - \vec{x}_2)^2} \right), \quad (4)$$

where $\epsilon_1 + \epsilon_2 \equiv 1$, and refer to the mass fraction of each lens. R_E now refers to the Einstein ring radius of the complete lens system ($M_1 + M_2$).

As with the single lens, Eqn. 4 represents a mapping from the image plane to the source plane. This mapping is well behaved, but the inverse mapping from the source plane to the image plane is multi-valued, with each point on the source plane mapping into either 3 or 5 points on the image plane. The boundaries between the regions of 3 and 5 images in the image plane are referred to as critical curves. These critical curves map into closed caustic curves (or caustics) in the source plane. The shape of a caustic curve is characterized by inwardly curved segments joined at outwardly spiked cusps.

A binary lens lightcurve can be described by 7 parameters, if the orbital motion of the lensing objects is neglected. These parameters include the 3 parameters for a single lens fit \hat{t} , u_{\min} , and t_0 , where u_{\min} and t_0 are now measured with respect to the lensing system’s center of mass. The 3 intrinsic binary parameters are the binary lens separation (scaled by R_E), a , the mass fraction, ϵ_1 , and the angle between the lens axis and the source trajectory, θ . A final parameter may be added if the source star crosses a caustic, the source radius crossing time t_* . This represents the time it takes the lens to move relative to the source by an angle equal to the source angular radius – typically an hour to a day. This may be constrained by observing the caustic crossing duration $2t_*/\sin \phi$, where ϕ is the angle between the relative motion vector and the caustic line. An

additional blending parameter f must also be included for each passband. An excellent treatment of binary microlensing can be found in Dominik (1998a).

When a source crosses near or over a caustic, the event lightcurve can differ quite significantly from the standard microlensing lightcurve. During a caustic crossing, the determinant of the lens mapping in Eqn. 4 goes to zero. This divergence of the magnification factor implies that a point source located on a caustic curve becomes infinitely bright. In this situation, two of the images either merge and disappear, or are created, such that the number of images is greater within the region bounded by the caustic surface. For a realistic source brightness profile, the observed magnification is the weighted mean of the magnification factor over the source, which always leads to finite values.

If one is able to observe a caustic crossing, the temporal width of the transit provides a measurement of t_* , if ϕ is sufficiently constrained by the global microlensing fit. An estimate of the true angular source size then yields the proper motion of the lensing system with respect to the source star. This provides an especially important constraint in binary lensing events seen towards the Magellanic Clouds, where there is a distinct difference between the expected relative proper motion of a binary lens in the Galactic dark halo ($\mu \sim 30 \text{ km s}^{-1} \text{ kpc}^{-1}$), and of a binary lens in the Magellanic Clouds, where the relative proper motion is a function of the velocity dispersion in the Cloud ($\mu \sim 1 \text{ km s}^{-1} \text{ kpc}^{-1}$). In general, once a caustic crossing event is detected (the first caustic crossing is unlikely to be resolved due to its short duration, but may be inferred from the enhanced magnification between caustics), one is guaranteed a second caustic crossing and, with dense enough sampling through the crossing, an estimate of the lens proper motion.

2.1. Estimates of the Binary Lensing Rate

The phenomenology of lensing by two point masses is well known (e.g. Schneider & Weiss 1986), and the lightcurve morphology expected in the Galactic microlensing limit well established (e.g. Mao & Paczyński 1991, Mao & Di Stefano 1995, and Di Stefano & Perna 1997). Mao & Paczyński (1991) predicted that $\sim 7\%$ of all events seen towards the Galactic bulge should show strong evidence of lens binarity, and that as many as $\sim 3\%$ of bulge events might show evidence of a high mass ratio (planetary) binary system, depending upon the abundance of giant planets. The prospect of detecting extra-solar planets through lens binarity has led to much investigation (Gould & Loeb 1992; Bolatto & Falco 1994; Bennett & Rhie 1996; Peale 1997; Gaudi, Naber, & Sackett 1998), and distinct methods and detection rates for multiple classes of planetary lensing (Griest & Safizadeh 1998; Di Stefano & Scalzo 1999a; Di Stefano & Scalzo 1999b).

The question of the fractional binary lensing rate has recently been analyzed in more detail by Di Stefano (1999), who argues that, in the extreme case where *all* lenses are binaries, $\sim 6\%$ of all events should exhibit caustic crossings. This fraction will obviously decrease if some lenses are single. Thus the majority of binary lensing events should result in multiply-peaked lightcurves

or low amplitude deviations from single lens lightcurves, without caustic features. However, Di Stefano (1999) appears to underestimate the observational bias towards low impact parameter (small u_{\min}) events. Di Stefano (1999) considers all events with $u_{\min} \leq 1$ to be detectable if they are sampled frequently, but in fact the MACHO analysis and Alert System trigger both explicitly exclude lensing events with $u_{\min} \gtrsim 0.75$. Additional cuts on the signal to noise of the stellar brightening also discriminate against the large u_{\min} events, which may lie within the relatively large error bars ($\sim 7\%$) of survey system photometry. Furthermore, most of the events seen towards both the Galactic bulge and the Magellanic Clouds are significantly blended, such that the true u_{\min} value is generally smaller than the observed value used for event selection. Fig. 2 of Di Stefano (1999) indicates that the fraction of caustic crossing events would be substantially higher if a smaller u_{\min} cut (*i.e.* $u_{\min} \lesssim 0.3$) were used to better reflect the survey team’s event selection criteria.

The current microlensing follow-up systems, including the Global Microlensing Alert Network (GMAN) (Alcock et al. 1997d), Microlensing Planet Search (MPS) team (Rhie et al. 1998a), and Probing Lensing Anomalies NETwork (PLANET) (Albrow et al. 1998a), avoid many of these difficulties with observing strategies optimized to detect short timescale, low level deviations in on-going events, with photometry at the $\sim 1 - 2\%$ level.

2.2. Previous Binary Lens Observations

The first unambiguous case of binary microlensing was reported by the OGLE collaboration (OGLE-7, Udalski et al. 1994), and later corroborated with data from the MACHO database (Bennett et al. 1995; Mao et al. 1994). Subsequent binary lens event publications include DUO 2 (Alard, Mao, & Guibert 1995), MACHO 95-BLG-12 (Pratt et al. 1996; Albrow et al. 1996), MACHO LMC-1 (Rhie & Bennett 1996; Dominik & Hirshfeld 1996), MACHO LMC-9 (Bennett et al. 1996b), MACHO 97-BLG-28 (Albrow et al. 1998b), and MACHO 98-SMC-1 (Alcock et al. 1999a; Afonso et al. 1999). In addition, there have been a number of binary lensing events discovered in progress and announced on the web sites of the various microlensing survey and follow-up programs¹.

¹ EROS [http://www-dapnia.ccea.fr/Spp/Experiences/EROS/alertes.html](http://www-dapnia cea.fr/Spp/Experiences/EROS/alertes.html)
MACHO <http://darkstar.astro.washington.edu>
MPS <http://bustard.phys.nd.edu/MPS/>
OGLE <http://www.astro.uw.edu.pl/~ftp/ogle/ogle2/ews/ews.html>
PLANET <http://www.astro.rug.nl/~planet/index.html>

3. Observations

The purpose of this paper is to present instances of binary lens type lightcurves that we have detected in our gravitational microlensing survey, using the 50-inch telescope at the Mount Stromlo Observatory (Alcock et al. 1997b; Hart et al. 1996; Marshall et al. 1994). These include events towards the Large Magellanic Cloud (LMC), Small Magellanic Cloud (SMC), and Galactic bulge. We have not made a complete assessment of our binary lens detection efficiency, and the events presented here were selected by a variety of different mechanisms. Most were originally discovered with the MACHO Alert System, and were subsequently observed to deviate from the standard microlensing lightcurve. Other events were discovered via our normal analysis procedure (see Alcock et al. 1997b), difference imaging analysis (DIA) on a subset of our database (Alcock et al. 1999b), or during testing of the Alert System software.

Many of the alert events, and most of the unusual events, from 1995-1998 were also followed with coordinated observations of the Global Microlensing Alert Network (GMAN) (Pratt et al. 1996) :

- These include nightly observations on the Cerro Tololo Interamerican Observatory (CTIO) ² 0.9m telescope at Cerro Tololo, Chile, with extremely flexible scheduling allowed by the staff to assist in characterizing the binary events presented here. The observing strategy was optimized in 1997 to target LMC/SMC events at highest priority (and paid off with the real-time detection of binary event MACHO 98-SMC-1 (Becker et al. 1998)), and thus the frequency of observations of our bulge events decreases.
- We have also coordinated observations on the Wise Observatory (WISE) 1.0m telescope at Mitzpe Ramon, Israel. These observations are generally requested in real-time for a subset of the bulge alert events which show unusual features.
- For the observing seasons 1995-1996, we were allotted approximately 50% of the bulge time at the University of Toronto Southern Observatory (UTSO) 0.6m telescope at Las Campanas, Chile for microlensing follow-up. Several events were followed at high frequency, and 3 of these appear here as binary candidates.
- Starting in 1997, we arranged microlensing follow-up observations at the Mount Stromlo Observatory 30" (MSO30) telescope in Canberra, Australia, with the Reynolds Amateur Photometry Team (RAPT). This group of amateur astronomers staffs the telescope nightly, on a volunteer basis.
- The Microlensing Planet Search (MPS) team began its pilot season of observations in 1997, and has obtained use of the MSO 74" (MSO74) telescope for rapid, precise monitoring of on-going Galactic bulge events.

²Cerro Tololo Interamerican Observatory, National Optical Astronomy Observatories, operated by the Association of Universities for Research in Astronomy, Inc. under cooperative agreement with the National Science Foundation.

The MACHO survey data from the Mt. Stromlo 50" telescope are generally reduced within hours after acquisition using the SoDOPHOT photometry routine (Bennett et al. 1993), which was developed from DOPHOT (Schechter, Mateo, & Saha 1993). The error bars presented here are the standard SoDOPHOT (or DOPHOT) error estimates with a 1.4% uncertainty added in quadrature. As the 50" data are reduced, the photometry is sent through the MACHO Alert filter for the purpose of detecting microlensing events in progress. Thirteen of the 21 events presented here were first detected with the MACHO Alert System, although two of these events were not found while in progress.

All CTIO, MSO30, and UTSO data are reduced in real-time using a suite of scripts, written in PERL, which make use of the DAOPHOT package (Stetson 1987). After the event has returned to baseline, CTIO, MSO30, UTSO, and WISE data are reduced *en-masse* using the ALLFRAME package (Stetson 1994). To assemble each lightcurve, the target star's brightness is finally normalized with respect to several hundred neighboring stars. The resulting photometric error bars are multiplied by a factor of 1.5, to account for additional scatter in the time-series not accounted for by the formal ALLFRAME error estimates, such as flat fielding and normalization errors. The MSO74 data are reduced and normalized using a slightly modified version of SoDOPHOT.

Finally, we would like to emphasize that for some of these fits there are probably degeneracies between model parameters. That is, the fit presented is not unique, but does represent a local minimum in parameter space. Is it likely that for some of these events, particularly the poorly sampled ones, there are different lens configurations whose lightcurves, as sampled by our observations, are similar to the fits presented here (see Dominik 1999). There are, however, systematic approaches to determining all physical solutions for a set of microlensing data (e.g. Di Stefano & Perna 1997 and Albrow et al. 1999b).

4. Binary Lensing Events

Characteristics of the MACHO objects that received the lensed flux are presented in Table 1. Each object is given an event name in addition to the MACHO star ID number which has been previously assigned. For each object, we include the transformation to Cousins V and $V - R$, calibrated using Alcock et al. (1999c). From the blending parameters included in the binary microlensing fit, we can also estimate the true brightness and color of the star which was lensed. This information is also included in Table 1. For all events, we will refer to the (sometimes blended) object identified in the MACHO database as the 'object', and refer to the 'source' as the actual star in the blend which was lensed. Fit parameters for these binary microlensing events are given in Tables 2 and 3. For each event, we present a lightcurve of these fits, as well as a schematic of the critical and caustic curves induced by the binary lens (Fig. 1 – 44). The data used in the fits may be found on the WWW at <http://wwwmacho.anu.edu.au/> and <http://wwwmacho.mcmaster.ca/>. Individuals are encouraged to attempt other binary lens fits to

these data.

Fig. 45 and Fig. 46 display the distribution of V , $V - R$ for $\sim 3,000$ neighboring sources in the same 5' "chunk" (1/64 of MACHO's focal plane) as the lensed object, for Magellanic Cloud and Galactic bulge sources, respectively. The solid circle indicates the location of the MACHO object, and the open circle represents the location of the lensed source, as determined from the blending parameters.

In the following, we discuss each of the 21 events individually.

4.1. LMC-1 (79.5628.1547)

This event was the first LMC microlensing event reported by the MACHO collaboration (Alcock et al. 1993). The lensed object does not significantly change color during the event, and its color and magnitude indicate that it is a slightly reddened red clump giant star in the LMC. We thus expect *a priori* that a large fraction of the MACHO object's brightness should be lensed. A difference image photometry (DIP, Tomaney & Crotts 1996) analysis of the event images indicates a very small centroid shift between the photometered object and lensed source, $0.1 \pm 0.1''$, also suggesting the clump giant was lensed.

The lightcurve is consistent with single lens microlensing, except for a shoulder shortly after the lightcurve peak. This suggests a short timescale structure which was not resolved at the sampling of the survey system. Binary fits for this event have been done by Dominik & Hirshfeld (1996), and the two fits displayed in Fig. 1 were previously presented by Rhie & Bennett (1996). The similarity to standard microlensing implies the fit resides in a class of fits with small lens separations (fit — in Fig. 1, and Fig. 2) or large mass ratios (fit - - - in Fig. 1, and Fig. 3).

The measured $\hat{t} \sim 35$ days for both of these fits yields an expectation value for the mass of the lensing system of $\sim 0.1M_{\odot}$ (Alcock et al. 1993; Dominik 1998b). For the large mass ratio fit, this implies a secondary companion of ~ 1 Jupiter mass. However, since there were no follow-up efforts in place at the time of this event, this degeneracy between fits cannot be broken.

4.2. LMC-9 (80.6468.2746)

LMC-9 is the most anomalous lensing event discovered toward the LMC, and it displays the lightcurve structure of a typical caustic crossing binary lens event with similar mass lenses (see Fig. 4). Prior analysis of this event can be found in Bennett et al. (1996b). The lensed object appears to be on the red side of the LMC main sequence, at the level of the clump. However, the fits suggest only $\sim 1/5$ of this light is lensed, and so the source likely resides further down the main sequence as a late A or early F star. The lensed source does appear $0.4 \pm 0.1''$ from the MACHO object, based upon DIP analysis.

The first caustic crossing appears to be resolved with two observations on its rise. If we assume the source is not itself a binary, we can estimate the source radius as $1.5 \pm 0.2 R_{\odot}$ from its color and magnitude. The measured $t_* = 0.65 \pm 0.10$ days yields a lens velocity projected to the LMC (assumed to be at 50 kpc) of $19 \pm 4 \text{ km s}^{-1}$, considerably lower than what one would expect from a halo lens. In fact, this velocity is low enough that it is only marginally consistent with a lens in the disk of the LMC, and would not be consistent with any LMC models including velocity dispersions in excess of the measured values.

Aubourg et al. (1999) have suggested an LMC model with a self-lensing optical depth large enough to explain the excess of lensing events observed towards the LMC. Aubourg et al. (1999) achieve a high microlensing optical depth without violating the virial relation between velocity dispersion and microlensing optical depth (Gould 1995) by arguing that the velocity dispersion of the lens population is much higher than the velocity dispersion of the stars with measured radial velocities (Cowley & Hartwick 1991; Zaritsky et al. 1999). However, even in such a model our projected velocity of $19 \pm 4 \text{ km s}^{-1}$ for LMC-9 would not be consistent with a lens in the LMC³.

Thus, there are two possible interpretations of the LMC-9 caustic crossing observations:

1. They imply that the lens resides in an LMC disk which contains enough mass to generate only a fraction of the observed LMC lensing events, or
2. The source star is itself a binary, and the two caustic crossing observations do not constrain the lens proper motion or its location.

Both of these possibilities have an *a priori* probability of about 10%. Clearly, better photometric coverage of the caustic crossings could have resolved this issue.

4.3. LMC-10 (18.3324.1765)

We include LMC-10 as a binary candidate as an example of variability which passes our microlensing cuts (Alcock et al. 1997b), and yet is almost certainly not standard single lens microlensing due to its asymmetry (Fig. 6). Explanations for this event include intrinsic stellar variability (we detect no recurrence of this behavior in 5 further years of observations), a background supernova (we find no obvious host galaxy down to $R \sim 21$), or possibly a weakly perturbed binary microlensing event. Such lightcurves are thought to compose a significant fraction of all binary lensing events (Di Stefano 1999). The best fit lightcurve does have a pair of caustic crossing, but they are separated by about 4 hours and occurred during daylight hours in Australia. For $t_* < 0.2$ days, these caustic crossings would not have been observable from

³An early version of Aubourg et al. (1999) incorrectly suggested that their model was consistent with the LMC-9 projected velocity (Aubourg 1999, private communication).

Australia, and the fit is a plausible explanation of the lightcurve. The microlensing interpretation of this event would be much more secure if such a lightcurve were seen in a time reversed order, since the observed rapid rise followed by a slow decay is common in known types of stellar variability. The one observational test that can still be performed is to obtain high resolution HST images of this object. The centroid of the variable source is well constrained by the DIP method of Tomaney & Crotts (1996), and appears $1.0 \pm 0.2''$ from the MACHO object. If the binary lens interpretation is correct, then this centroid should be centered on a $R = 21.4$ star. Alternatively, the HST frame might also reveal a background galaxy which will make the supernova explanation most plausible.

4.4. 98-SMC-1 (208.15683.4237)

Alert 98-SMC-1, detected on May 25 1998, was the second microlensing event seen towards the SMC. Nightly GMAN followup observations of the early lightcurve detected evidence of a caustic crossing near June 6.5 UT 1998 (day 2347.5 in Fig. 8) (Becker et al. 1998). The prospect of resolving the second caustic crossing, allowing an estimate of the lens location, prompted the microlensing community to commit significant observational resources to this event. Following predictions of the second caustic crossing date by Bennett et al. (1998) and the PLANET collaboration, the event was followed by the EROS (Afonso et al. 1998), PLANET (Albrow et al. 1999a), MACHO/GMAN (Alcock et al. 1999a), OGLE (Udalski et al. 1998), and MPS collaborations (Rhie et al. 1998a). In each case, the analysis of event data leads to a relatively long caustic crossing timescale, with the robust conclusion that 98-SMC-1 is due to SMC-SMC self lensing. A joint paper incorporating all event data is in preparation (Afonso et al. 1999).

The fit we present here, originally from Alcock et al. (1999a), exhibits a $t_* = 0.116 \pm 0.010$ days. We estimate $R_* = 1.1 \pm 0.1 R_\odot$, and assuming the source resides in the SMC at 60 kpc we find a lens velocity projected to the SMC of $\hat{v} = 76 \pm 10 \text{ km s}^{-1}$. The probability for a Galactic halo lens to produce a \hat{v} value this small is of order 0.1 %.

4.5. OGLE-7/MACHO-119-A (119.20226.2119)

This caustic crossing event was initially detected by the OGLE collaboration (Udalski et al. 1994), and later verified with data from the MACHO database (Mao et al. 1994). As OGLE-7, it was the first reported case of binary microlensing. 119-A is a moderately blended event, with $f \sim 0.4$, and the source appears to be located near the top of the bulge main sequence.

The fit presented in Fig. 10, and the geometry of the lensing encounter in Fig. 11, are qualitatively similar to the analysis of Udalski et al. (1994). A comparison of event parameters (MACHO:OGLE) yields $\hat{t} = (169 : 160)$, $u_{\min} = (0.08 : 0.05)$, $a = (1.05 : 1.14)$, $\epsilon_1 = (0.55 : 0.50)$, $\theta = (-0.94 : 0.84)$, where the difference in θ is due to a different orientation of coordinate

systems. Fortunately, the MACHO dataset provides better sampling of the lightcurve, and thus more tightly constrains the global fit. The data presented here include 2 observations on the falling portion of the second caustic crossing, yielding an additional constraint of $t_* = 0.21 \pm 0.03$ days.

4.6. MACHO-403-C (403.47793.2961)

Event 403-C exhibits a series of photometric deviations near Aug 18, 1996 (day 1690 in Fig. 12) which are, for the most part, achromatic. It is plausible these deviations are due to gravitational microlensing. However, this event does not appear to be consistent with single lens microlensing, and is only marginally consistent with binary microlensing. The sparse sampling and relatively large error bars prevent tight constraints on the binary microlensing event parameters.

4.7. 94-BLG-4 (118.18141.731)

94-BLG-4 exhibits features similar to LMC-1, with a high- σ deviation near the peak of the event which is unresolved by the survey system. This event was initially reported in Bennett et al. (1997), after discovery during testing of the MACHO Alert System. The 2 observations apparently taken between caustic crossings are not enough to completely constrain the lensing system, thus Fig. 14 and Fig. 15 are probably not unique interpretations of this sparsely sampled lightcurve.

The lensed object is a clump giant, with $V = 17.9$, $V - R = 1.1$, based upon its position in Fig. 46. The binary fit blend fraction of $f \sim 1$ indicates the clump giant itself was lensed, avoiding fit ambiguities introduced by unknown or unconstrained blend fractions, which directly influence our measurement of \hat{t} . The event duration is relatively short, $\hat{t} = 10.7$ days. If we assume “typical” parameters for the lensing object ($v_{\perp} = 150 \text{ km s}^{-1}$ and a distance 80% of the way to the Galactic bulge) we arrive at the relationship $\hat{t} \sim 70 \sqrt{m/M_{\odot}}$ days (Paczýński 1991). This implies an overall lens mass of $0.02 M_{\odot}$ – however, we expect the shortest of our events to be drawn from lenses residing closer to the source, so the actual mass is likely to be much larger than this. If we take an upper limit of $0.2 M_{\odot}$ as the total lens mass, then the mass ratio of 1/18 implies a secondary lens of $\lesssim 10$ Jupiter masses, for this particular fit.

4.8. 95-BLG-12 (120.21263.1213)

This 12th Alert of the 1995 bulge season was detected on May 15, at a magnification of $A \sim 2$. Real-time follow-up observations by both GMAN (Pratt et al. 1996) and PLANET (Albrow et al. 1996) detected deviations from the standard fit near Jun 5, making 95-BLG-12 the first binary event detected in real-time. Data on this event from the PLANET collaboration are presented in Albrow et al. (1998a).

The lensed object is located on the subgiant branch of the bulge, below the clump. However, because subgiants are rare, we expect that the majority of objects in this location of the color-magnitude diagram are actually blends of multiple fainter stars. Thus, it is no surprise that the binary lens fit indicates blend fractions of $\sim 0.2 - 0.3$. 95-BLG-12 is a good example of a significantly perturbed, non-caustic crossing binary lensing event (Fig. 16). The multiple peaks are caused by the source approaching cusps in the caustic curve, as displayed in Fig. 17. The extensive follow-up data are able to constrain the event at nearly the 1% level for much of its duration.

4.9. 96-BLG-3 (119.19444.2055)

This event was discovered at the beginning of the 1996 bulge season, and announced by the MACHO Alert System on Mar 12, 1996. After an initial peak (due to a cusp approach) which resembled a normal lensing event, the star jumped to a large magnification on Mar 25, 1996, implying a caustic crossing had likely occurred. Based upon the available MACHO data, Bennett et al. (1996a) were able to successfully predict the second caustic crossing to within 0.15 days. The important features at the time of this prediction were the initial peak in Fig. 18, due to a cusp approach, and the sparsely sampled U-shape between caustics. These global constraints on the lightcurve provided enough leverage for an accurate caustic crossing prediction, although this is not necessarily possible with more local constraints, even a well sampled caustic crossing (Albrow et al. 1999b).

Follow-up data taken at the CTIO 1.5m provided the first ever resolution of a binary caustic crossing, as shown in Fig. 18. In addition, spectroscopic observations of the object were taken during the crossing (Lennon et al. 1996). As the source crossed out of the caustic region, its brightness peaked at extremely high magnification, $A_{\max} \sim 120$. However, the observed magnification of the MACHO object was considerably less, as it is a significant blend ($f \sim 0.2$ for MACHO). Thus, while Lennon et al. (1996) report their spectrum of that of a G0 subgiant, the blend fractions indicate that the source is a G0 dwarf.

Lennon et al. (1996) showed that the source is not a spectroscopic binary, and estimated from their spectra an effective temperature of $T_{\text{eff}} = 6100$ K. Their comparison to evolutionary tracks leads to an angular source radius of $\theta_* = 0.94\mu\text{as}$. Since these spectra were taken while the source was highly magnified, their T_{eff} should represent the temperature of the lensed source. However, their estimate of the distance to the source, and hence its angular size, depended upon the baseline brightness of the object ($V = 19.2$), instead of the recovered brightness of the lensed source ($V = 20.8$). Our analysis in Sec. 5.2.2, Table 4, indicates our estimate of $T_{\text{eff}} = 6200\text{K}$ is in excellent agreement with Lennon et al. (1996), and de-blending the event reasonably leads to a smaller $\theta_* = 0.53\mu\text{as}$.

4.10. 96-BLG-4 (105.21417.101)

96-BLG-4 displays a repeating variability (Fig. 20), which would generally exclude it as a microlensing candidate. The first peak is well fit by standard microlensing ($\chi^2/dof = 1.2$), and was not a binary candidate until the MACHO Alert System re-triggered on this event ~ 550 days after the first peak. The color of this object ($V = 16.2, V - R = 1.1$) indicates it is unlikely to be a long period variable (LPV), and any periodic variability is ruled out by prior observations. The object does appear to be a bright giant, located close to the tip of the red giant branch.

As is the case with many of our giant sources, we do not detect a significant color shift during the event, and the binary lens fit is consistent with zero blending ($f = 1$). The multiple achromatic peaks suggest lensing of a single giant source by a binary lens, or lensing of a binary system by a single lens. Fig. 46 indicates that the source appears ~ 1.3 mag brighter than the red clump in this region, so a single lens, binary source event seems plausible (the probability of a chance superposition of giant stars is extremely small). Stars generally spend only a few percent of their lives on the giant branch (Iben 1967), so it is unlikely for two members of a binary system to reside on the giant branch at the same time. But, given the sample of ~ 350 candidate events that our binary lens sample has been selected from, one binary giant source event is plausible.

Another interpretation of this event is a very widely separated ($a = 7.5R_E$) binary lens acting upon a single background giant source. It has been recognized by Di Stefano & Mao (1996) that lensing by widely separated binary systems ($a > 2.5R_E$) should occur with $\sim 10\%$ the frequency of close binary events. As shown in Fig. 21, the caustics for this event are extremely small, which indicates that this event, unlike any of the others presented in this paper, is very much like the superposition of two single lens lightcurves. This makes it difficult to unambiguously discriminate between binary lens and binary source models for this event.

4.11. 97-BLG-1 (113.18674.756)

97-BLG-1 was initially announced as microlensing on Mar 3, 1997. A substantial deviation from standard microlensing was noticed Mar 11, 1997. This sharp decline, seen in Fig. 22, signified the source exiting the caustic region, and follow-up efforts were only able to sample the final cusp approach (see Fig. 23).

This MACHO object appears to be a clump giant, relatively unreddened compared with the other events in our sample. There is little blending in this event, such that the giant is likely the lensed source. The second caustic crossing in this model is resolved with 2 MACHO observations, which leads to an estimate of $t_* = 0.53 \pm 0.03$ days. However, the lack of information prior to the start of the bulge season severely limits our ability to parameterize this event, so we expect that our fit may not be unique. The only strong constraints on this lensing encounter are the magnitude of the final cusp approach and the likelihood of minimal blending for a clump giant

source.

4.12. 97-BLG-24 (101.20650.1216)

The MACHO lightcurve for 97-BLG-24 (Fig. 24) exhibits a significant deviation from point source microlensing, similar to LMC-1 (Fig. 1). However, this deviation was noticed in real-time, allowing immediate follow-up observations to be undertaken with the MSO 30" telescope. These data reveal an unusual increase in the object's brightness before observations ended for the evening.

Unfortunately, the lensed source appears $\sim 1.2''$ from the MACHO object, in a region of high crowding. It is difficult to independently photometer the lensed source even in the follow-up photometry, and the data presented here represent the change in brightness of the brightest neighbor to the lensed source – i.e. the event is strongly blended. Nevertheless, we are able to resolve evidence of lens binarity in the deviation near the peak of the lightcurve. This deviation is more heavily sampled than LMC-1, but still suffers from the same model degeneracy. (We note that Fig. 24 displays the apparent brightening of the MACHO object, not the lensed source, due to the different blend fractions between the two fits presented in Tables 2 and 3.)

The solid and dashed line fits in Fig. 24 display \hat{t} of 30.7 and 45.5 days, implying overall lens masses of 0.19 and $0.42M_{\odot}$, respectively. The former fit includes a binary system with components of 0.16 and $0.03M_{\odot}$, likely a stellar - brown dwarf system. The latter dashed fit, with a mass ratio of $29 : 1$, implies lens masses of 0.41 and $0.014M_{\odot}$, consistent with a stellar lens with a companion of ~ 14 Jupiter masses.

4.13. 97-BLG-28 (108.18951.593)

After being detected and alerted upon May 29, 1997, this event began to increase in brightness at an unexpected rate on Jun 14, 1997 (day 1990 in Fig. 27), and both MACHO/GMAN and PLANET issued secondary alerts for a binary lensing event in progress. The PLANET collaboration was able to obtain nearly constant coverage of this event, resulting in parameterization of the limb-darkening coefficients for the source, and an estimate of the lens proper motion of $\mu = 19.4 \pm 2.6 \text{ km s}^{-1} \text{ kpc}^{-1}$ (Albrow et al. 1998b).

The results presented here are similar to those of Albrow et al. (1998b). The fit to microlensing suggests a moderate amount of un-lensed blue light in the photometered object, and the object is likely a lensed clump giant source blended with objects of bluer color. The trajectory of the source plotted in Fig. 28 indicates the lightcurve deviation was due to a cusp crossing. Resolution of the source face during this crossing allows a measurement of $t_* = 0.760 \pm 0.014$ days. A comparison of event parameters (MACHO:PLANET) with model LD1 of Albrow et al.

(1998b) yields $\hat{t} = (52.8 : 54.4)$, $u_{\min} = (0.225 : 0.215)$, $a = (0.71 : 0.69)$, $\epsilon_1 = (0.17 : 0.19)$, $\theta = (1.44 : 1.42)$, $t_* = (0.76 : 0.78)$.

Following the procedure outlined in Section 5.2.2 and Table 4, we estimate the reddening to be $E(V - R) = 0.67 \pm 0.04$, which yields de-reddened source magnitudes of $V = 15.52 \pm 0.19$ and $R = 14.94 \pm 0.15$. From this we determine $T_{\text{eff}} = 4500 \pm 200\text{K}$ for the source star. Using a bolometric correction of $BC_V = -0.48$, we find an angular source radius of $\theta_* = 6.58 \pm 0.90\mu\text{as}$. For comparison, the PLANET group find a de-reddened $V = 15.27$, $T_{\text{eff}} = 4350\text{K}$, and $\theta_* = 8.74 \pm 1.17\mu\text{as}$, so our results are in reasonably good agreement.

4.14. 97-BLG-41 (402.47862.1576)

This event was detected and alerted upon on 18 Jun, 1997. This event exhibited what appeared to be a fairly normal rise and fall for a microlensing event. However, after peak the event did not decline to baseline magnification, but leveled off at $A \sim 1.5$, and began a slow rise, which itself was fit well by a longer duration microlensing event. The deviation from a normal single lens lightcurve was noted and announced by both the MACHO/GMAN and PLANET collaborations. Near the peak of the event is an apparent caustic or cusp crossing. The MACHO and GMAN data have been plotted in Fig. 29.

Considerable effort has been made to fit this lightcurve to a binary lens model, but no satisfactory model has been found, even when the possible orbital motion of the lens was included. However, a satisfactory multiple lens fit has been found by Bennett et al. (1999).

4.15. 98-BLG-12 (179.21577.1740)

98-BLG-12 was detected on Apr 8, 1998, and initially thought to be a rapidly rising, high magnification event. This behavior, evident in Fig. 30, was a result of the source exiting its first passage through the caustic structure (Fig. 31). It was not recognized as a binary lensing event until the source re-entered the caustic structure near May 17.5 UT, 1998 (day 2327.5), and was subsequently observed at high magnification by the survey telescope on May 17.74 UT, 1998 (day 2327.74). The < 3 days spent between caustics allowed little time for follow-up observations to constrain event parameters. Interestingly, in all passbands, this event appears heavily blended ($f \sim 0.2$).

4.16. 98-BLG-14 (401.48408.649)

This brightening of this apparent clump giant object was detected and alerted on Apr 26, 1998. Initially, it was not clear if the asymmetry in Fig. 32 was due to the parallax effect (Refsdal

1966; Alcock et al. 1995), and initial data allowed fits of similar significance for both binary and parallax models. However, the higher precision photometry from CTIO and MSO74 observations clearly favor the binary interpretation over the best fit parallax lightcurve ($\Delta\chi^2 = 115.75$ with 1 less degree of freedom), while the MACHO data also provide $\Delta\chi^2 = 30.32$. Unfortunately, there does remain a degeneracy between binary lens models. Fig. 33 and Fig. 34 indicate this is a non-caustic crossing binary event, similar to 95-BLG-12.

The blend fraction for the best fit (fit — in Fig. 32, and Fig. 33) is $f \sim 0.5$ for all 4 passbands of coverage, but there is another fit that is almost as good with $f \gtrsim 1$ (fit - - - in Fig. 32, and Fig. 34). The best fit suggests a blend of clump giant stars, where they are constrained to lie within a seeing disk, or $\sim 1''$. 98-BLG-14 is located closer to the Galactic center than most of our events at $l = 1.96$, $b = -2.29$, where the surface density of giants is quite high. The average separation of clump giants is $5.3''$ in the vicinity of 98-BLG-14, so we expect that $\sim 10\%$ of clump giants will be blended with another clump giant. The de-reddened brightness of the MACHO object would place it at the bright tip of the clump. In the best fit, the lensed source would be somewhat lower than the mean clump brightness. It is thus reasonable for the lensed clump giant source to be blended with an unlensed clump giant. The second-best fit differs from the first by $\Delta\chi^2 = 5$, and from the event timescale of $\hat{t} = 74$ days and lens mass ratio of $12 : 1$, we can estimate a lens system comprised of a $1.03M_\odot$ primary and $0.088M_\odot$ companion.

4.17. 98-BLG-16 (402.47863.110)

98-BLG-16 was detected and alerted on Apr 28, 1998, and thought to be a high magnification, short timescale event. The initial sharp rise in Fig. 35 was due to a cusp approach (Fig. 36). Subsequent lightcurve interpretation was hindered by a significant amount of scatter in the MACHO Red passband, due to a defective amplifier, and a centroid offset of $\sim 1.3''$ between the MACHO object and the lensed source. Follow-up data from the CTIO 0.9m were able to resolve these objects, which allowed them to be independently photometered. Inspection of the CTIO dataset indicates the lensed source has a baseline flux of $\sim 7\%$ of the brightest (constant) neighboring star which serves as the target of MACHO photometry. The binary lens fit determines blend fractions consistent with this, $f_{MACHO} \sim 0.04$ and $f_{CTIO} \sim 1$, indicating there is no significant flux contribution from the lensing objects. The CTIO data from May 4.3 UT, 1998 (day 2314.3) provide a constraint on the lens proper motion for this particular fit, $t_* = 0.163 \pm 0.003$ days.

4.18. 98-BLG-42 (101.21045.2528)

98-BLG-42 was detected and alerted on Aug 22, 1998 at a magnification of ~ 4.0 . The source at this point in time was inside the caustic region depicted in Fig. 38. The event was immediately

followed up by the MPS effort, on the MSO 74" telescope. Over the next 3 nights the source began to rapidly increase in brightness. The PLANET collaboration issued an Anomaly Alert on Aug 26.0 UT, 1998 (day 2428.0) indicating the source underwent a caustic crossing between Aug 25.0 and 25.7 UT, 1998. Our fit presented here indicates a caustic crossing date of Aug 25.77 UT, with a source radius crossing time of $t_* = 0.109 \pm 0.016$ days.

4.19. 97-BLG-d2 (108.19073.2291)

This event was detected in the 3-year difference image analysis (DIA) of MACHO field 108, originally presented in Alcock et al. (1999b). The event is most closely associated with MACHO object 108.19073.2291, however the DIA technique uniquely identifies the time-varying source. The lightcurve associated with this analysis is purely a lightcurve of residuals around the source's baseline flux, which is not determined. For consistency with the notation of the other fits in this paper, we have added an arbitrary amount of flux to the residual lightcurve, and fit for the fraction of the combined lightcurve that is lensed. In this way we are able to estimate the baseline brightness of the lensed source. The source trajectory in Fig. 40 includes 2 cusp approaches, and passage through a caustic structure, which is suggested by 2 MACHO data points at high magnification.

4.20. MACHO-108-E (108.19333.1878)

This event was detected in the course of the MACHO bulge 5-year analysis (Alcock et al. 1999d). The deviation occurred with the Alert System in place. However, the Alert System was not triggered since all but 3 of the MACHO Blue data points are removed from the lightcurve due to the object's proximity to the edge of a detector. For this reason we are unable to realistically estimate properties of the lensed source, or set meaningful limits on the lens brightness. The lightcurve (Fig. 41) is characterized by approaches to 2 of the 3 caustics in the source plane (Fig. 42).

4.21. MACHO-176-A (176.19219.978)

Event 176-A was also detected in the bulge 5-year analysis, and is a good example of a poorly sampled binary lens event. The magnitude of the initial caustic approach is unconstrained, and the fit presented here places the one relevant data point at its peak (Fig. 43). The U-shape of the subsequent data suggests a caustic crossing and gradual decline to baseline. The critical and caustic curves are presented in Fig. 44.

5. What Can We Learn?

With our ensemble of 21 binary microlensing candidates, we can begin to consider mapping the properties of the binary events to the lensing population as a whole (Di Stefano 1999; Kerins & Evans 1998). This is most difficult towards the Magellanic Clouds, where we have the additional uncertainty of an unknown or unmodelled lensing population.

5.1. Towards the Magellanic Clouds

We have presented 3 candidate LMC binary events out of the 8 events published in Alcock et al. (1997b), and detect no more unambiguous binary lens candidates in the ~ 20 events (Alcock et al. 1999e) in our 5-year analysis (we do however detect one binary source candidate, 96-LMC-2 (Becker et al. 1997)). A color-magnitude diagram, incorporating the de-blended magnitudes of the Magellanic sources from Table 1, can be found in Figure 45.

LMC-9 is a resolved caustic crossing event, where the measured t_* (assuming a single lensed source) is consistent with the lensing system residing in the LMC (Bennett et al. 1996b), but only if the velocity dispersion and the self-lensing optical depth (Gould 1995) of the LMC are both small. If the LMC self-lensing optical depth is large enough to explain most of the microlensing events seen towards the LMC, as in the model of Aubourg et al. (1999), then the proper motion of LMC-9 is not consistent with an LMC lens, unless the source star is actually a pair of binary stars of similar brightness. However, in this case, we can no longer constrain the proper motion of the lens.

As emphasized by Di Stefano (1999), we should also expect events without obvious caustic crossings, similar to LMC-10. This event is consistent with a binary lens event, but the asymmetry of the lightcurve also resembles what might be expected for some types of stellar variability. A future HST frame of this object could confirm the microlensing prediction for the amount of blending.

Event 98-SMC-1 was recognized to be a caustic crossing event in real time with the GMAN follow-up observations presented here. An unprecedented response by the majority of the microlensing community resulted in dense coverage of the event, including resolution of the second caustic crossing by the PLANET and EROS collaborations. Important constraints on the initial caustic crossing date were provided by the OGLE and MPS collaborations. The lens proper motion derived from each of these datasets is most consistent with a SMC lens. This is the strongest constraint that has yet been placed on the location of the lensing population towards the Magellanic Clouds. However, as Palanque-Delabrouille et al. (1998) point out, the SMC is expected to have a large self-lensing optical depth, so that a large fraction of SMC events are likely to be due to self-lensing, even if most of the LMC events are due to halo lenses.

Kerins & Evans (1998) reach the conclusion that, if the caustic crossing events LMC-9 and

98-SMC-1 are both due to Magellanic lenses, than the bulk of lensing seen so far towards the Magellanic Clouds is most likely due to self-lensing, where the lenses may reside in Magellanic stellar or dark halos. However, the suggestive evidence that the LMC-9 lens may reside in the LMC only applies for LMC models with a low self-lensing optical depth. Furthermore, as Honma (1999) has pointed out, there is probably a bias in favor of detecting long timescale caustic crossing events. Thus, we may be more likely to detect and characterize caustic crossing features for self-lensing events than for halo lensing events, if the latter tend to have shorter timescales. A potentially more serious bias may be that there may be very few binary lenses in the halo. If most of the LMC events are due to lenses in the Galactic halo, then they comprise a previously unknown population with an unknown binary fraction. So, it is possible that the sample of binary events themselves selects against the halo lensing events. If so, we might expect a smaller fraction of binary lensing events towards the LMC than towards the bulge when the event samples get larger.

5.2. Towards the Galactic Bulge

A more representative sample of binary lenses can be found amongst the 17 Galactic bulge candidates. For the duration 1994-1998, the Alert System triggered on 196 Galactic bulge microlensing events. Twelve of the Alert events are presented here as binary lens candidates. Since the Alert System is tuned to detect generic variability, it is reasonable to make the assumption that the 12 binary events out of the 196 Alert events are representative of the detectable binary fraction of the lensing population as a whole. This is consistent with theoretical estimates of a binary lensing rate of order 10% (Mao & Paczyński 1991).

A color-magnitude diagram, incorporating the de-blended magnitudes of the lensed sources from Table 1, can be found in Figure 46. It is interesting to note that clump giants are over-represented in our sample, implying our binary lens detection efficiency is highest with these bright sources. It is also important to note that for the 6 clump giants lensed, in most cases the blending fraction is quite close to 1 (with the possible exception of 98-BLG-14), indicating there is insignificant contamination from neighboring sources and, most importantly, from the lensing system. This is contrary to the distributions of blending in the majority of binary microlensing events that have been reported in the literature thus far (Di Stefano 1999).

Two of the binary events (97-BLG-24 and 98-BLG-16) are heavily blended in the MACHO data, but the lensed source star is resolved in the follow-up GMAN data, at separations of $1.2''$ and $1.3''$, respectively. However, the 97-BLG-24 field is crowded enough that it is difficult to independently photometer the MACHO object and lensed source. For 98-BLG-16, the microlensing fit to CTIO data exhibits no blending, indicating the lens is in fact relatively dark. Candidates 95-BLG-12, 96-BLG-3, and 98-BLG-12 are strongly blended in all passbands (70 – 80% contamination), and it is possible in these cases that the lens contributes significant flux to the source brightness. High resolution photometry of strongly blended events can disentangle blending

due to crowding, and blending due to lens luminosity.

Excluding event 97-BLG-24 for which we have two fits, we find 12 (9) caustic crossing events from our ensemble of 16 (only the 11 Alert) bulge candidates. While not all of the GMAN follow-up data for the interval 1995-1998 have yet been reduced, we so far have found no weakly perturbed systems, at the $\sim 1\%$ level (see however Becker 2000). Di Stefano (1999) indicates that several of these weakly perturbed events should exist for each caustic crossing event (but see Sec. 2.1). That we have detected no such events indicates our efficiency at detecting them, or characterizing them as binary microlensing, is currently quite low.

5.2.1. Mass Ratio Distribution

While some of the events here are poorly constrained, and thus can be characterized by multiple combinations of event parameters, we can begin to probe the distribution of mass ratios of the binary lensing population towards the Galactic bulge, given the above fits. Distributions of the binary parameters θ and a are less informative, with θ representing a random orientation between the lens separation axis and motion with respect to the source, and a the projection of the lens separation at a random (unknown) orbital phase. Figure 47 contains a histogram of the distribution of mass ratios (q , defined to be ≤ 1) which we find from our bulge events. The 2 fits each for events 97-BLG-24 and 98-BLG-14 are represented by additional shaded areas. The distribution here is free of inclination uncertainties present in studies of spectroscopic binaries (SB), but does likely suffer from non-uniqueness of fits in several cases.

The binary mass ratio distribution function $N(q)$ has been studied by, e.g. Trimble (1990), who examines SB systems with both giant and relatively bright main sequence primaries. Similar morphologies are found between samples, generally characterized by $N(q) \propto q^{-1}$, with a possible peak near $q \sim 0.3$. However, we expect many of our lenses to be drawn from the lower, more populated portion of the main sequence. Given the apparent dependence of $N(q)$ on spectral type (Abt 1983), it would be more appropriate to compare Fig. 47 with the study of solar-type SB by Mazeh et al. (1992). They find, with a considerably smaller sample than Trimble (1990), a relatively flat $N(q)$, possibly rising towards larger q . We therefore compare two models, $N(q) \propto q^{-1}$ and $N(q) = \text{constant}$, against the events with $0.1 < q < 1$ using the one-sided Kolmogorov-Smirnov (KS) test. We find probabilities of 0.07 and 0.41, respectively, of finding a KS deviation between data and model as large as that observed. A $N(q) \propto q^{-1}$ is clearly inconsistent with our measured distribution, while a flat $N(q)$ is consistent with our data.

5.2.2. Reddening Estimates

For 10 of our bulge events, the microlensing fits provide a measurement of t_* . However, it is our coverage of events 119-A (Fig. 10), 96-BLG-3 (Fig. 18), 97-BLG-28 (Fig. 27), and 98-BLG-42

(Fig. 37) which most reliably constrain t_* .

We therefore have 4 events where we believe we have a reliable measurement of the time it takes the lens to transit the source face, $2t_*$. To arrive at an estimate of the proper motion of the lensing system, we must first determine the angular size of the source. This can be done by assuming the source is a blackbody and estimating its effective temperature T_{eff} and apparent bolometric magnitude m_{bol} . We first need to determine the extinction, A_V , and reddening, $E(V - R)$, to the source – in the following, we assume $A_V = 3.97E(V - R)$ (Rieke & Lebofsky 1985).

Stanek (1996), in a study of red clump stars in Baade’s Window, finds a range of A_V from 1.26 to 2.79, even though this is the clearest and most uniform window through the bulge. This suggests it would be unwise to apply an “average” extinction correction to all of our events. Instead, we estimate the reddening for each source using neighboring RR Lyrae stars, whose intrinsic colors are well known. An intrinsic color-period (P) relationship has been established for field RR Lyrae by Caputo & De Santis (1992), in the form of

$$(B - V)_0 = 0.658 + 0.097 [\text{Fe}/\text{H}] + 0.710 \log P. \quad (5)$$

We assume $[\text{Fe}/\text{H}] = -1$, after Walker & Terndrup (1991), and transform to $(V - R)_0$ with the relation (Alcock et al. 1997a)

$$(V - R)_0 = 0.004 + 0.566(B - V)_0. \quad (6)$$

We then compute the reddening to all RR Lyrae within $10'$ of the source, excluding significant outliers, and apply the reddening and extinction corrections to our lensed source star. The results of this are listed in the first columns of Table 4. We note that two of the events, 119-A and 96-BLG-3, occurred within Baade’s Window, but both sources are just outside the extinction grid reported by Stanek (1996).

We next interpolate the ATLAS9 and NMARCS model atmospheres presented in Bessell, Castelli, & Plez (1998) (assuming solar metallicity, $\log g = 2.0$ for giants, and $\log g = 4.5$ otherwise) to determine the source’s T_{eff} and bolometric correction in V (BC_V), given its unreddened $(V - R)_0$. It is then straightforward to calculate the angular size of the source θ_* using the bolometric flux method of Gray (1992), and to determine the relative proper motion $\mu = \theta_*/t_*$ between the lens and the source, further described in Sec. 5.2.3.

5.2.3. Lens Proper Motions

The determination of the lens proper motion with respect to the source, μ , yields an additional constraint on the parameters of the lensing system. For most lensing events, the only observable parameter which constrains the distance, D_{ol} , total mass, M_{tot} , and the transverse velocity, v_{\perp} , of

the lens system is the event timescale, \hat{t} . However, for caustic crossing events, we have seen that it is also possible to measure the lens proper motion, which is related to the distance and transverse velocity of the lens by

$$\mu = \frac{v_{\perp}}{D_{ol}}. \quad (7)$$

Thus, for the four events with measured μ values, we have two constraints on three parameters, so there is a one-parameter family of solutions, namely

$$M_{\text{tot}} = \frac{\mu^2 \hat{t}^2}{16G} \frac{D_{ol} (D_{ol} + D_{ls})}{D_{ls}}. \quad (8)$$

These solutions are shown in Figure 48. We see that M_{tot} grows as function of the lens distance, and passes through the expected lens masses of $0.1 - 2M_{\odot}$ at distances of $2 - 7.5$ kpc.

We can make a more accurate estimate of the lens parameters if we make use of our knowledge of the velocity distributions of the source and lens populations. This requires that we specify a Galactic model, and we select the simple bar model of Han & Gould (1995). The kinematics of the bulge using giants has been measured by Minniti (1996). We assume velocity dispersions of 30 km s^{-1} in each transverse direction for disk lenses, and 80 km s^{-1} in each transverse direction for both lenses and source stars located in the central bar. We have assumed a distance of $R_0 = 8$ kpc to the Galactic center and 8.5 kpc to each source star. We have done a likelihood analysis to determine the most probable lens distance and mass for each of the four events with reliable proper motion measurements, and the results are summarized in Figure 48 and Table 5. The measured proper motions of $\mu = 1.8 - 3.2 \text{ mas/yr}$ are most consistent with lens systems residing in the bulge, and the best fit primary lens masses are consistent with main sequence stars fainter than the Sun. The only exception is the heavier lens mass for event 96-BLG-3, which has a best fit mass of $1.2M_{\odot}$ with an uncertainty of a factor of two.

If the heavier 96-BLG-3 lens is a main sequence star, then we must have $M_2 \leq 1.3M_{\odot}$ to be consistent with our measurement of the unlensed flux observed at the position of the source star. High resolution imaging of the source might be able to tighten this constraint by resolving some of the unlensed flux into separate stars. Similar constraints apply for the other stars, but are significantly weaker because the implied masses are much lower. However, these constraints do not apply for stellar remnant lenses, which may make up of order 20% of the lens population (Gould 1999).

6. Conclusions

After a survey of the MACHO database, it is very apparent that microlensing by binary lens systems has been detected, and at a rate that is roughly consistent with theoretical predictions for known stellar populations. However, a rigorous search has not yet been implemented, and we cannot set hard limits on the binary microlensing rate, nor on the characteristics of binary

systems in the lensing population. This includes the incidence of planets around lensing stars. However, follow-up efforts such as MPS (Rhie et al. 1998b) and PLANET (Gaudi et al. 1998) are undertaking dense lightcurve sampling, and are beginning to set meaningful limits on planetary companions on an event-by-event basis.

It is also apparent that there are difficult degeneracies between binary microlensing fits which cannot be resolved with the sparse sampling (\sim once per night) of the microlensing survey telescopes. This is especially important in short duration and/or low level deviations, such as caustic crossings or planetary ‘spikes’. In both cases important information is contained in a small fraction of the lightcurve. It is thus important that microlensing follow-up continues with dense (tens of observations per night), precise ($\sim 1\%$) sampling of event lightcurves. The limitations of undersampled datasets are apparent in the analysis of 97-BLG-24, where we are sure of a binary (possibly even planetary) signal, but are not able to uniquely characterize it.

Three of our bulge events (95-BLG-12, 96-BLG-3 and 98-BLG-12) are strongly blended in all MACHO and GMAN follow-up passbands, indicating the lensing objects may be luminous at a detectable level. High resolution observations of these sources may eventually reveal the appearance of a “new” source, as the lens proper motion separates it from the lensed source at the rate of \sim milli-arcseconds/yr. This can be accomplished with the HST, or adaptive optics imaging available on systems such as Gemini. On the other hand, our binary events on giant sources tend to show little blending. Event 98-BLG-16, a main-sequence source which is highly blended in the MACHO photometry, is resolved into separate objects in GMAN follow-up data, and fit blend fractions indicate the lensing objects are in fact dark.

We have recovered a distribution of mass ratios for 16 of our Galactic bulge microlensing candidates, and a distribution of lens proper motions for 4 of these events where we have, to some degree, resolved a caustic crossing. The mass ratio distribution is consistent with the relatively flat distribution seen in solar-type spectroscopic binary systems. The lens proper motions, when combined with the likelihood analysis in Sec. 5.2.3, imply a population of binary lenses residing in the Galactic bulge at a distance of 7 ± 1 kpc. The lens masses generally appear sub-solar.

Finally, we would like to caution against over-interpretation of this dataset, in particular the Magellanic Cloud subset, which is admittedly incomplete. In fact, there are undoubtedly a number of unquantified biases in our ability to discriminate between the single-lens and binary-lens case, although actual event detection is more a function of the significance of the deviation from baseline than lightcurve morphology. However, observations of on-going binary lensing events towards the Magellanic Clouds, such as 98-SMC-1, may on an event-by-event basis allow us to examine the role the lensing populations play in the larger context of Galactic dark matter.

Acknowledgments

We are very grateful for the skilled support given our project by S. Chan, S. Sabine, and the technical staff at the Mt. Stromlo Observatory. We especially thank J.D. Reynolds for the network software that has made this effort successful. We would like to thank the many staff and observers at CTIO and UTSO who have helped to make the GMAN effort successful.

Work performed at LLNL is supported by the DOE under contract W7405-ENG-48. Work performed by the Center for Particle Astrophysics personnel is supported in part by the Office of Science and Technology Centers of NSF under cooperative agreement AST-8809616. Work performed at MSSSO is supported by the Bilateral Science and Technology Program of the Australian Department of Industry, Technology and Regional Development. Astronomy at Wise Observatory is supported by a grant from the Israel Science Foundation. KG acknowledges support from DOE grant DEFG03-90-ER 40546 and a Cottrell Scholar award. DM is also supported by Fondecyt 1990440. CWS thanks the Packard Foundation for their generous support. WJS is supported by a PPARC Advanced Fellowship.

REFERENCES

- Abt, H. A. 1983, *ARA&A*, 21, 343
- Afonso, C., et al. 1998, *A&A*, 337, L17
- Afonso, C., et al. 1999, in preparation
- Alard, C., et al. 1995, *ESO Messenger*, 80, 31
- Alard, C., Mao, S., & Guibert, J. 1995, *A&A*, 300, L17
- Albrow, M., et al. 1996, in *Astrophysical Applications of Gravitational Lensing: Proceedings of the 173rd Symposium of the International Astronomical Union*, ed. C. S. Kochanek & J. N. Hewitt, International Astronomical Union Symposium Series No. 173 (Kluwer Academic Publishers), 227
- Albrow, M., et al. 1998a, *ApJ*, 509, 687
- Albrow, M., et al. 1998b, *astro-ph/9811479*
- Albrow, M. D., et al. 1999a, *ApJ*, 512, 672
- Albrow, M., et al. 1999b, *astro-ph/9903008*
- Alcock, C., et al. 1993, *Nature*, 365, 621
- Alcock, C., et al. 1995, *ApJ*, 454, L125
- Alcock, C., et al. 1997a, *ApJ*, 482, 89
- Alcock, C., et al. 1997b, *ApJ*, 486, 697
- Alcock, C., et al. 1997c, *ApJ*, 490, L59
- Alcock, C., et al. 1997d, *ApJ*, 491, 436
- Alcock, C., et al. 1998a, *ApJ*, 492, 190
- Alcock, C., et al. 1998b, *ApJ*, 494, 396
- Alcock, C., et al. 1998c, *ApJ*, 499, L9
- Alcock, C., et al. 1999a, *ApJ*, 518, 44
- Alcock, C., et al. 1999b, *Accepted*, *ApJ*
- Alcock, C., et al. 1999c, *Submitted*, *PASP*
- Alcock, C., et al. 1999d, in preparation

- Alcock, C., et al. 1999e, in preparation
- Aubourg, E., et al. 1993, *Nature*, 365, 623
- Aubourg, E., et al. 1999, astro-ph/9901372
- Becker, A. C. 2000, Ph.D. thesis, University of Washington, in preparation
- Becker, A. C., et al. 1997, American Astronomical Society Meeting, 191, 8305
- Becker, A. C., et al. 1998, *IAU Circ.*, 6935, 1
- Bennett, D. P., et al. 1993, *BAAS*, 183, 7206
- Bennett, D. P., et al. 1995, in *Dark Matter*, ed. Holt, S. S. and Bennett, C. L. , AIP Conference Proceedings No. 336, 77
- Bennett, D., et al. 1996a, *IAU Circ.*, 6361, 1
- Bennett, D. P., et al. 1996b, in *Nucl. Phys. B (Proc. Suppl.)*, Vol. 51B, Sources and Detection of Dark Matter in the Universe: Proceedings of the International Symposium on Sources and Detection of Dark Matter in the Universe, ed. D. Cline (Elsevier Science), 131
- Bennett, D. P., et al. 1997, in *Proceedings of Planets Beyond the Solar System and the Next Generation of Space Missions*, astro-ph/9612208, held at STScI, October 16-18, 1996
- Bennett, D., et al. 1998, *IAU Circ.*, 6939, 1
- Bennett, D. P., et al. 1999, in preparation
- Bennett, D. P., & Rhie, S. H. 1996, *ApJ*, 472, 660
- Bessell, M. S., Castelli, F., & Plez, B. 1998, *A&A*, 333, 231
- Bolatto, A. D., & Falco, E. E. 1994, *ApJ*, 436, 112
- Caputo, F., & De Santis, R. 1992, *AJ*, 104, 253
- Cowley, A. P., & Hartwick, F. D. A. 1991, *ApJ*, 373, 80
- Di Stefano, R. 1999, astro-ph/9901035
- Di Stefano, R., & Mao, S. 1996, *ApJ*, 457, 93
- Di Stefano, R., & Perna, R. 1997, *ApJ*, 488, 55
- Di Stefano, R., & Scalzo, R. A. 1999a, *ApJ*, 512, 564
- Di Stefano, R., & Scalzo, R. A. 1999b, *ApJ*, 512, 579

- Dominik, M. 1998a, A&A, 329, 361
- Dominik, M. 1998b, A&A, 330, 963
- Dominik, M. 1999, A&A, 341, 943
- Dominik, M., & Hirshfeld, A. C. 1996, A&A, 313, 841
- Gaudi, B. S., et al. 1998, American Astronomical Society Meeting, 193, 10807
- Gaudi, B. S., Naber, R. M., & Sackett, P. D. 1998, ApJ, 502, L33
- Gould, A. 1995, ApJ, 441, 77
- Gould, A. 1999, ApJsubmitted, astro-ph/9906472
- Gould, A., & Loeb, A. 1992, ApJ, 396, 104
- Gray, D. F. 1992, The Observation and Analysis of Stellar Photospheres (Second ed.) (Cambridge University Press)
- Griest, K., & Safizadeh, N. 1998, ApJ, 500, 37
- Han, C., & Gould, A. 1995, ApJ, 447, 53
- Hart, J., et al. 1996, PASP, 108, 220
- Honma, M. 1999, ApJ, 511, L29
- Iben, J., I. 1967, ARA&A, 5, 571
- Kerins, E., & Evans, N. 1998, astro-ph/9812403
- Lennon, D. J., Mao, S., Fuhrmann, K., & Gehren, T. 1996, ApJ, 471, L23
- Mao, S., & Paczyński, B. 1991, ApJ, 374, L37
- Mao, S., & Di Stefano, R. 1995, ApJ, 440, 22
- Mao, S., et al. 1994, BAAS, 185, 1705
- Marshall, S., et al. 1994, in IAU Symposium #161: Astronomy From Wide Field Imaging, ed. H. T. MacGillivray et al., 67
- Mazeh, T., Goldberg, D., Duquennoy, A., & Mayor, M. 1992, ApJ, 401, 265
- Minniti, D. 1996, ApJ, 459, 579
- Paczynski, B. 1986, ApJ, 304, 1

- Paczynski, B. 1991, *ApJ*, 371, L63
- Paczynski, B., & Stanek, K. Z. 1998, *ApJ*, 494, L219
- Paczynski, B., Stanek, K. Z., Udalski, A., Szymański, M., et al. 1994, *ApJ*, 435, L113
- Palanque-Delabrouille, N. 1997, Ph.D. thesis, Université de Paris 7
- Palanque-Delabrouille, N., et al. 1998, *A&A*, 332, 1
- Peale, S. J. 1997, *Icarus*, Vol. 127, p. 269-289 (1997), 127, 269
- Pratt, M., et al. 1996, in *Astrophysical Applications of Gravitational Lensing: Proceedings of the 173rd Symposium of the International Astronomical Union*, ed. C. S. Kochanek & J. N. Hewitt, International Astronomical Union Symposium Series No. 173 (Kluwer Academic Publishers), 221
- Refsdal, S. 1966, *MNRAS*, 134, 315
- Renault, C., et al. 1997, *A&A*, 324, L69
- Rhie, S. H., & Bennett, D. P. 1996, in *Nucl. Phys. B (Proc. Suppl.)*, Vol. 51B, Sources and Detection of Dark Matter in the Universe: Proceedings of the International Symposium on Sources and Detection of Dark Matter in the Universe, ed. D. Cline (Elsevier Science), 86
- Rhie, S. H., et al. 1998a, *astro-ph/9812252*
- Rhie, S. H., et al. 1998b, American Astronomical Society Meeting, 193, 10805
- Rieke, G. H., & Lebofsky, M. J. 1985, *ApJ*, 288, 618
- Schechter, P. L., Mateo, M., & Saha, A. 1993, *PASP*, 105, 1342
- Schneider, P., & Weiss, A. 1986, *A&A*, 164, 237
- Stanek, K. Z. 1996, *ApJ*, 460, L37
- Stanek, K. Z., Mateo, M., Udalski, A., Szymański, M., Kaluzny, J., & Kubiak, M. 1994, *ApJ*, 429, L73
- Stetson, P. 1987, *PASP*, 99, 191
- Stetson, P. B. 1994, *PASP*, 106, 250
- Tomaney, A. B., & Crotts, A. P. S. 1996, *AJ*, 112, 2872
- Trimble, V. 1990, *MNRAS*, 242, 79
- Udalski, A., Kubiak, M., & Szymański, M. 1997, *Acta Astronomica*, 47, 319

- Udalski, A., Szymański, M., Mao, S., Di stefano, R., et al. 1994, ApJ, 436, L103
- Udalski, A., et al. 1998, astro-ph/9808077
- Walker, A. R., & Terndrup, D. M. 1991, ApJ, 378, 119
- Zaritsky, D., Sheckman, S. A., Thompson, I., Harris, J., & Lin, D. N. C. 1999, AJ, 117, 2268
- Zhao, H., Rich, R. M., & Spergel, D. N. 1996, MNRAS, 282, 175

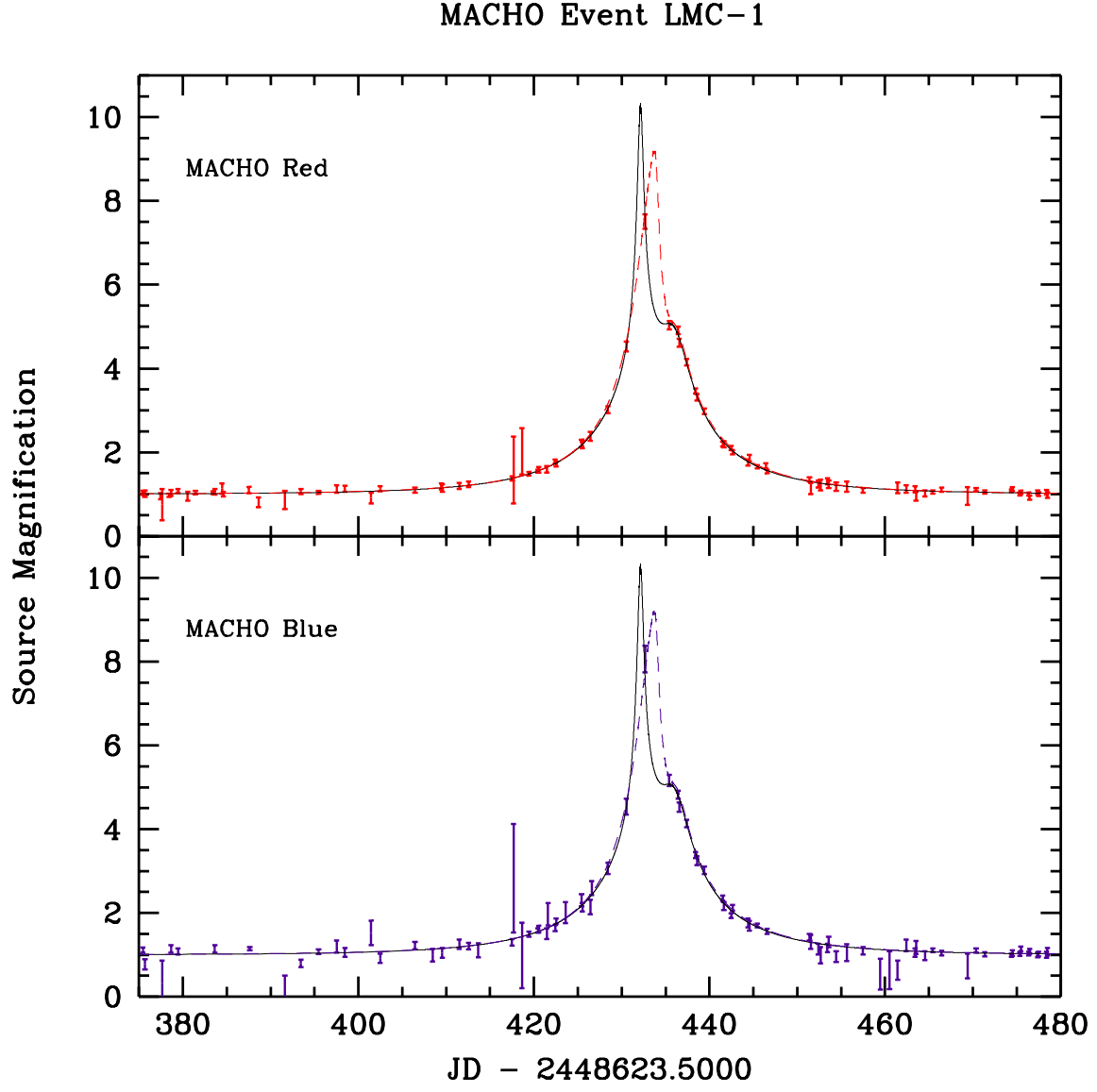


Fig. 1.— Lightcurve of MACHO event LMC-1, including fits indicating a 'planetary' mass secondary lens (---) and a more standard binary system (—).

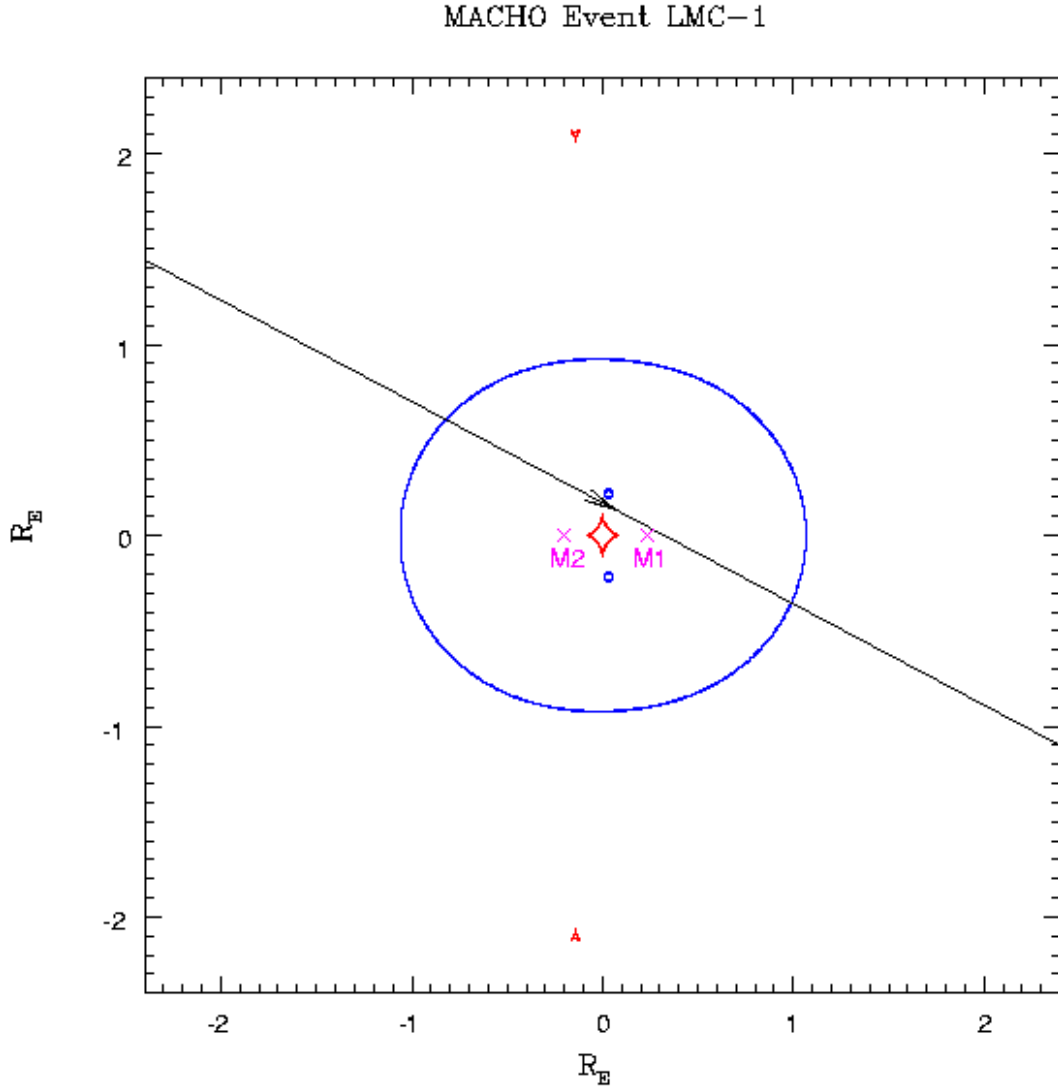


Fig. 2.— Location of the (red) caustic and (blue) critical curves for the LMC-1 standard binary lens fit (—) presented in Fig. 1. The coordinate system, whose origin is at the center of mass, indicates distance in units of the system’s Einstein ring radius R_E . Also shown are the locations of the lensing objects, and the trajectory of the source through the caustic structure.

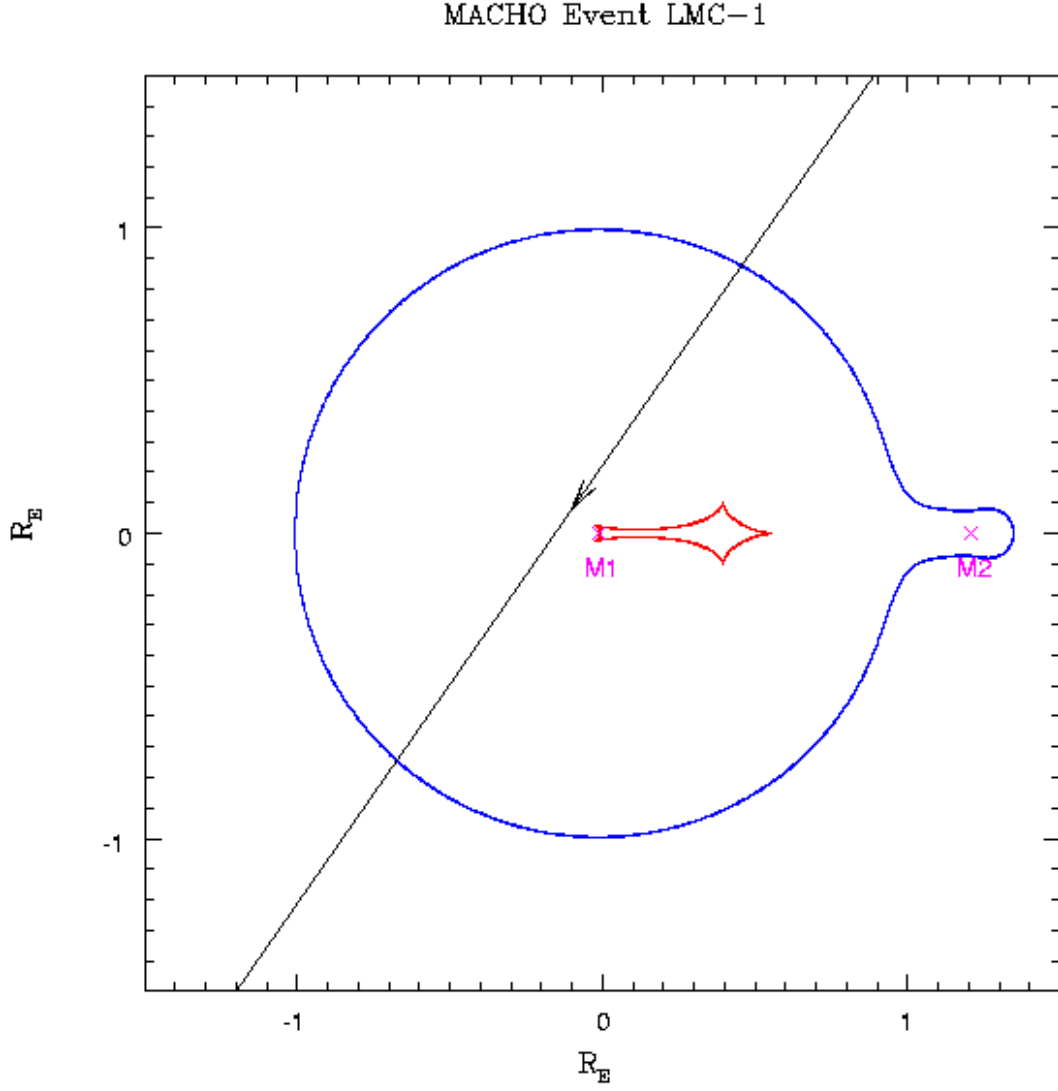


Fig. 3.— Location of the (red) caustic and (blue) critical curves for the LMC-1 ‘planetary’ binary lens fit (– – –) presented in Fig. 1. The coordinate system, whose origin is at the center of mass, indicates distance in units of the system’s Einstein ring radius R_E . Also shown are the locations of the lensing objects, and the trajectory of the source through the caustic structure.

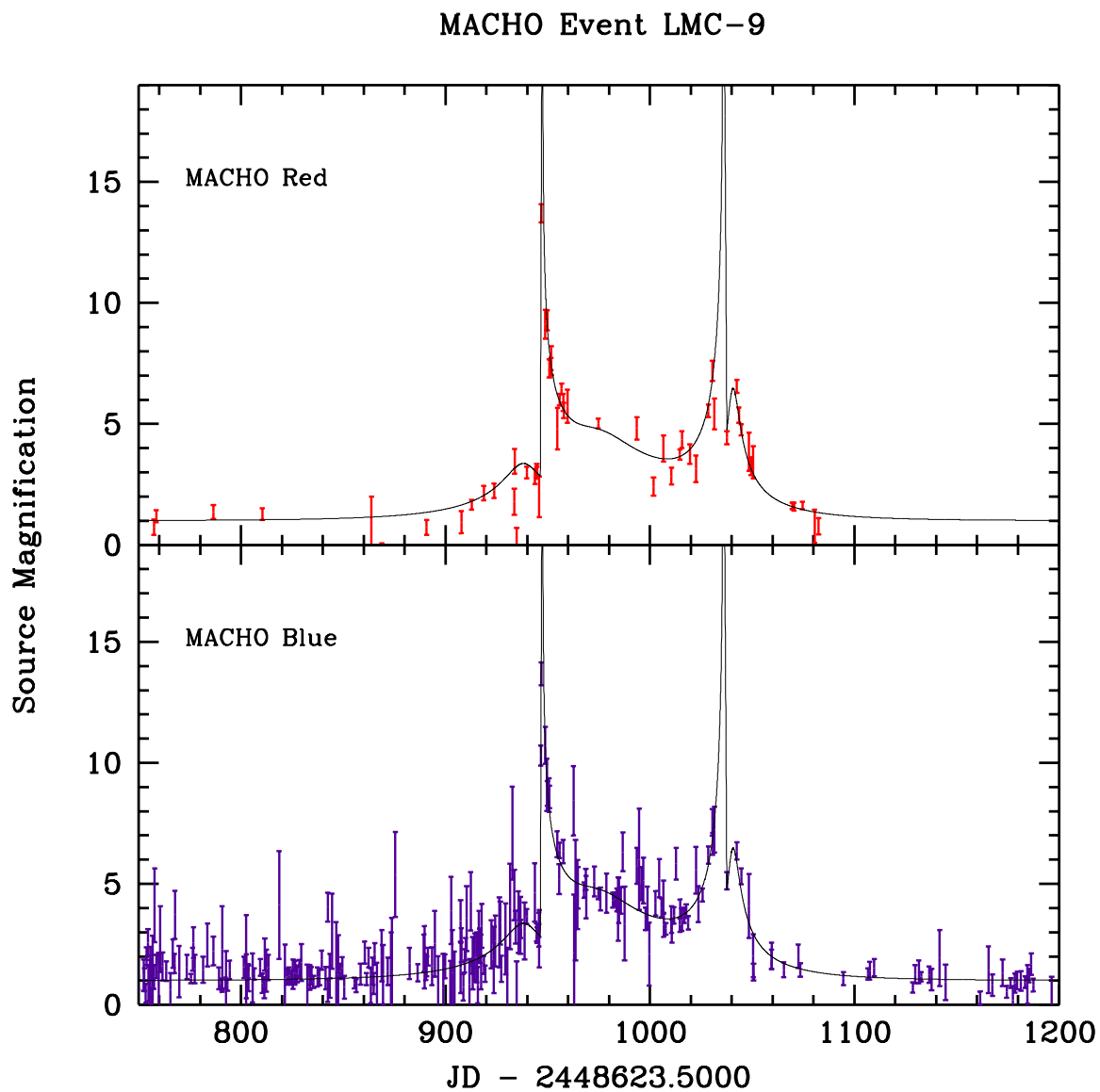


Fig. 4.— Lightcurve of MACHO event LMC-9, including our fit to binary microlensing.

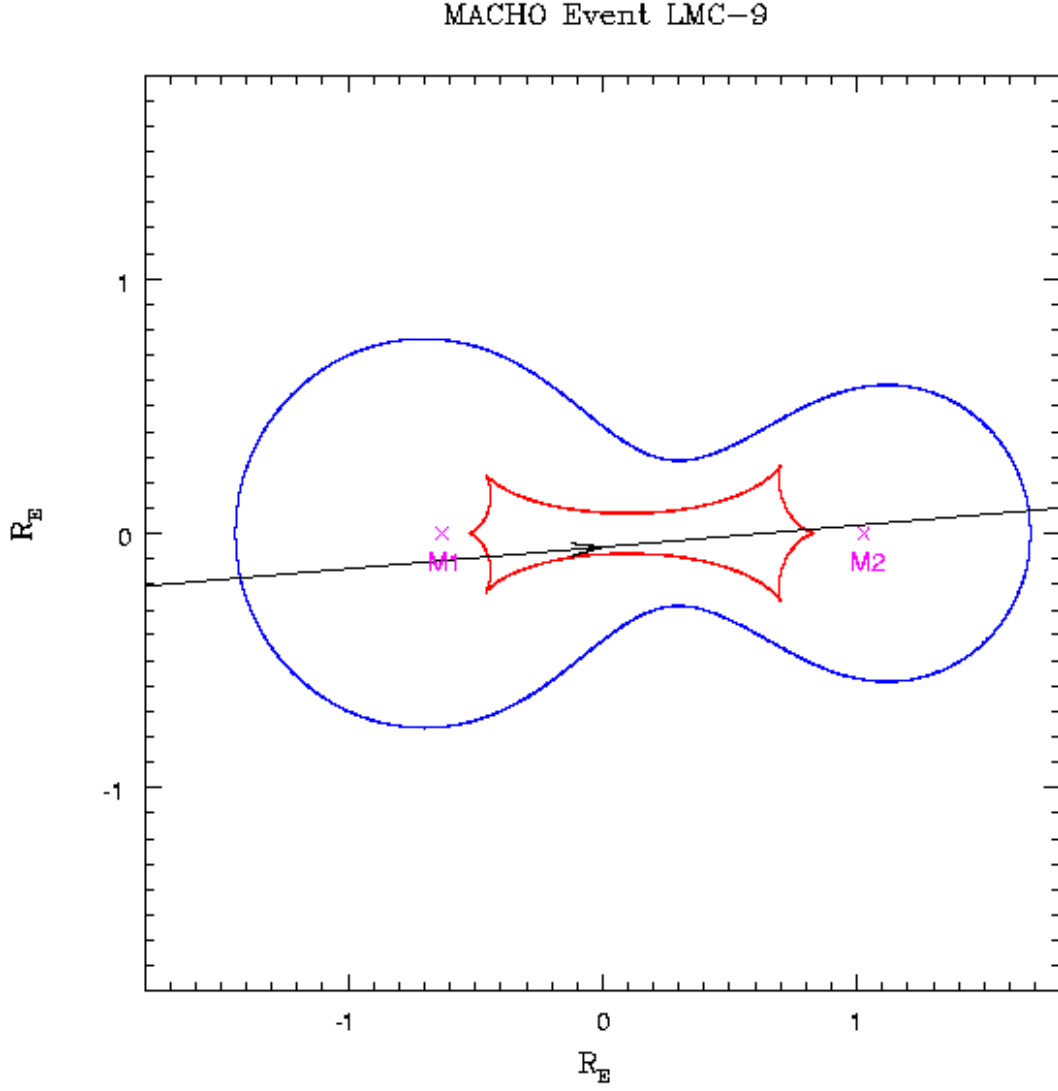


Fig. 5.— Location of the (red) caustic and (blue) critical curves for the LMC-9 binary lens fit presented in Fig. 4. The coordinate system, whose origin is at the center of mass, indicates distance in units of the system’s Einstein Ring radius R_E . Also shown are the locations of the lensing objects, and the trajectory of the source through the caustic structure.

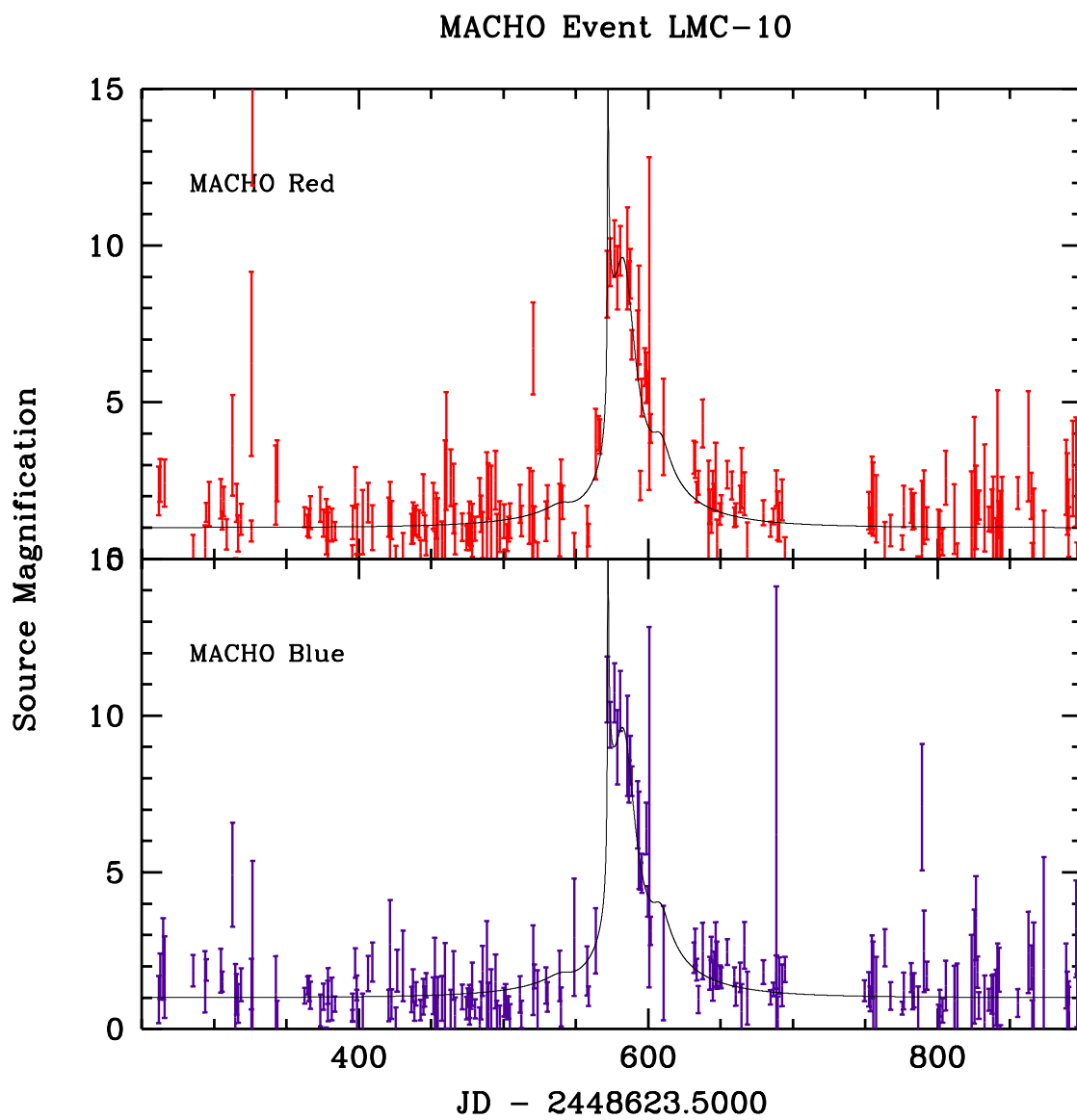


Fig. 6.— Lightcurve of MACHO event LMC-10, including our fit to binary microlensing.

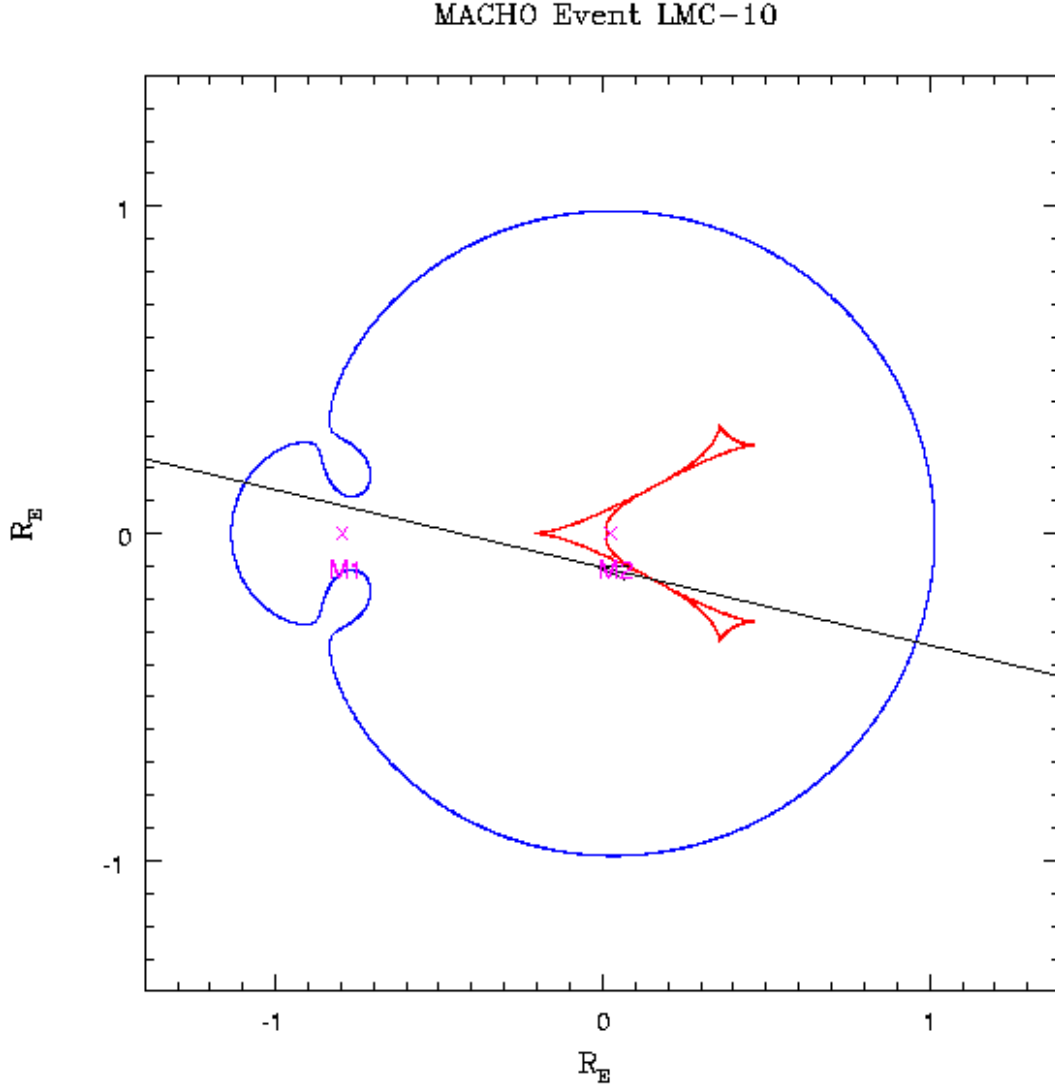


Fig. 7.— Location of the (red) caustic and (blue) critical curves for the LMC-10 binary lens fit presented in Fig. 6. The coordinate system, whose origin is at the center of mass, indicates distance in units of the system’s Einstein Ring radius R_E . Also shown are the locations of the lensing objects, and the trajectory of the source through the caustic structure.

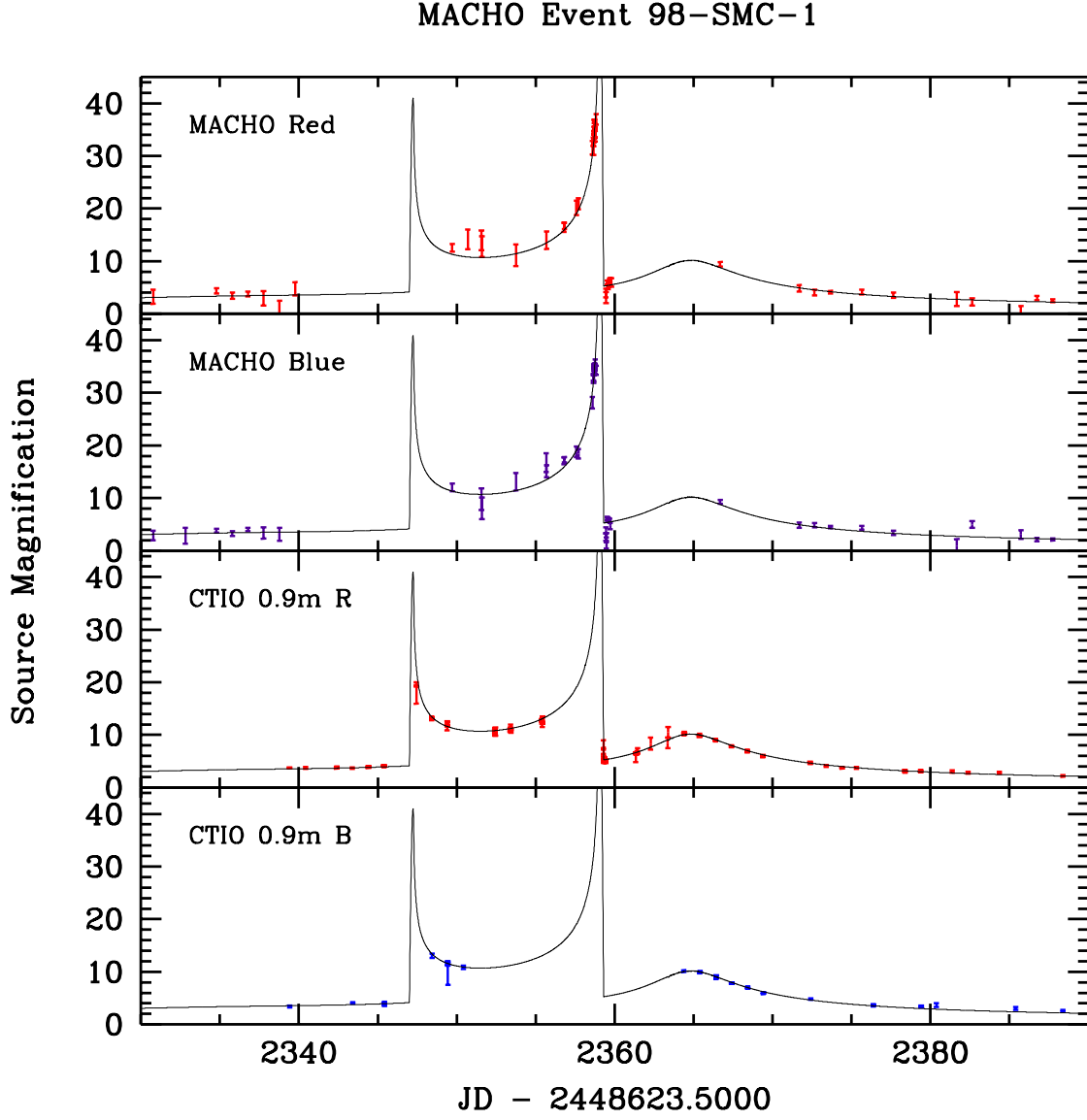


Fig. 8.— Lightcurve of MACHO event 98-SMC-1, including our fit to binary microlensing.

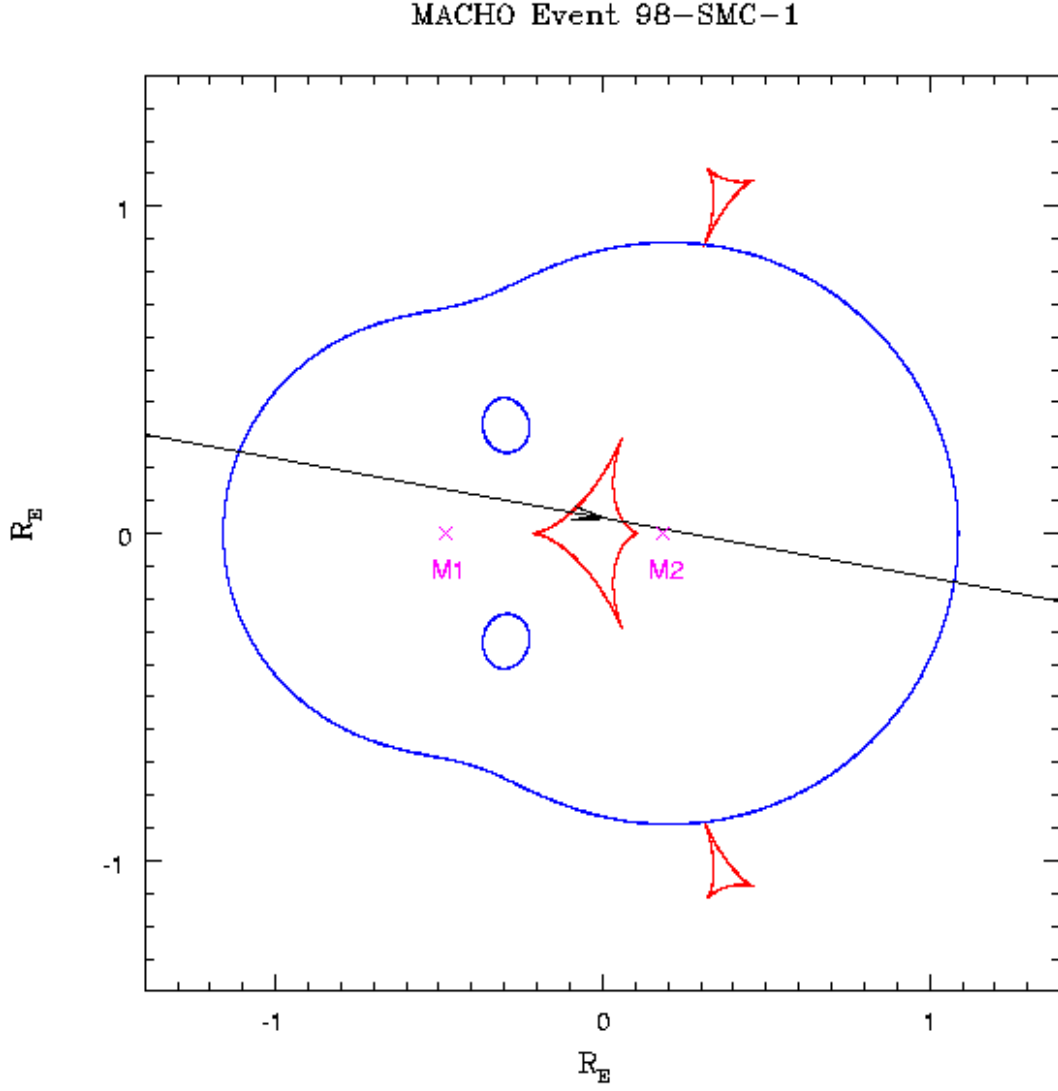


Fig. 9.— Location of the (red) caustic and (blue) critical curves for the 98-SMC-1 binary lens fit presented in Fig. 8. The coordinate system, whose origin is at the center of mass, indicates distance in units of the system’s Einstein Ring radius R_E . Also shown are the locations of the lensing objects, and the trajectory of the source through the caustic structure.

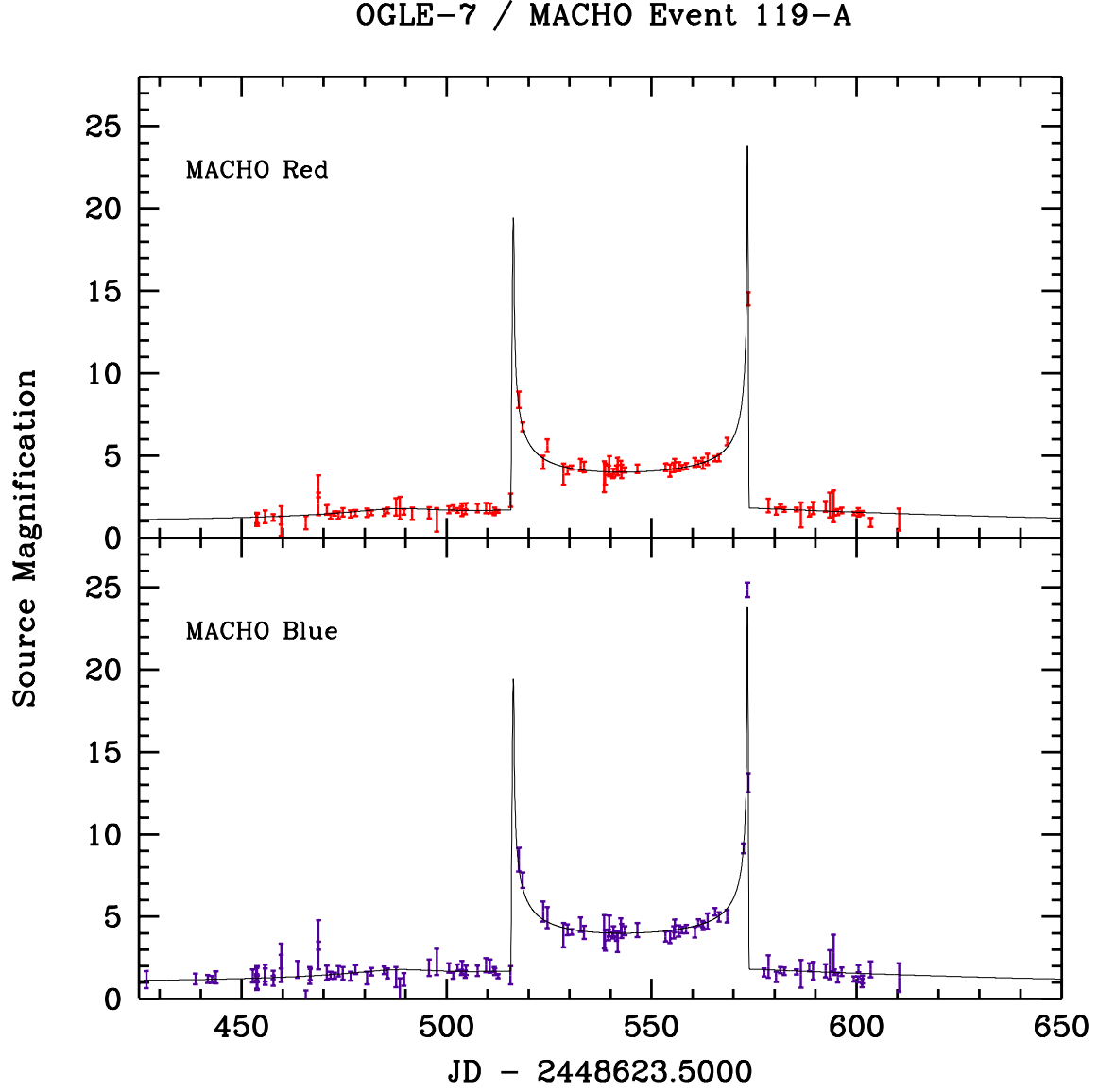


Fig. 10.— Lightcurve of MACHO event 119-A, including our fit to binary microlensing.

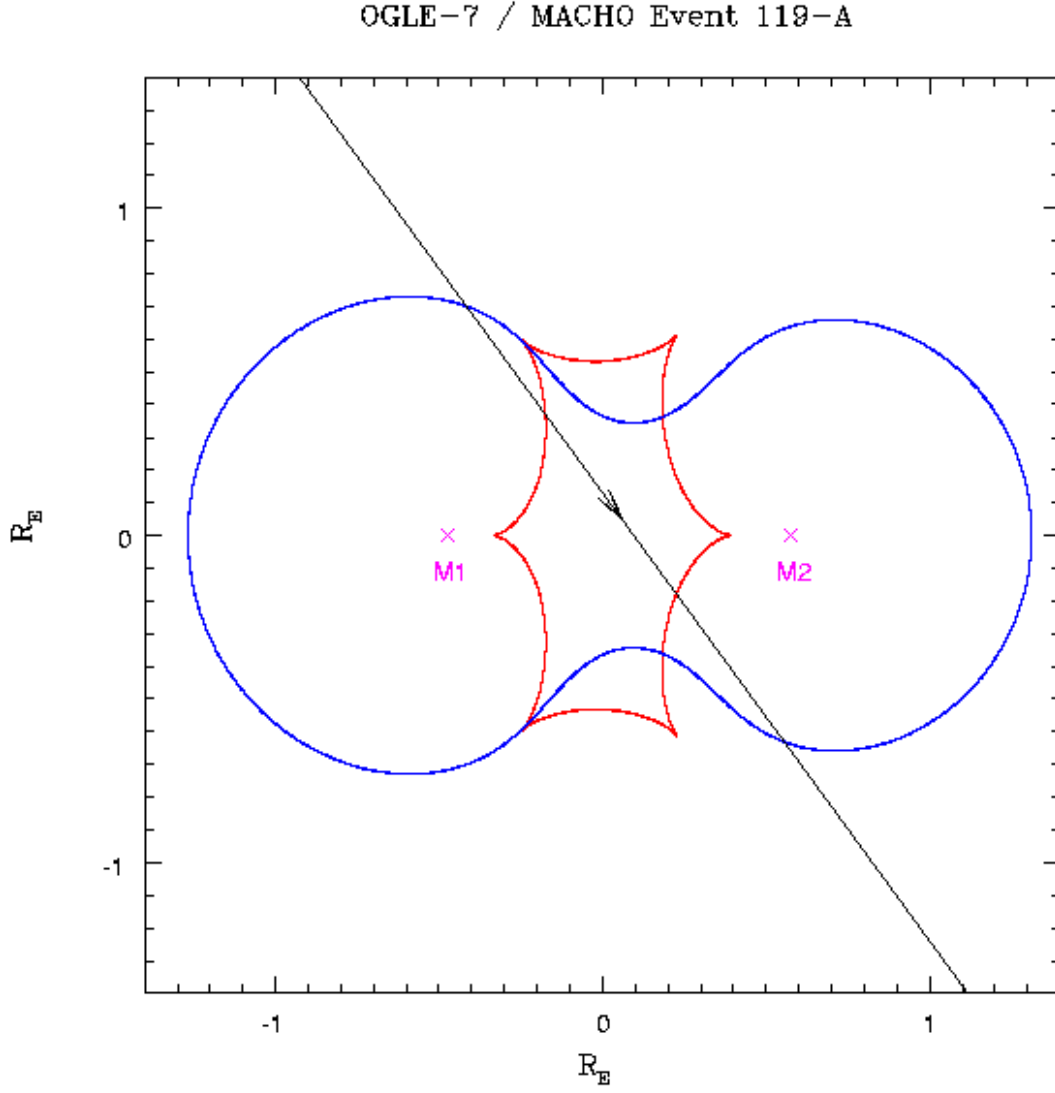


Fig. 11.— Location of the (red) caustic and (blue) critical curves for the 119-A binary lens fit presented in Fig. 10. The coordinate system, whose origin is at the center of mass, indicates distance in units of the system’s Einstein Ring radius R_E . Also shown are the locations of the lensing objects, and the trajectory of the source through the caustic structure.

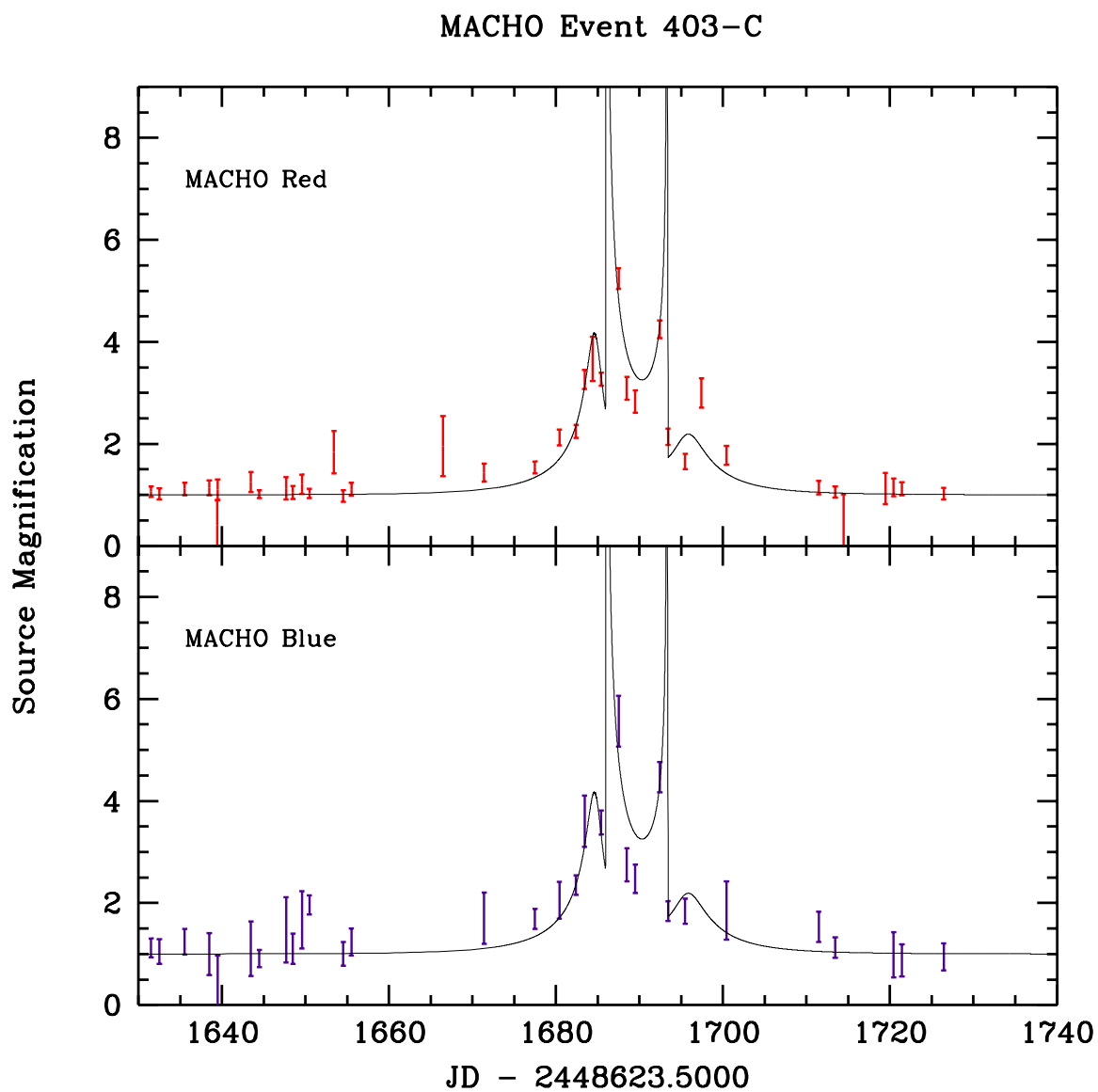


Fig. 12.— Lightcurve of MACHO event 403-C, including our fit to binary microlensing.

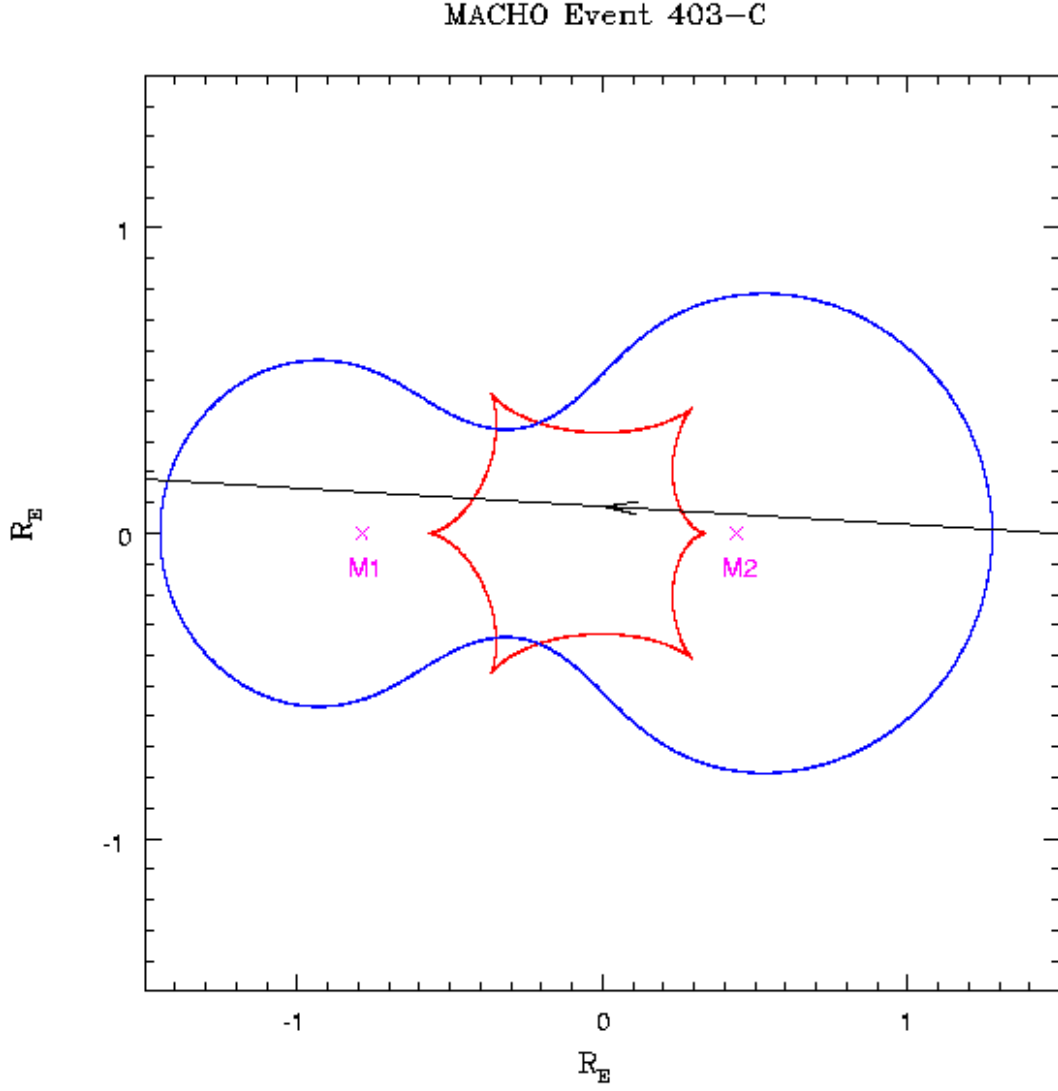


Fig. 13.— Location of the (red) caustic and (blue) critical curves for the 403-C binary lens fit presented in Fig. 12. The coordinate system, whose origin is at the center of mass, indicates distance in units of the system’s Einstein Ring radius R_E . Also shown are the locations of the lensing objects, and the trajectory of the source through the caustic structure.

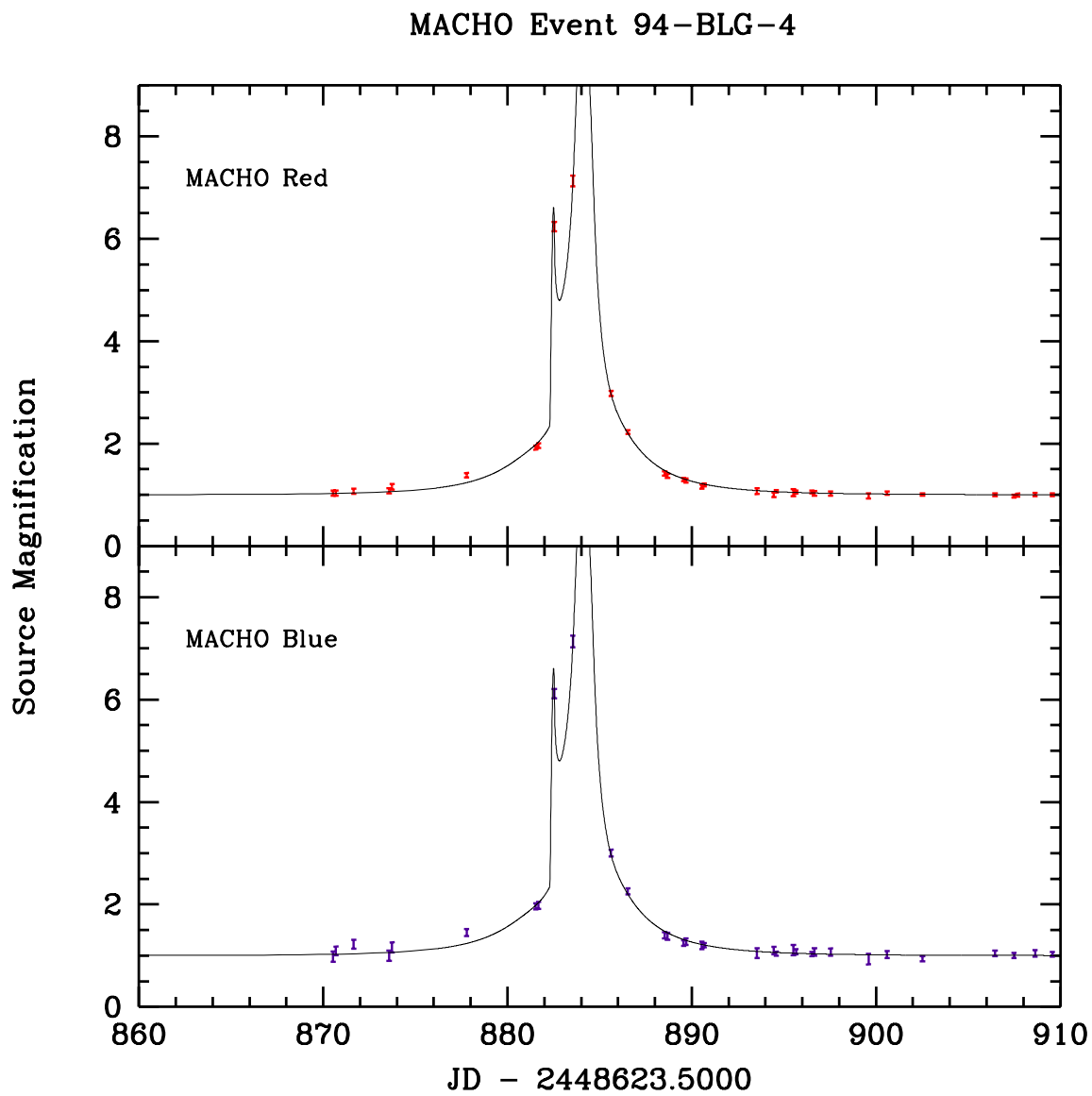


Fig. 14.— Lightcurve of MACHO event 94-BLG-4, including our fit to binary microlensing.

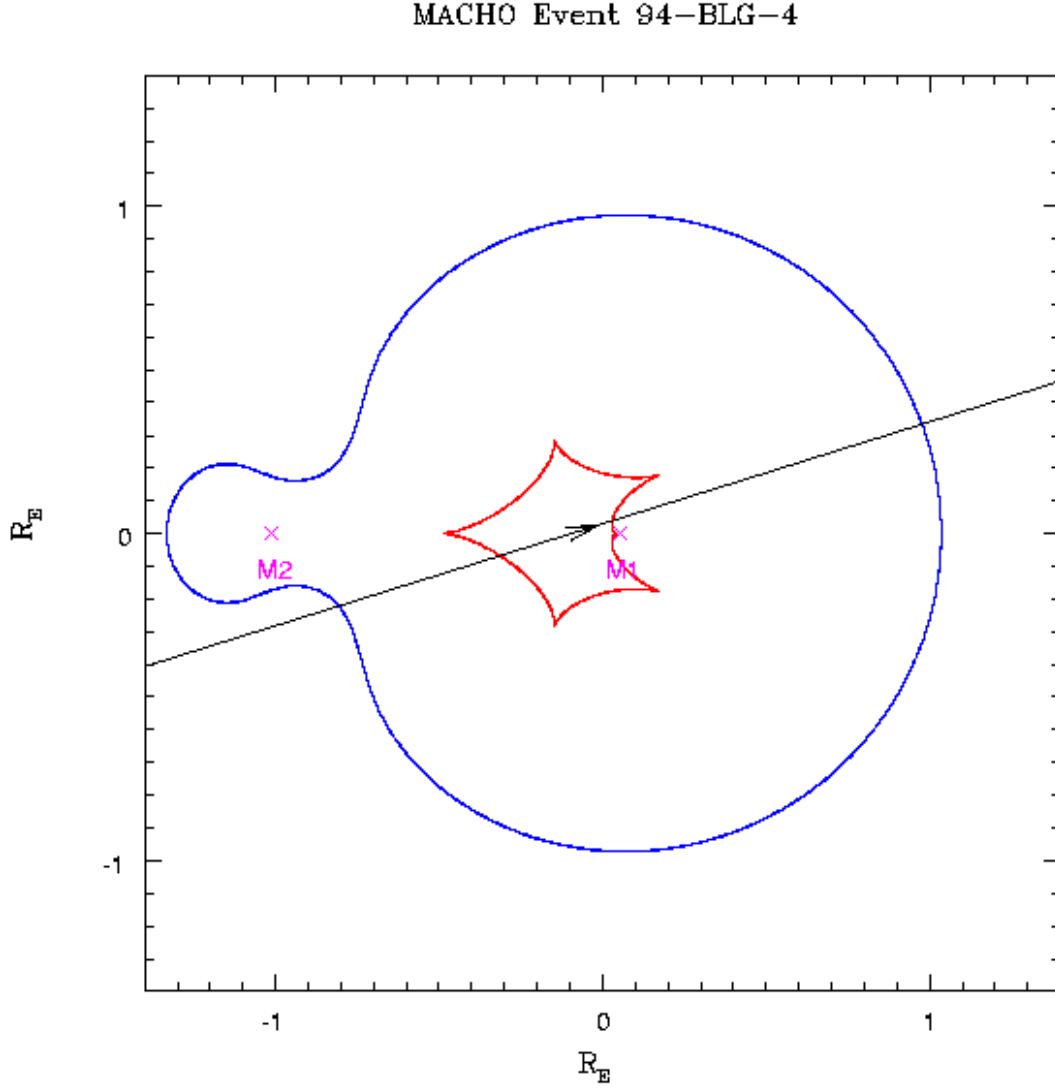


Fig. 15.— Location of the (red) caustic and (blue) critical curves for the 94-BLG-4 binary lens fit presented in Fig. 14. The coordinate system, whose origin is at the center of mass, indicates distance in units of the system’s Einstein Ring radius R_E . Also shown are the locations of the lensing objects, and the trajectory of the source through the caustic structure.

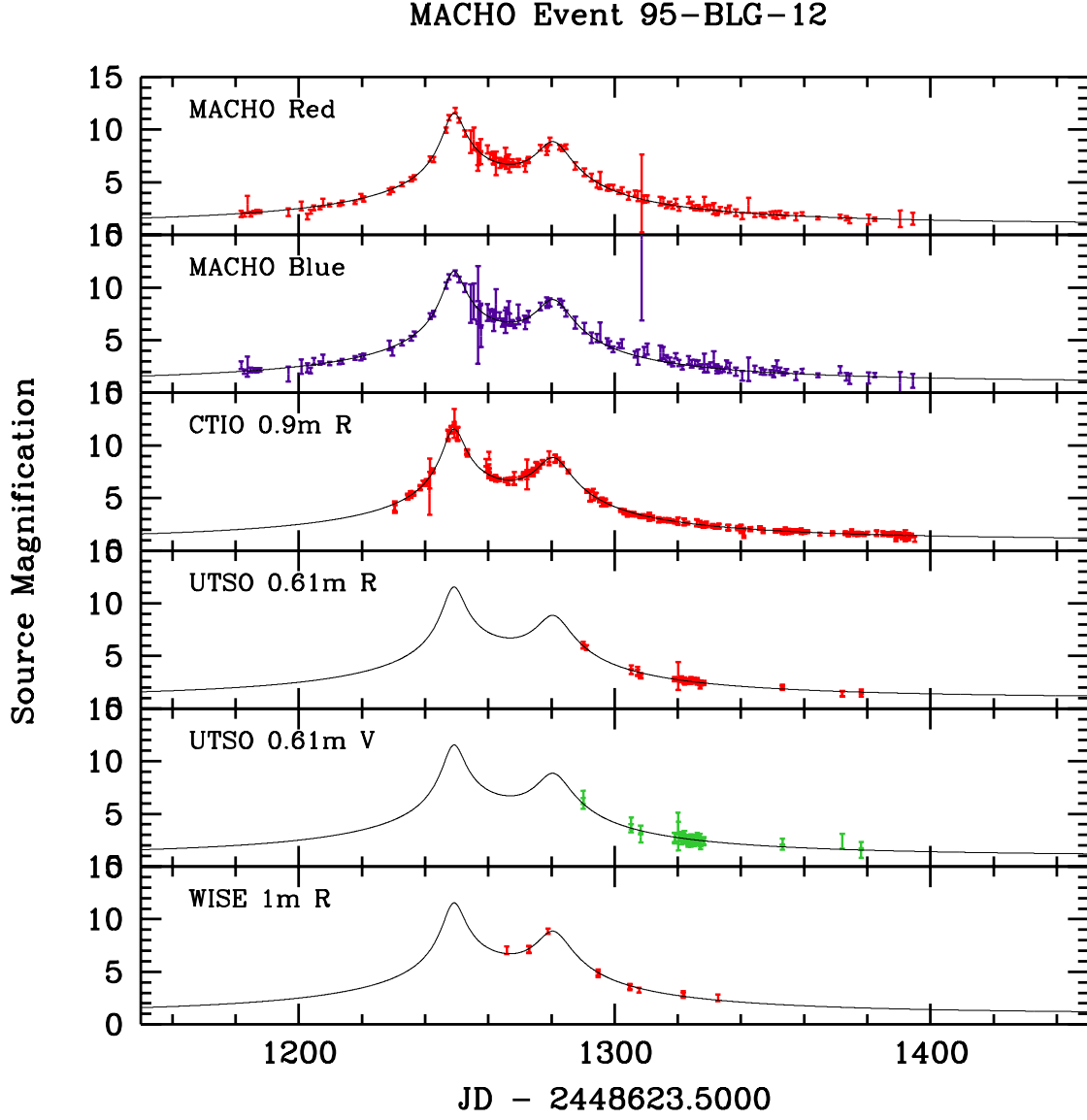


Fig. 16.— Lightcurve of MACHO event 95-BLG-12, including our fit to binary microlensing.

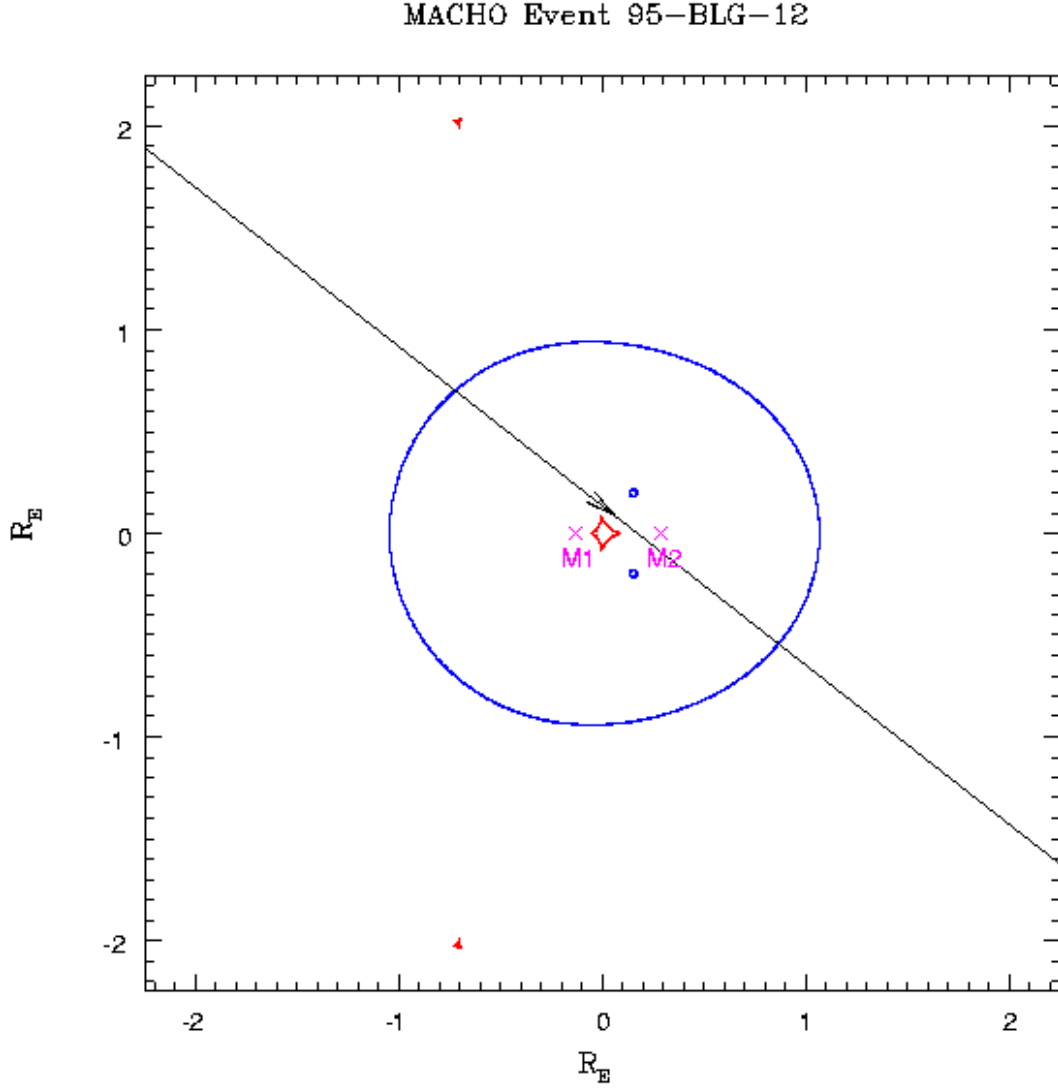


Fig. 17.— Location of the (red) caustic and (blue) critical curves for the 95-BLG-12 binary lens fit presented in Fig. 16. The coordinate system, whose origin is at the center of mass, indicates distance in units of the system’s Einstein Ring radius R_E . Also shown are the locations of the lensing objects, and the trajectory of the source through the caustic structure.

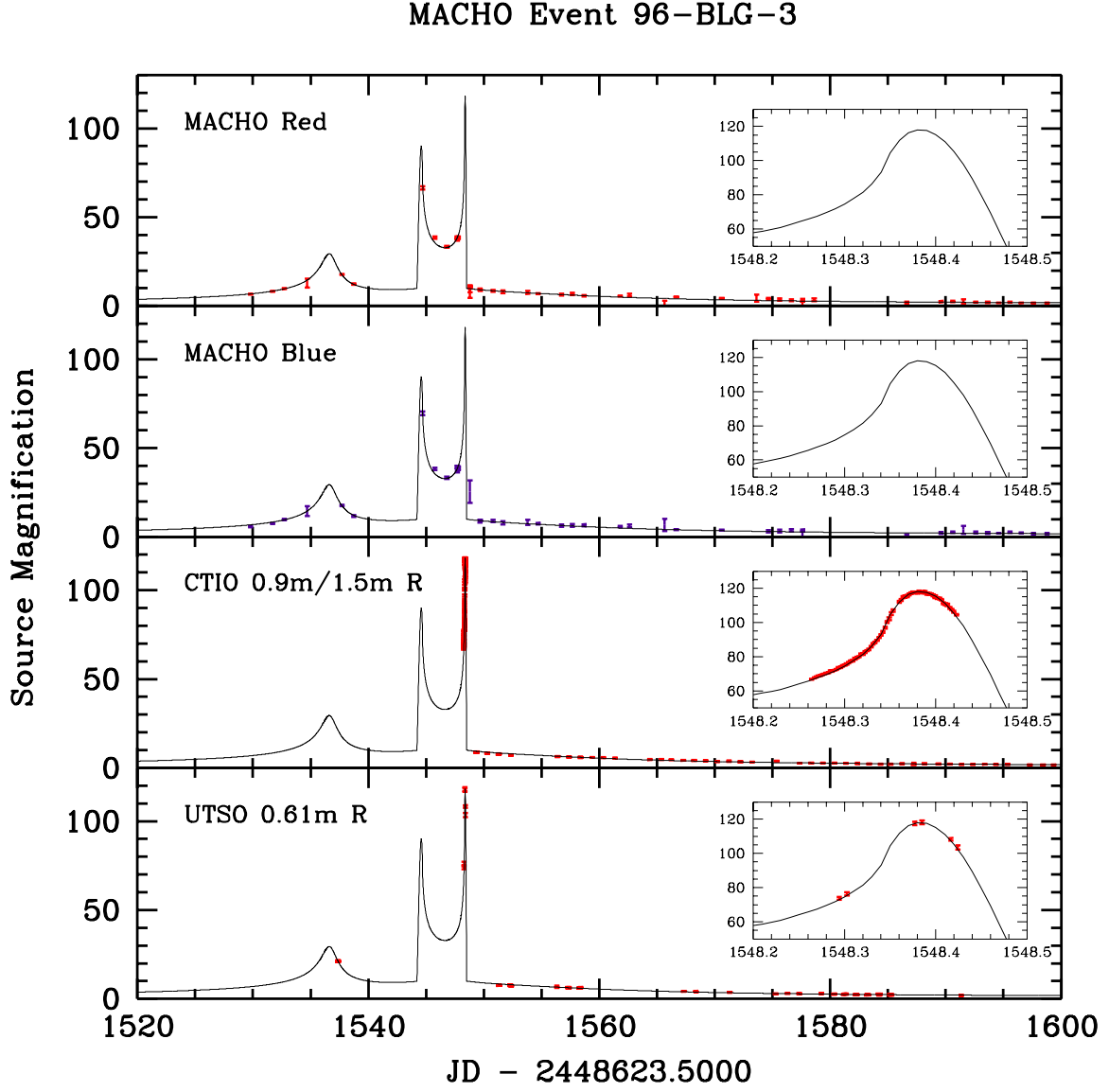


Fig. 18.— Lightcurve of MACHO event 96-BLG-3, including our fit to binary microlensing.

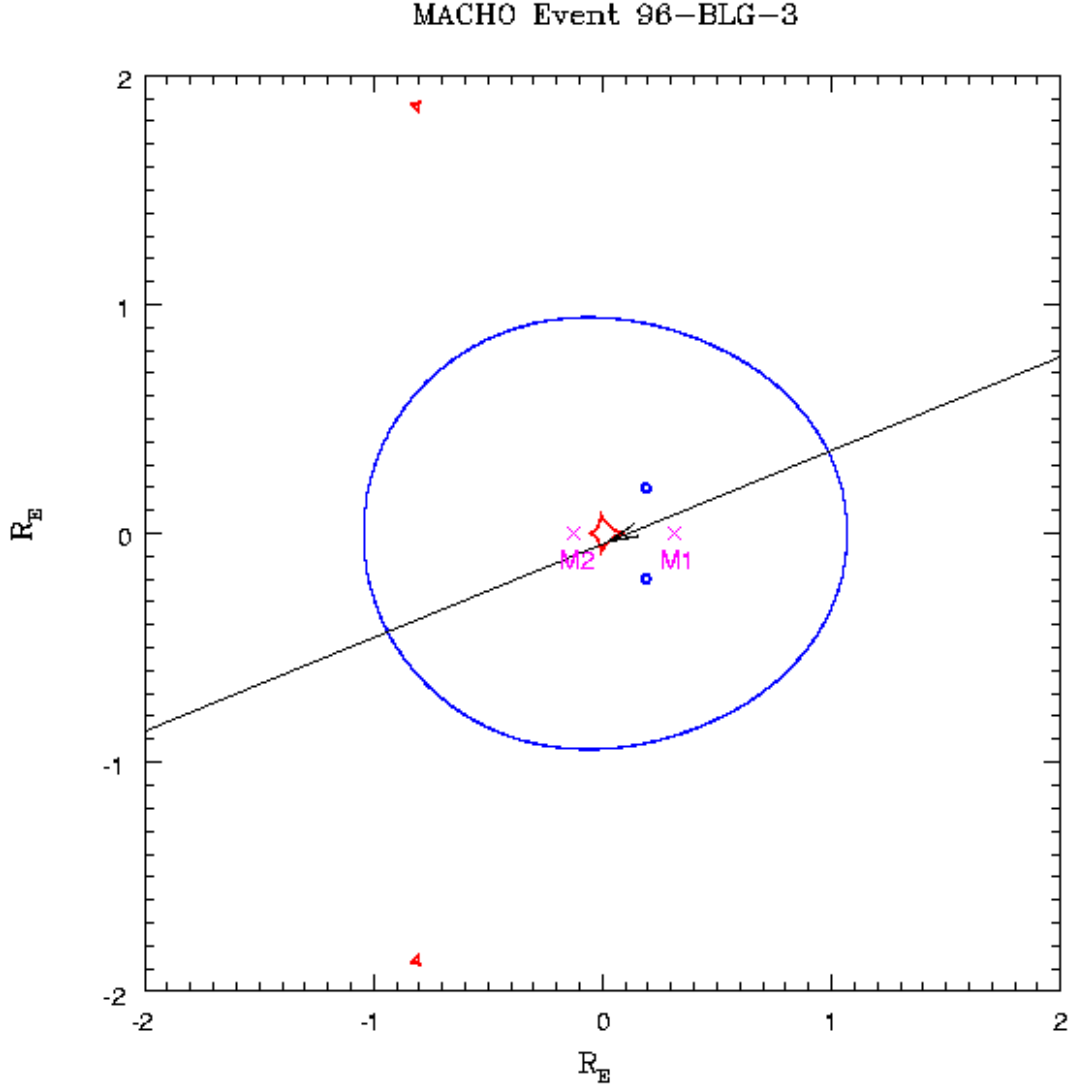


Fig. 19.— Location of the (red) caustic and (blue) critical curves for the 96-BLG-3 binary lens fit presented in Fig. 18. The coordinate system, whose origin is at the center of mass, indicates distance in units of the system’s Einstein Ring radius R_E . Also shown are the locations of the lensing objects, and the trajectory of the source through the caustic structure.

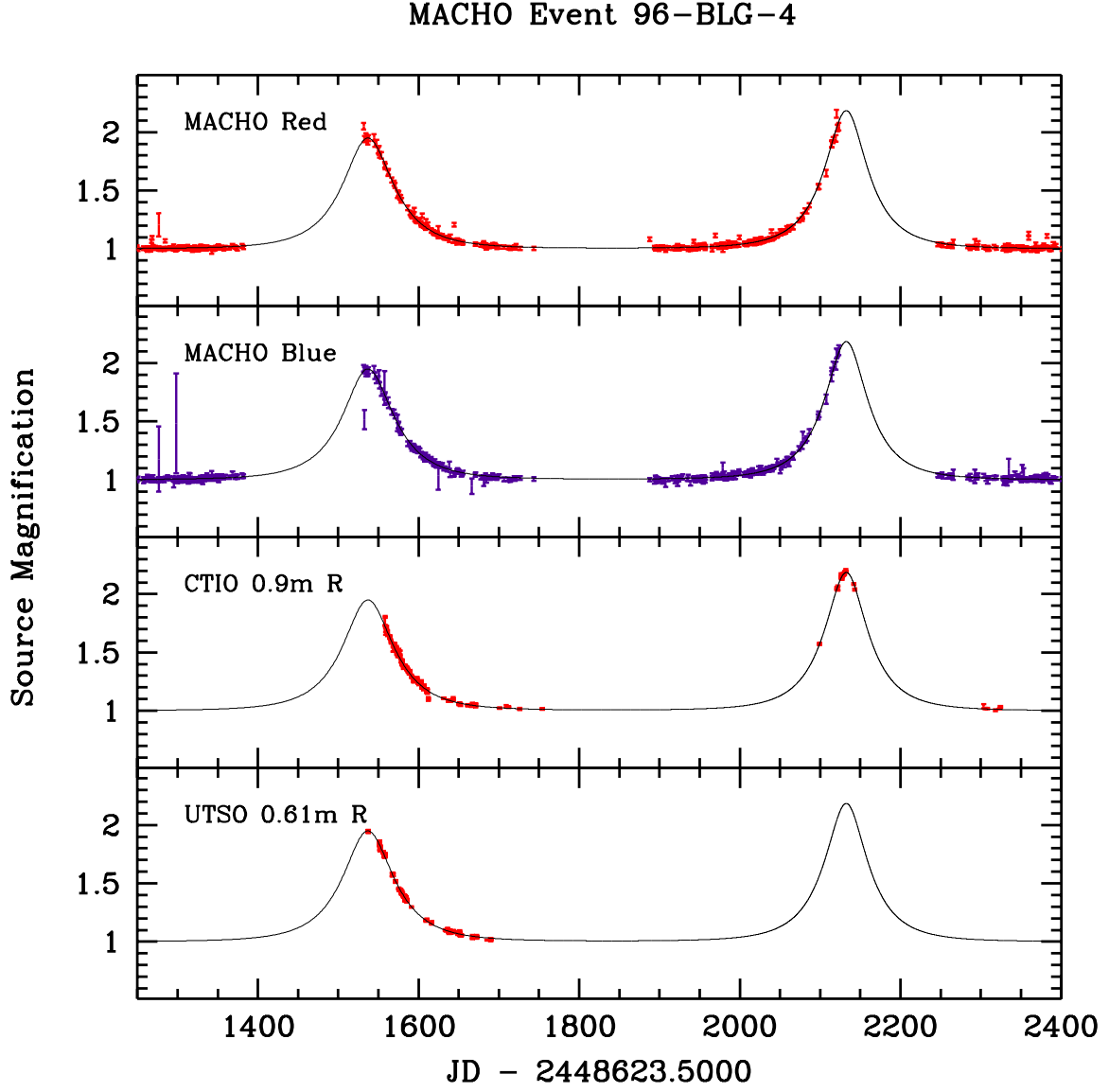


Fig. 20.— Lightcurve of MACHO event 96-BLG-4, including our fit to binary microlensing.

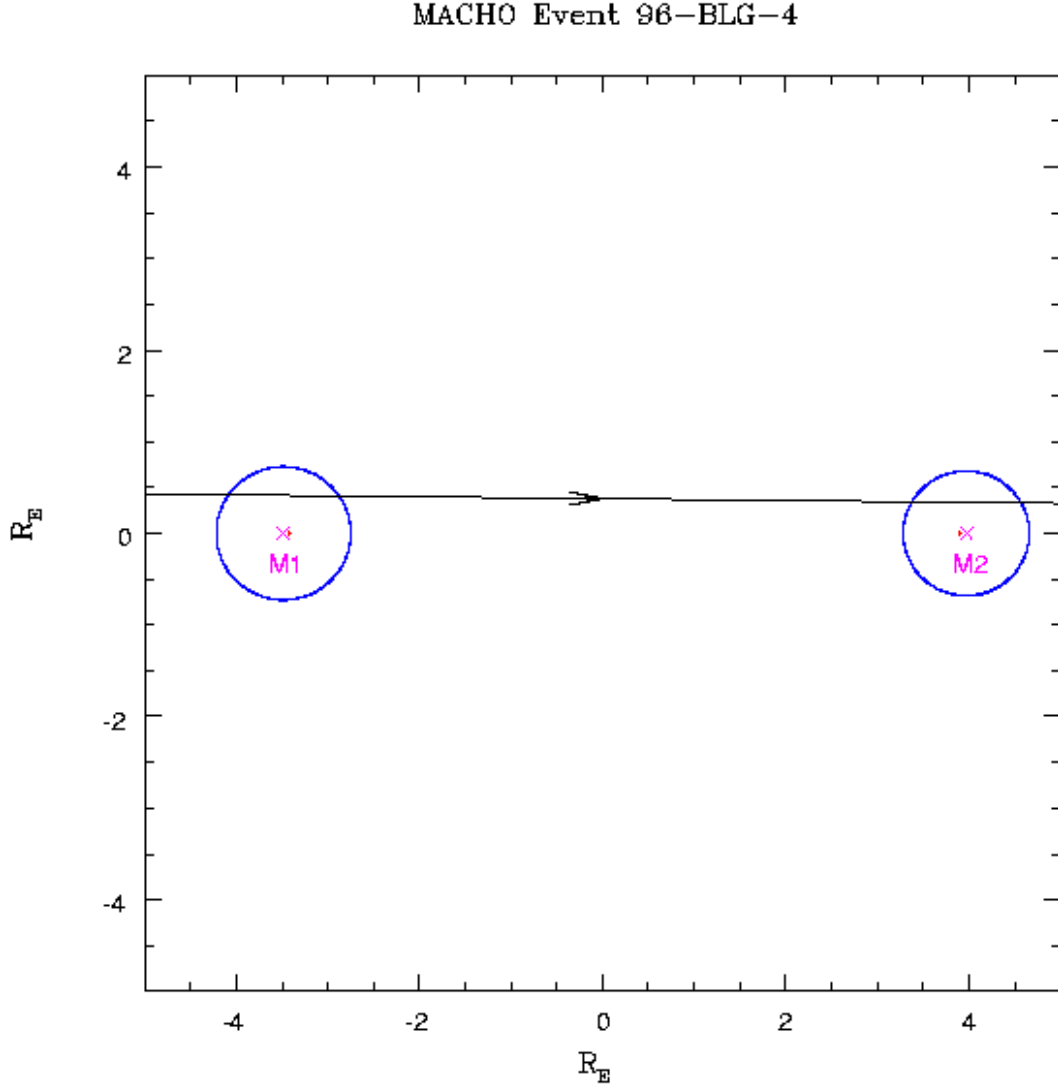


Fig. 21.— Location of the (red) caustic and (blue) critical curves for the 96-BLG-4 binary lens fit presented in Fig. 20. The coordinate system, whose origin is at the center of mass, indicates distance in units of the system’s Einstein Ring radius R_E . Also shown are the locations of the lensing objects, and the trajectory of the source through the caustic structure.

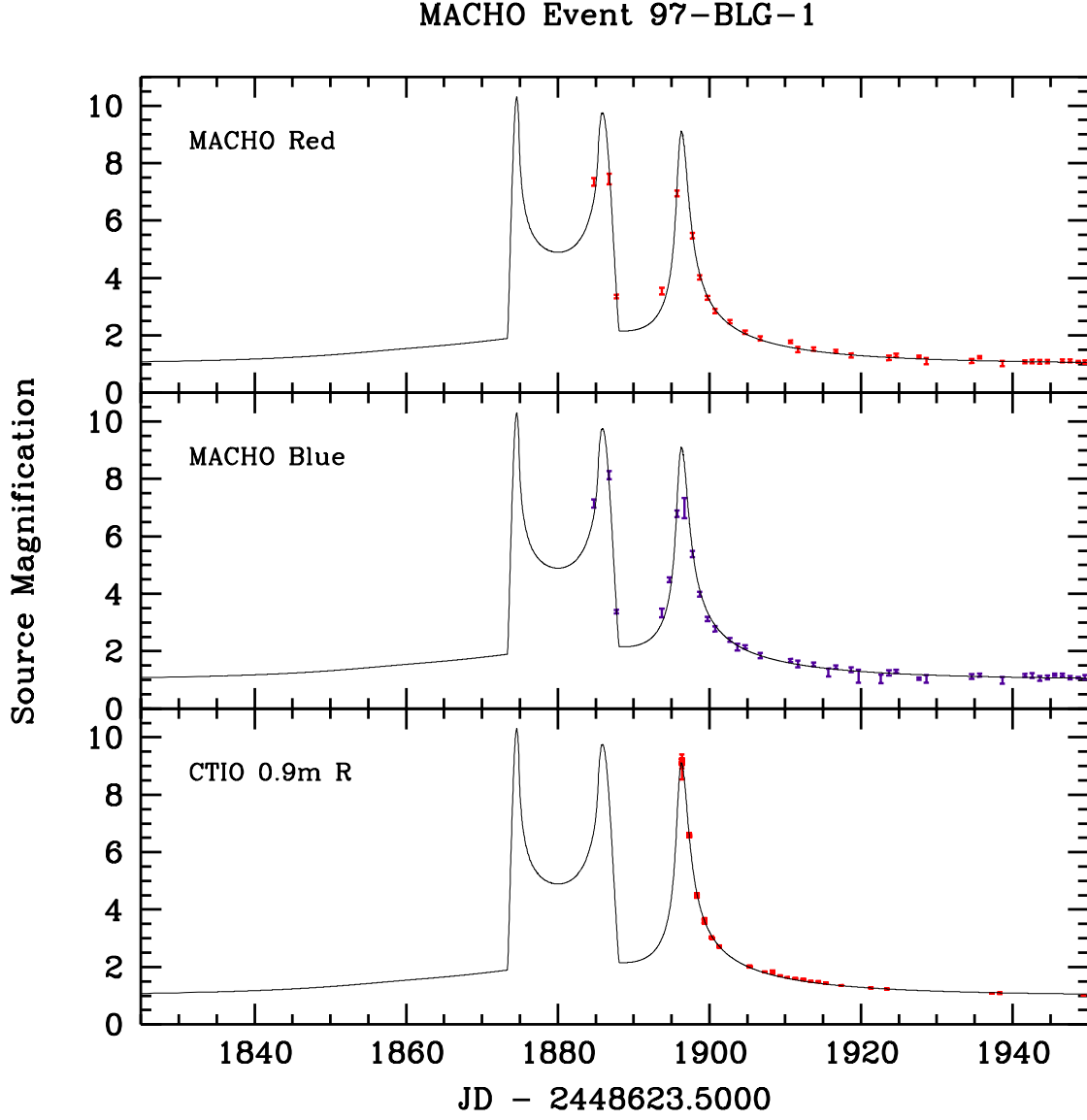


Fig. 22.— Lightcurve of MACHO event 97-BLG-1, including our fit to binary microlensing.

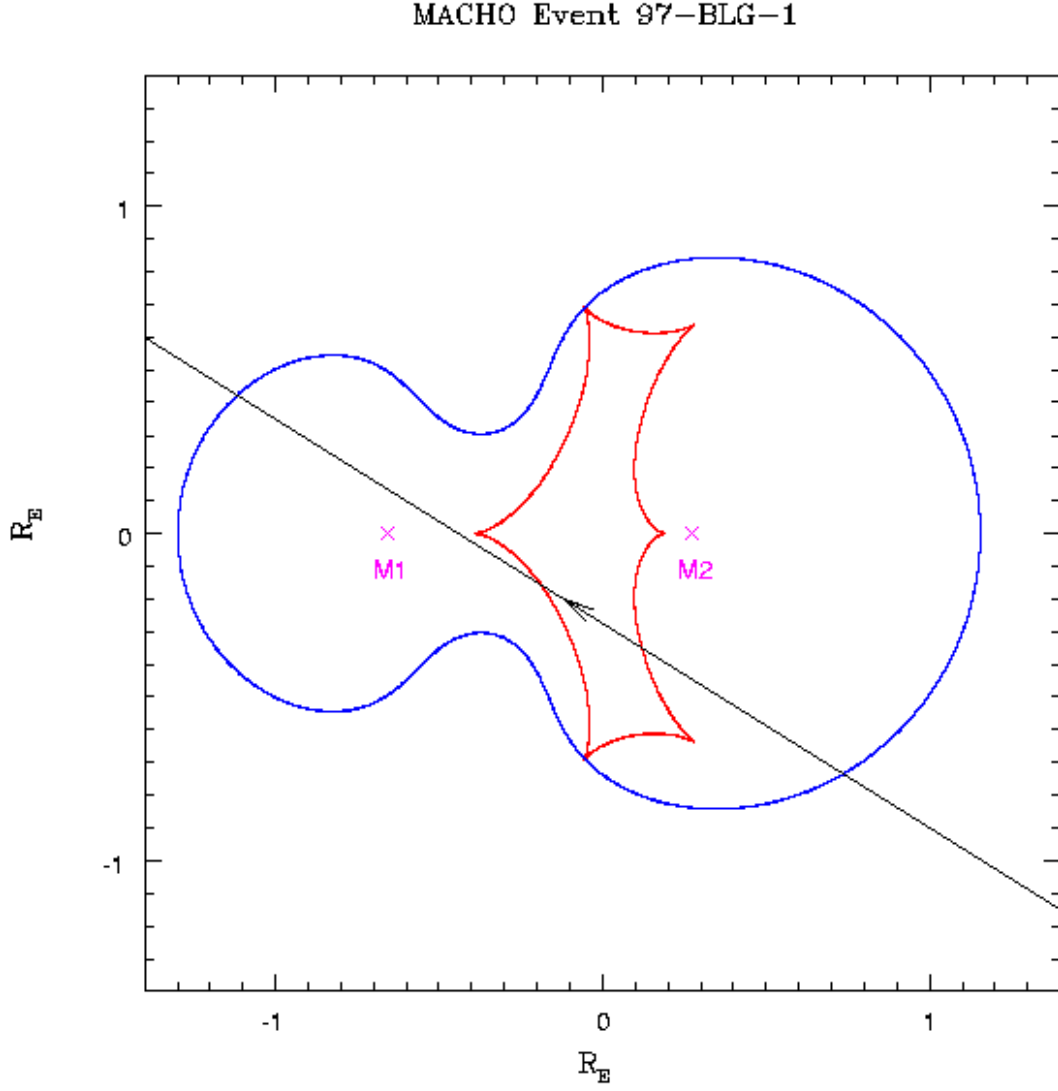


Fig. 23.— Location of the (red) caustic and (blue) critical curves for the 97-BLG-1 binary lens fit presented in Fig. 22. The coordinate system, whose origin is at the center of mass, indicates distance in units of the system’s Einstein Ring radius R_E . Also shown are the locations of the lensing objects, and the trajectory of the source through the caustic structure.

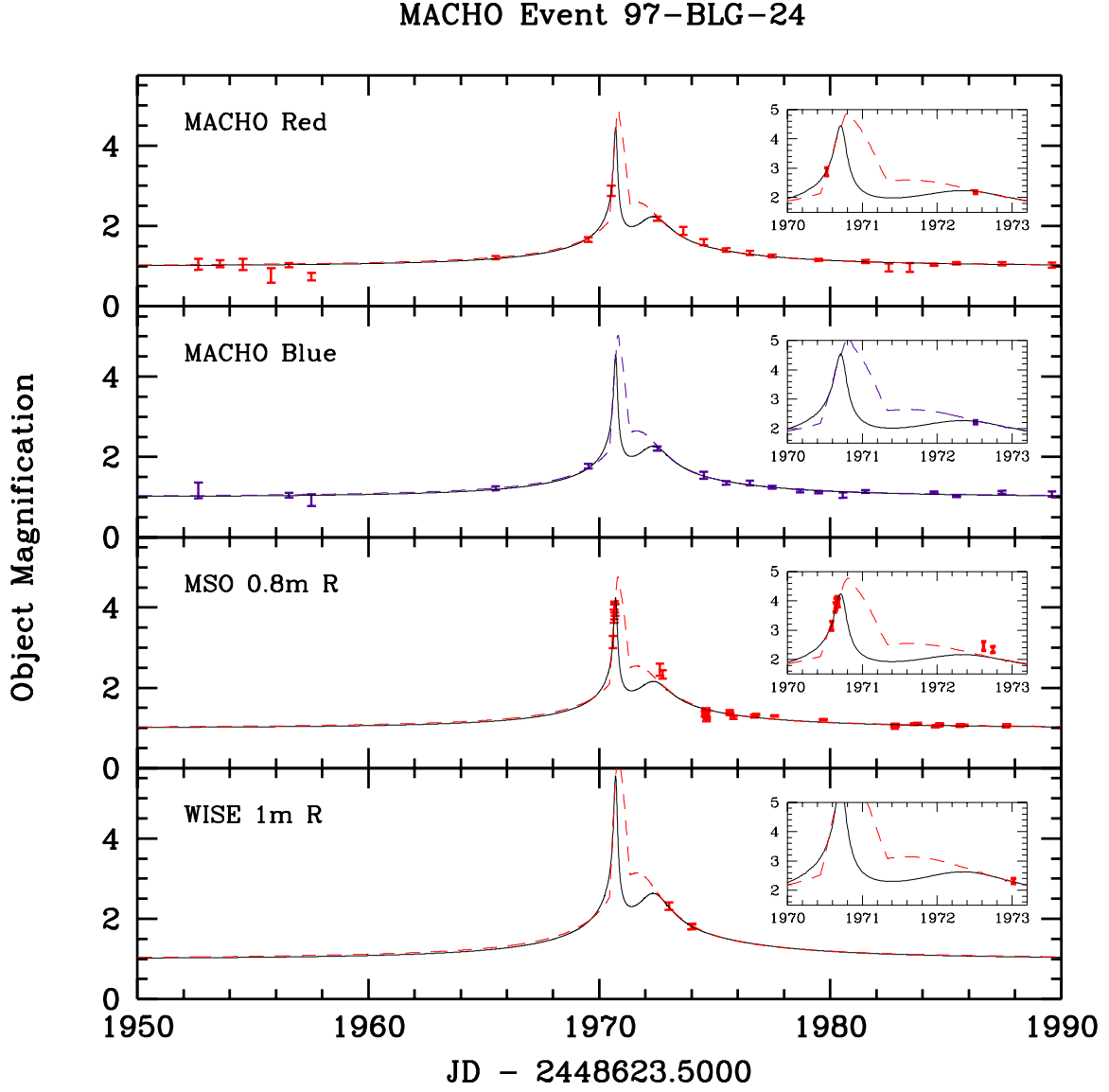


Fig. 24.— Lightcurve of MACHO event 97-BLG-24, including our fits to binary microlensing. Due to the different blending parameters between fits, we plot the observed magnification of the MACHO object, as opposed to the actual lensed source.

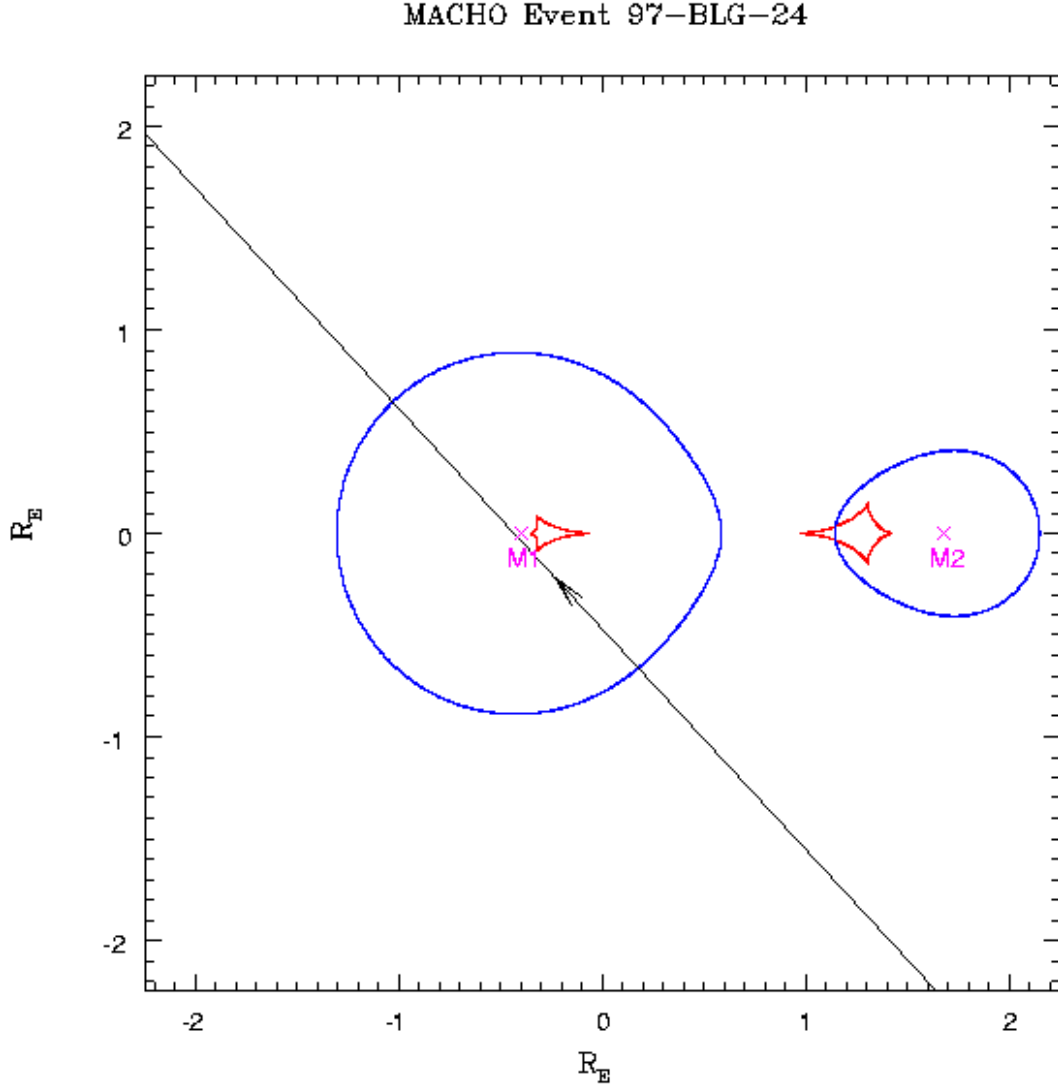


Fig. 25.— Location of the (red) caustic and (blue) critical curves for the 97-BLG-24 standard binary lens fit (—) presented in Fig. 24. The coordinate system, whose origin is at the center of mass, indicates distance in units of the system’s Einstein ring radius R_E . Also shown are the locations of the lensing objects, and the trajectory of the source through the caustic structure.

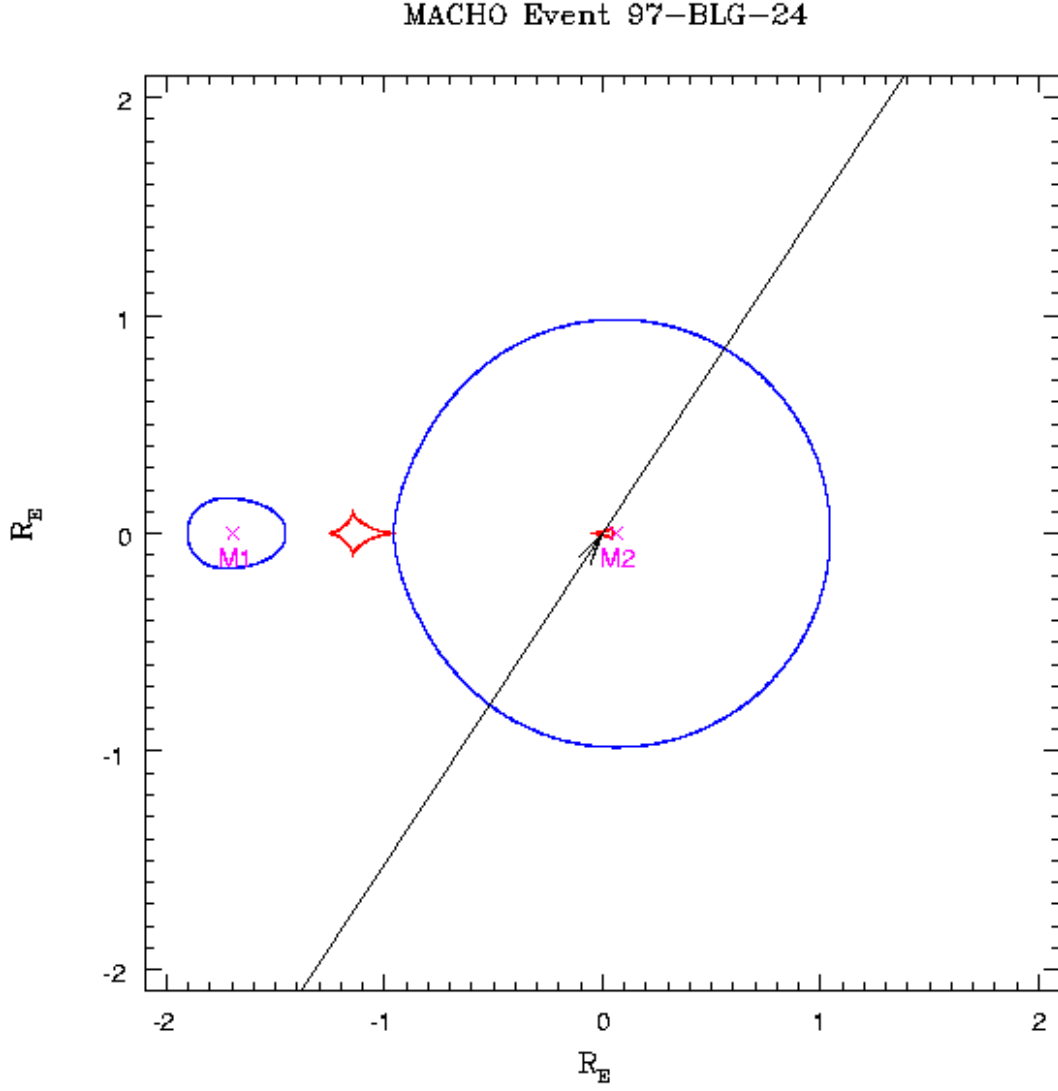


Fig. 26.— Location of the (red) caustic and (blue) critical curves for the 97-BLG-24 ‘planetary’ binary lens fit (– – –) presented in Fig. 24. The coordinate system, whose origin is at the center of mass, indicates distance in units of the system’s Einstein ring radius R_E . Also shown are the locations of the lensing objects, and the trajectory of the source through the caustic structure.

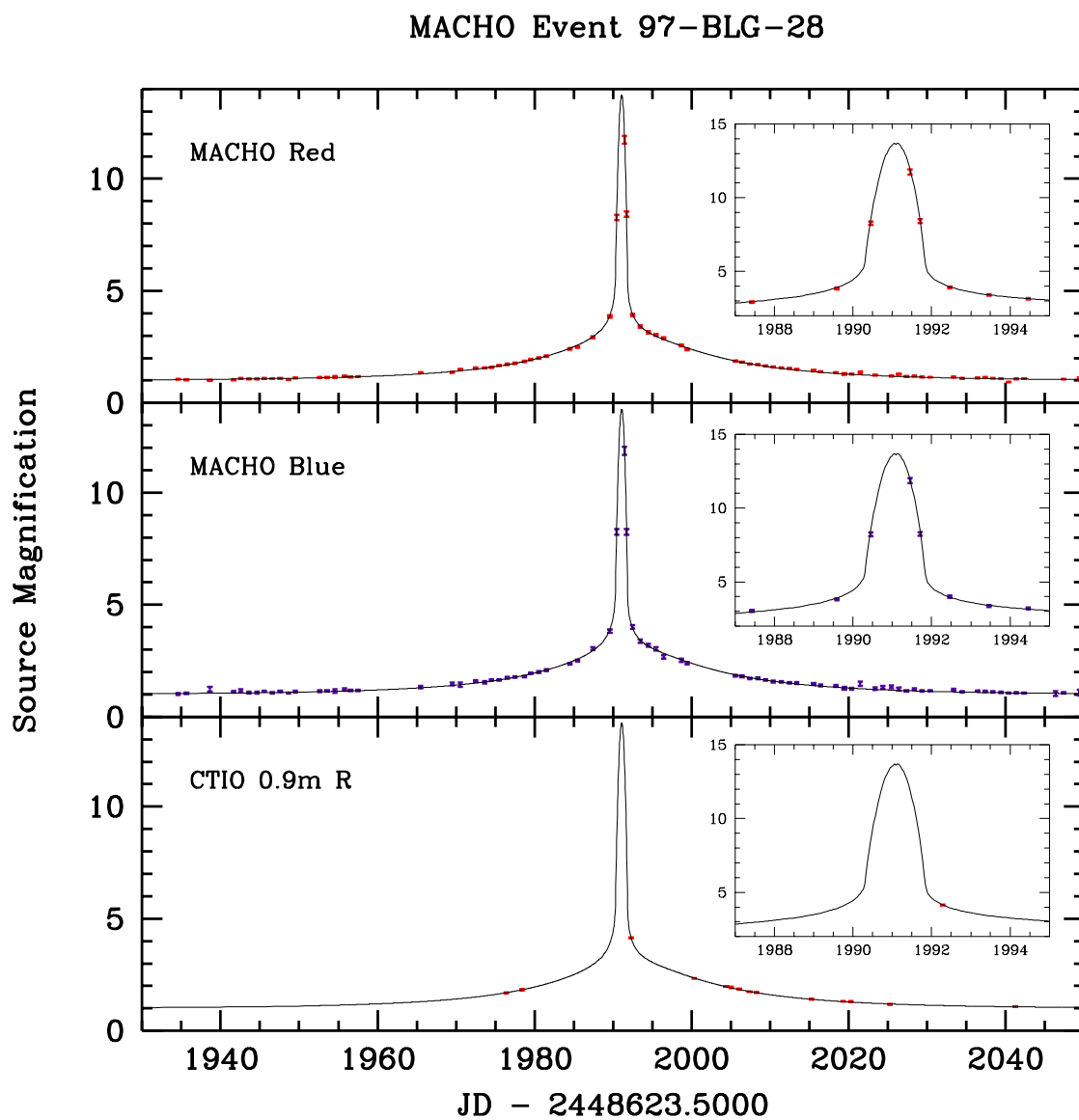


Fig. 27.— Lightcurve of MACHO event 97-BLG-28, including our fit to binary microlensing.

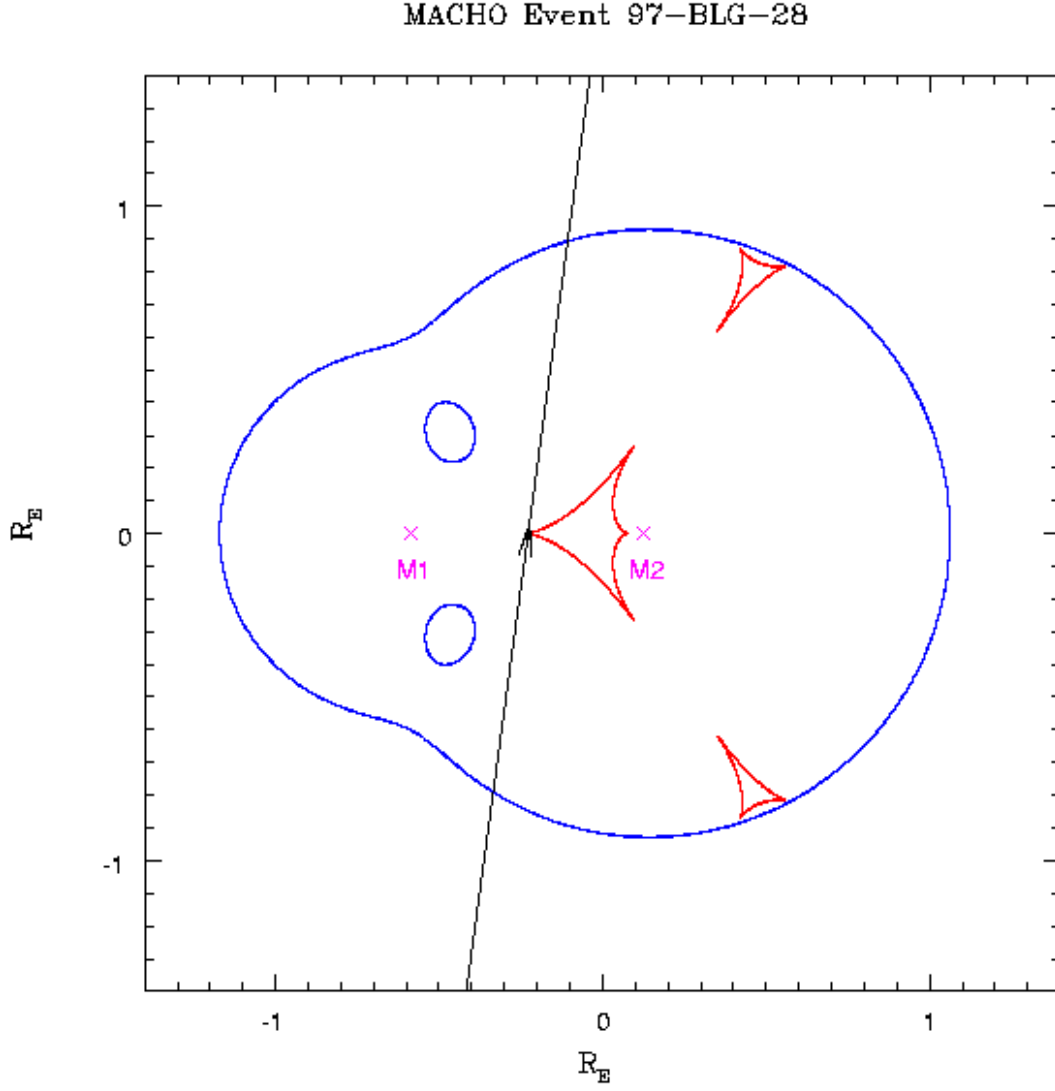


Fig. 28.— Location of the (red) caustic and (blue) critical curves for the 97-BLG-28 binary lens fit presented in Fig. 27. The coordinate system, whose origin is at the center of mass, indicates distance in units of the system’s Einstein Ring radius R_E . Also shown are the locations of the lensing objects, and the trajectory of the source through the caustic structure.

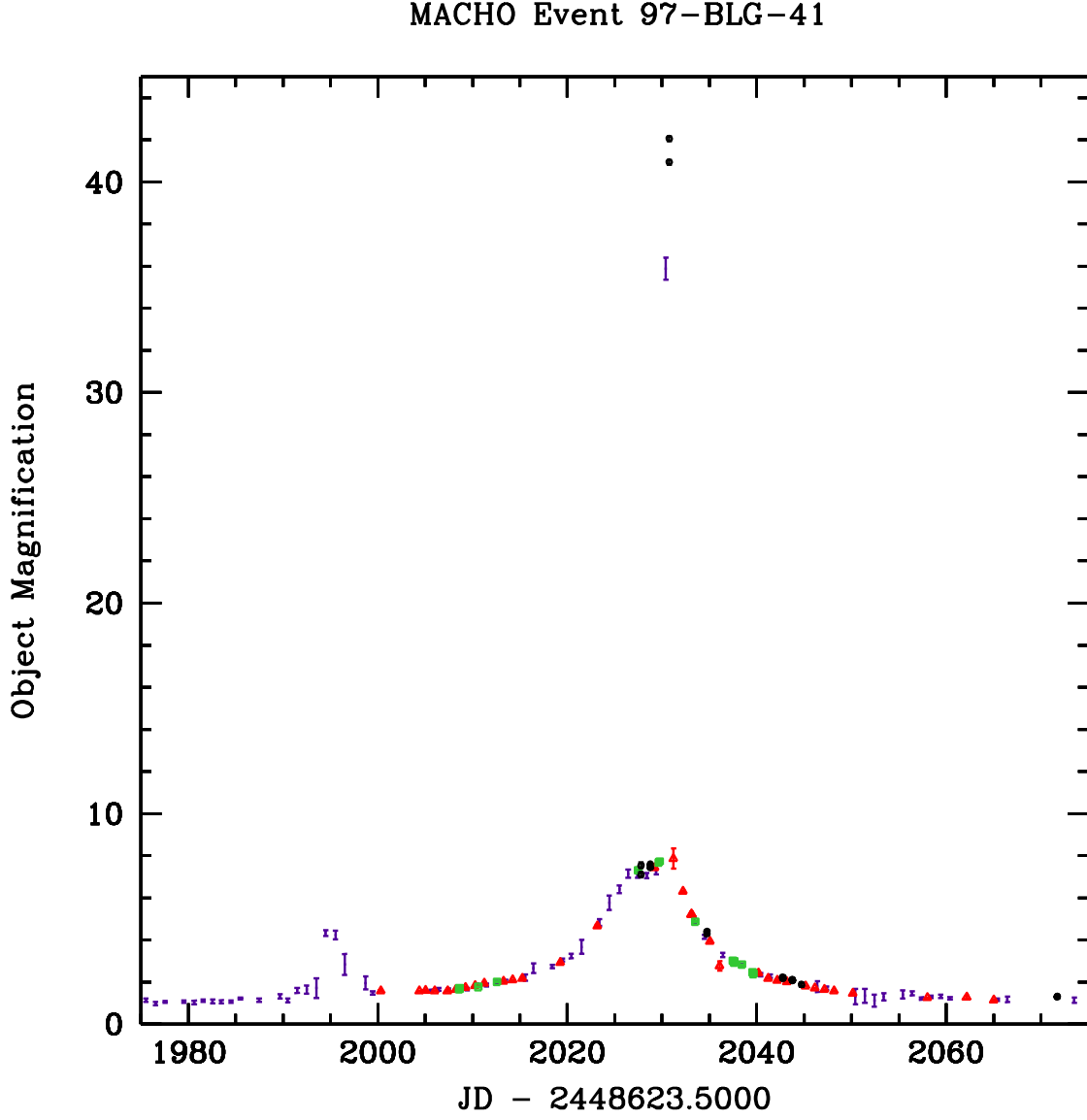


Fig. 29.— Lightcurve of MACHO event 97-BLG-41, with an approximate baseline determined from a fit to the second peak, disregarding the caustic features. Plotted are the MACHO-B (blue points), CTIO-r (red triangles), MSO30-r (green squares) and WISE-r (black circles) data.

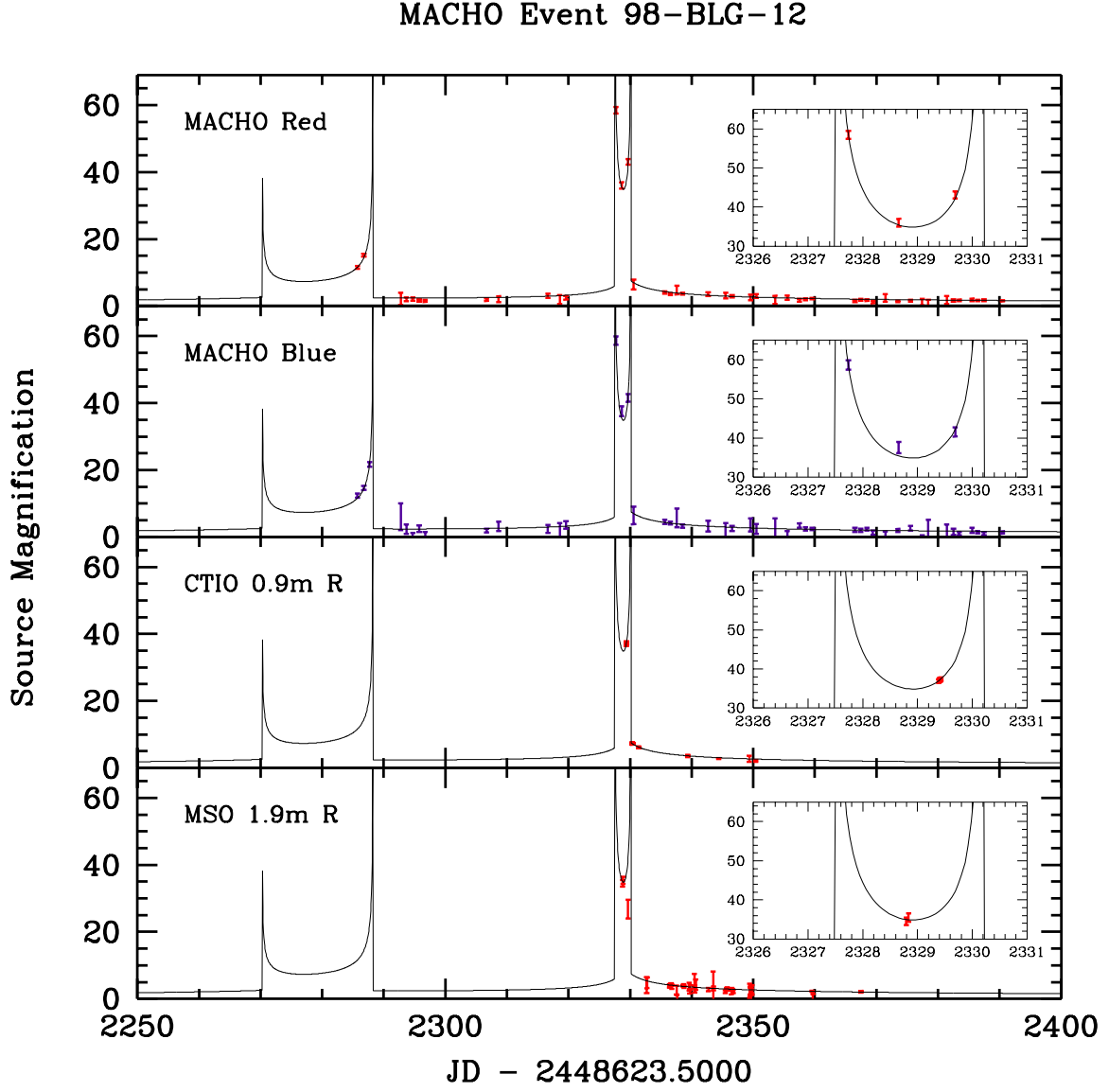


Fig. 30.— Lightcurve of MACHO event 98-BLG-12, including our fit to binary microlensing.

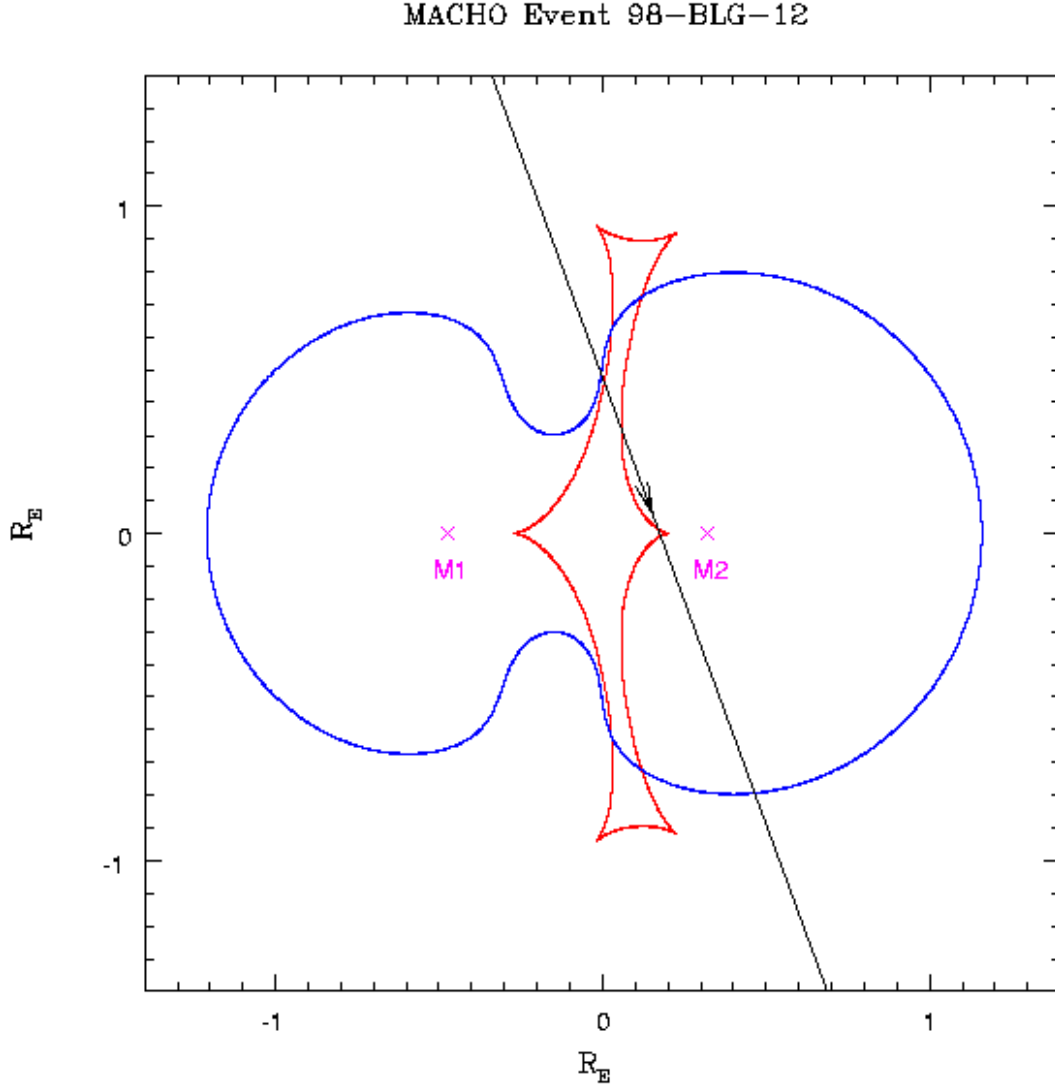


Fig. 31.— Location of the (red) caustic and (blue) critical curves for the 98-BLG-12 binary lens fit presented in Fig. 30. The coordinate system, whose origin is at the center of mass, indicates distance in units of the system’s Einstein Ring radius R_E . Also shown are the locations of the lensing objects, and the trajectory of the source through the caustic structure.

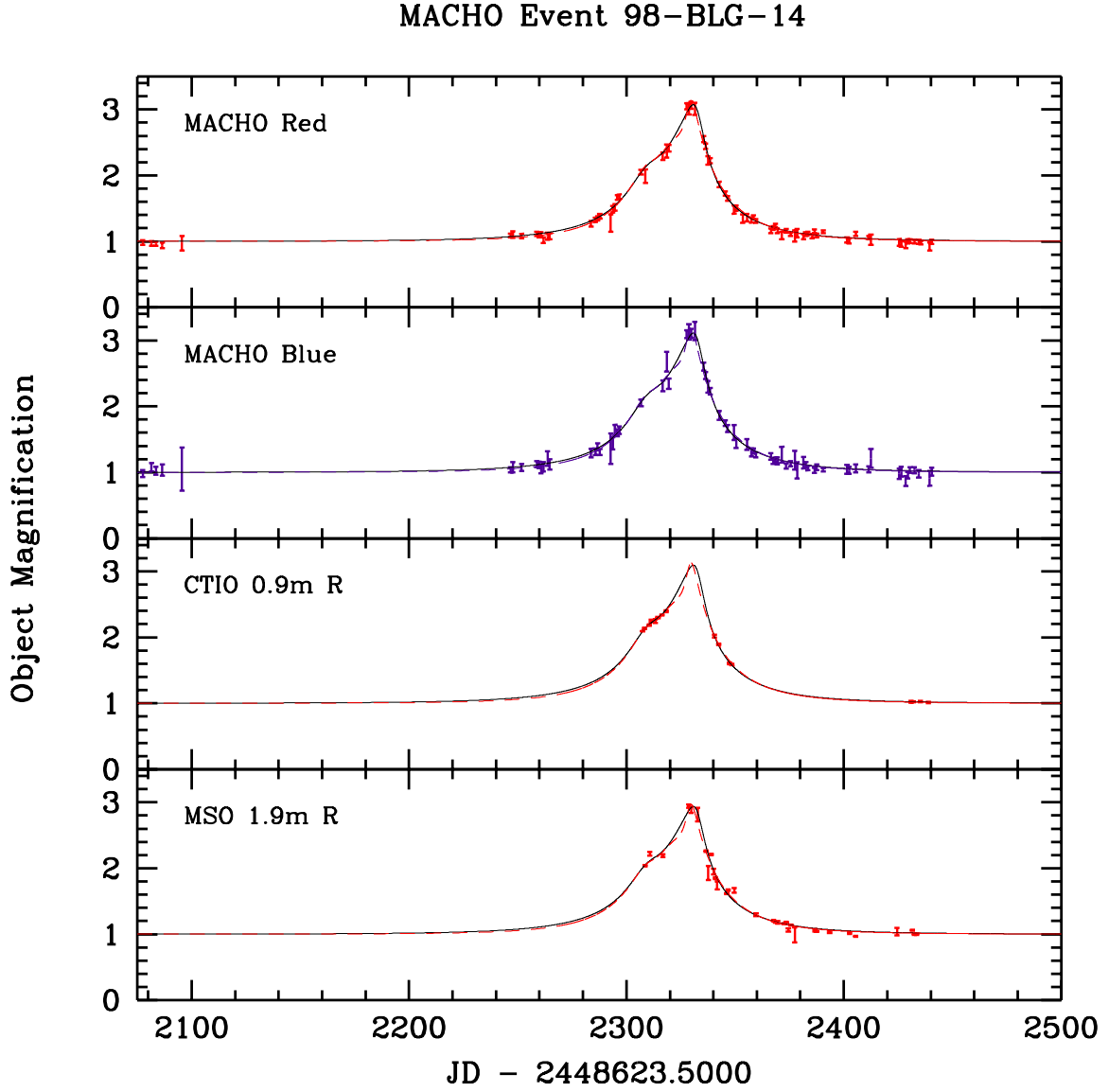


Fig. 32.— Lightcurve of MACHO event 98-BLG-14, including our fits to binary microlensing. Due to the different blending parameters between fits, we plot the observed magnification of the MACHO object, as opposed to the actual lensed source. The MSO74 data have been averaged into 1 day bins.

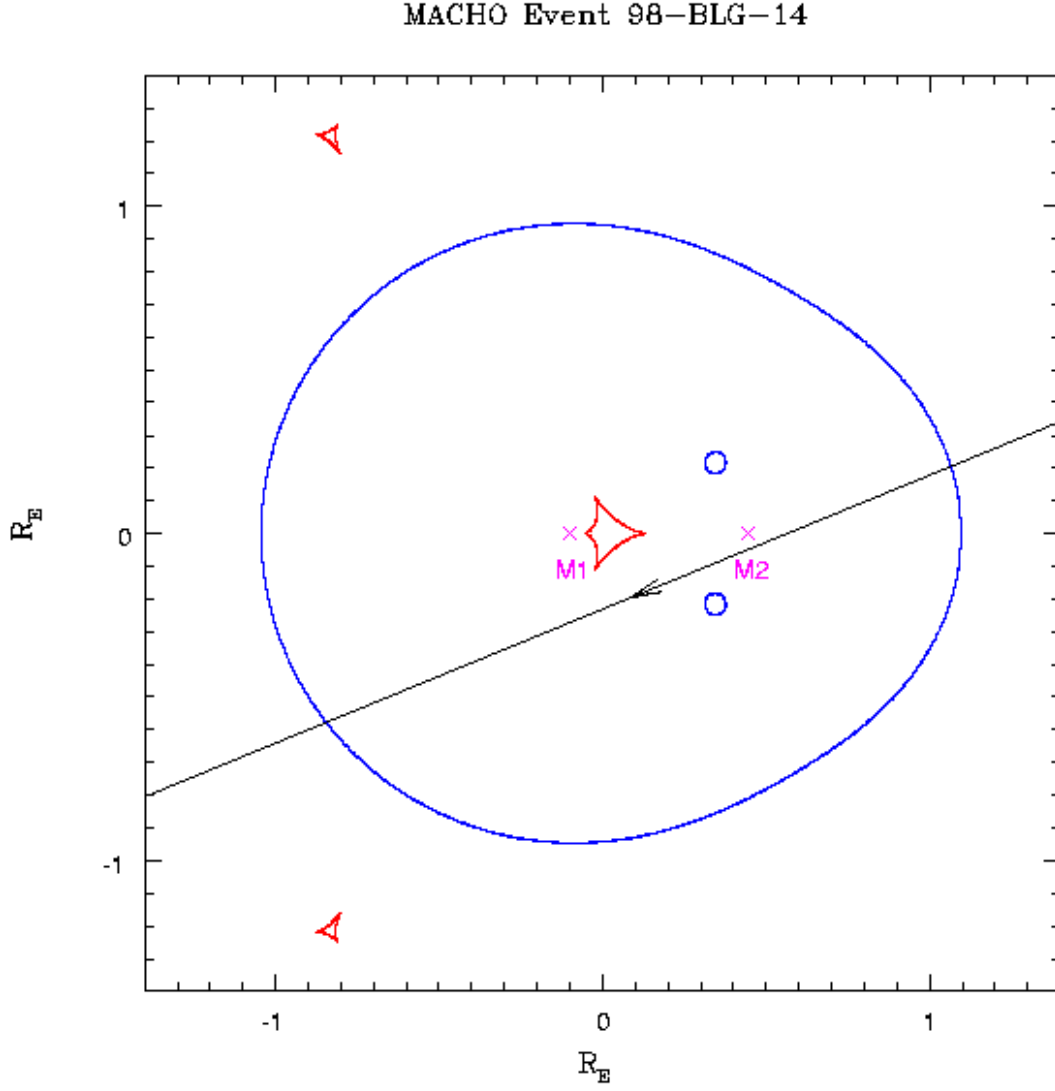


Fig. 33.— Location of the (red) caustic and (blue) critical curves for the solid 98-BLG-14 binary lens fit (—) presented in Fig. 32. The coordinate system, whose origin is at the center of mass, indicates distance in units of the system’s Einstein Ring radius R_E . Also shown are the locations of the lensing objects, and the trajectory of the source through the caustic structure.

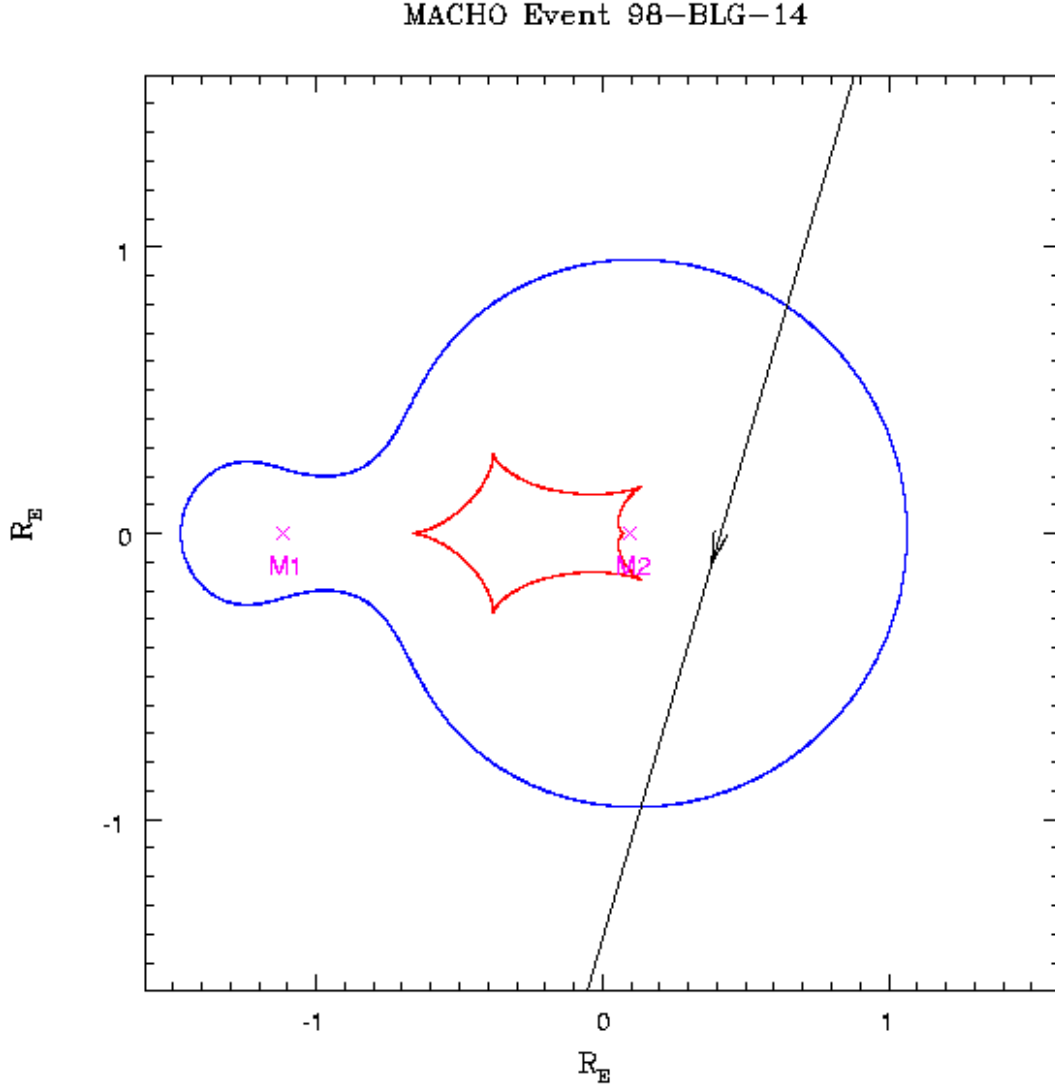


Fig. 34.— Location of the (red) caustic and (blue) critical curves for the dashed (large mass ratio) 98-BLG-14 binary lens fit (---) presented in Fig. 32. The coordinate system, whose origin is at the center of mass, indicates distance in units of the system’s Einstein Ring radius R_E . Also shown are the locations of the lensing objects, and the trajectory of the source through the caustic structure.

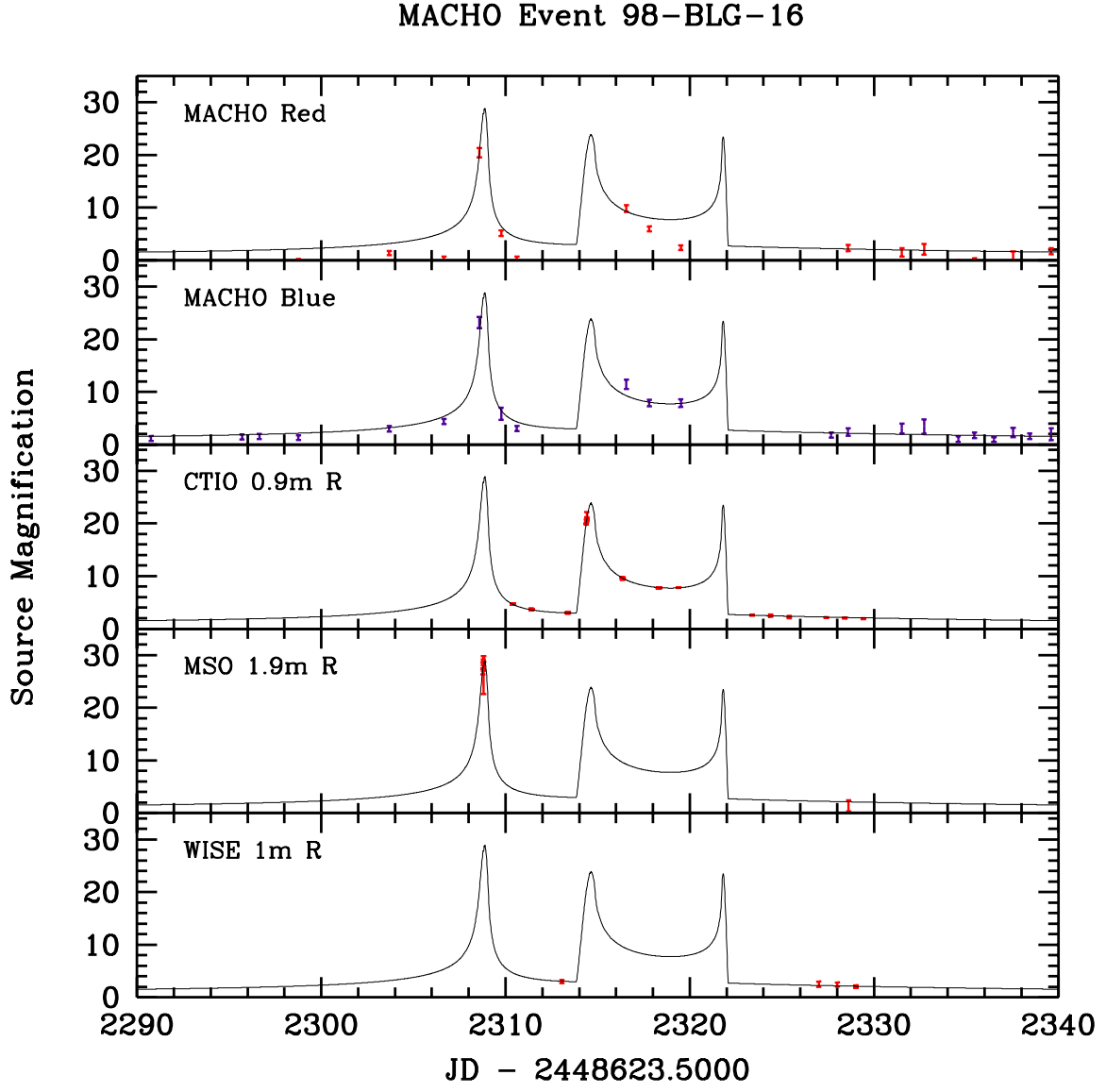


Fig. 35.— Lightcurve of MACHO event 98-BLG-16, including our fit to binary microlensing. The MACHO Red data exhibit excessive scatter due to a defective amplifier.

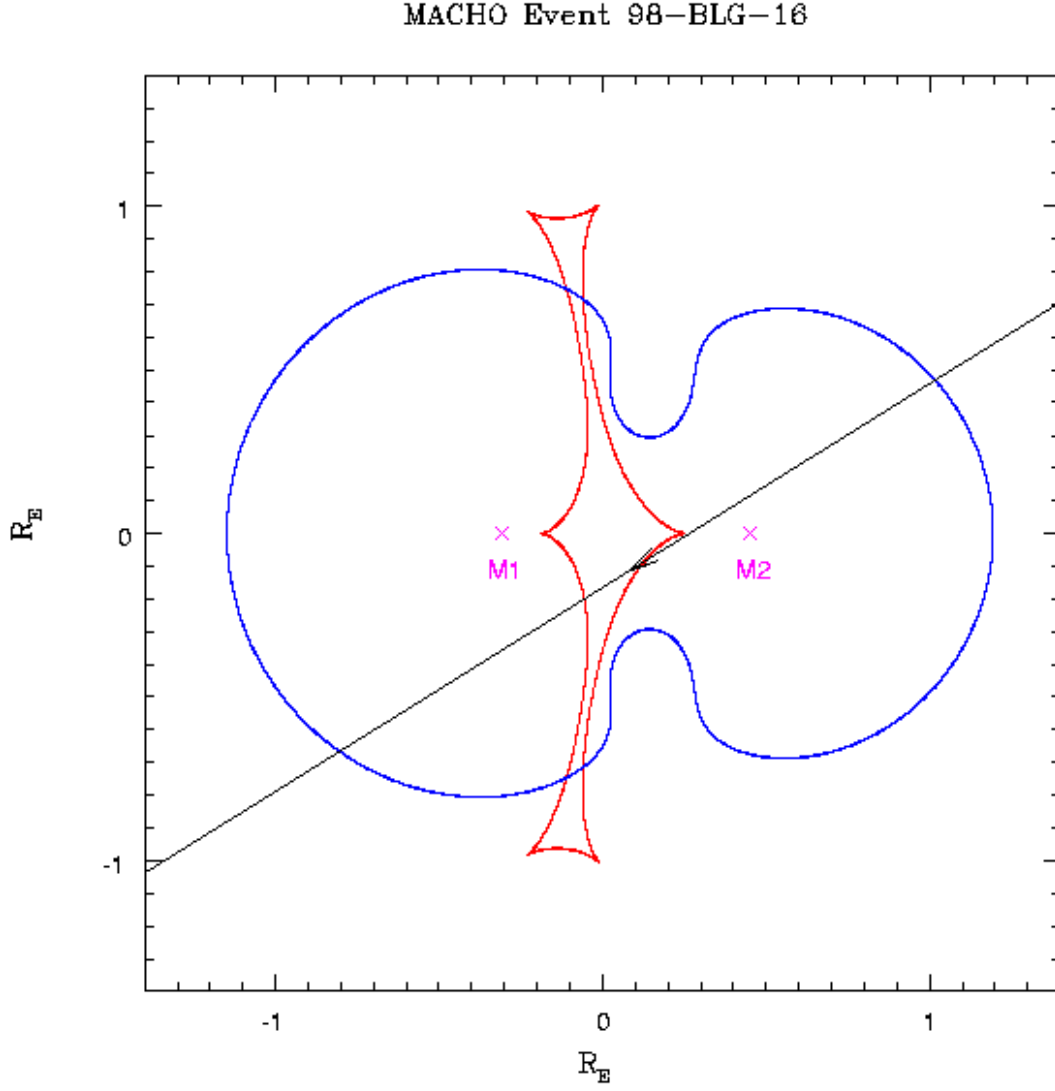


Fig. 36.— Location of the (red) caustic and (blue) critical curves for the 98-BLG-16 binary lens fit presented in Fig. 35. The coordinate system, whose origin is at the center of mass, indicates distance in units of the system’s Einstein Ring radius R_E . Also shown are the locations of the lensing objects, and the trajectory of the source through the caustic structure.

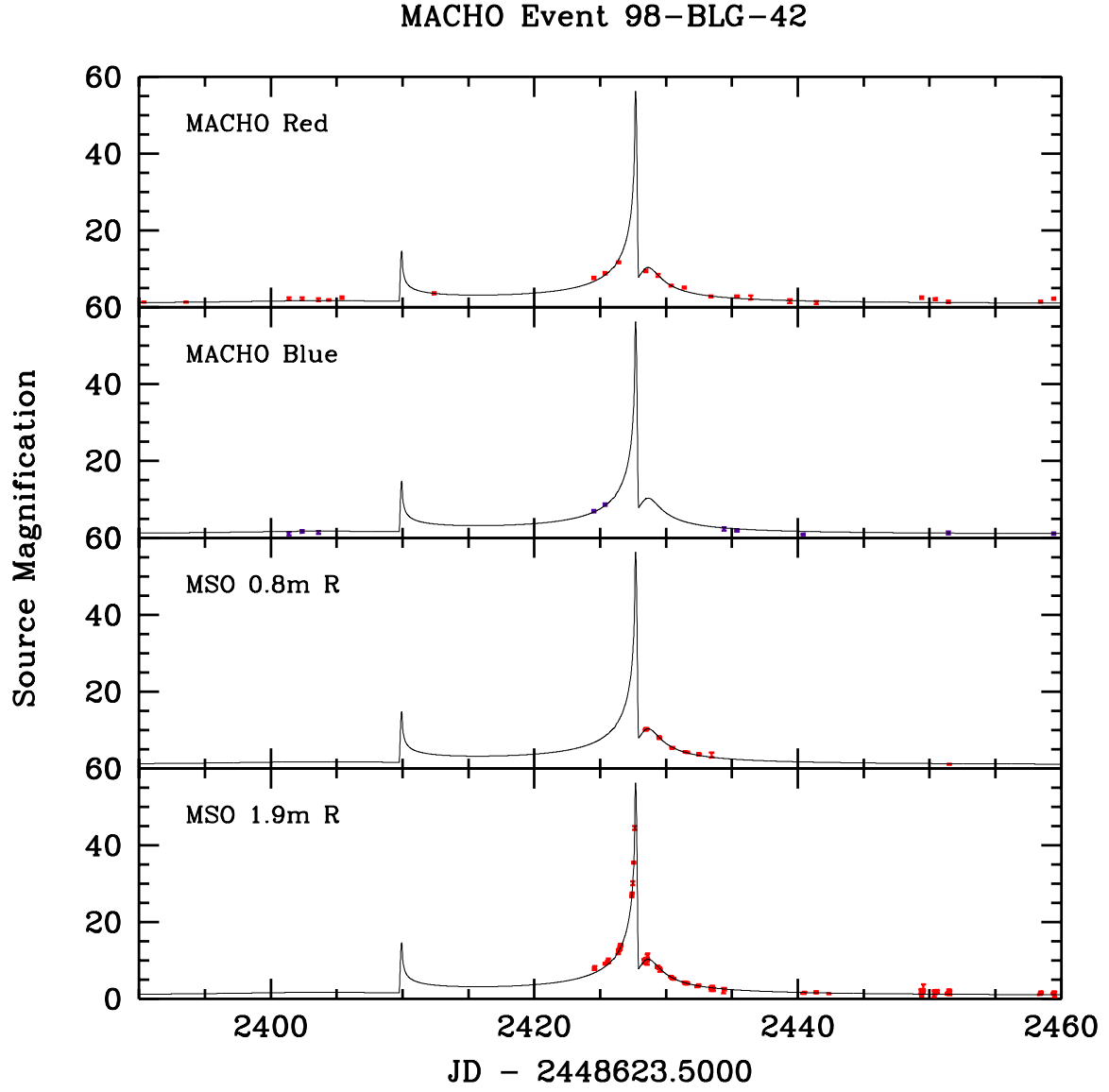


Fig. 37.— Lightcurve of MACHO event 98-BLG-42, including our fit to binary microlensing.

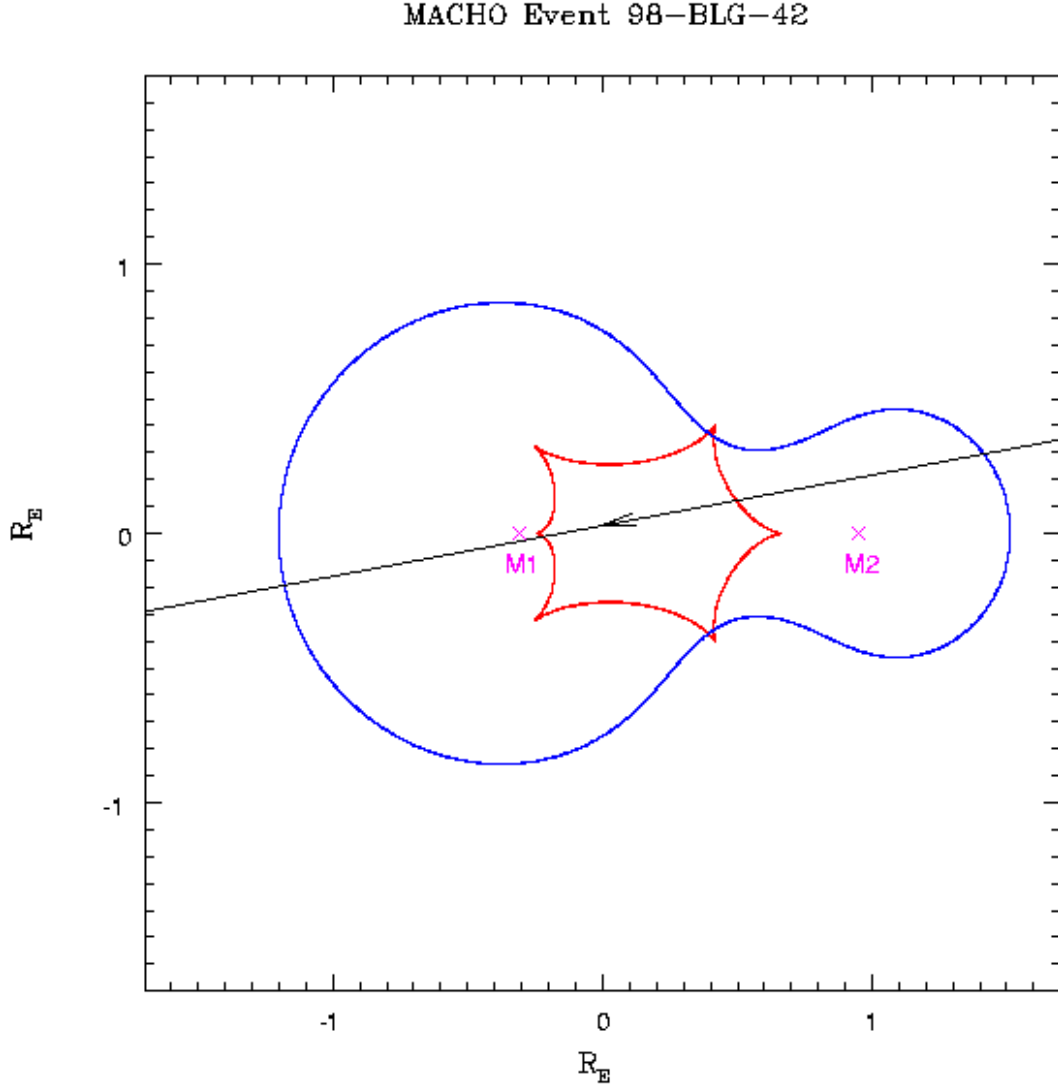


Fig. 38.— Location of the (red) caustic and (blue) critical curves for the 98-BLG-42 binary lens fit presented in Fig. 37. The coordinate system, whose origin is at the center of mass, indicates distance in units of the system’s Einstein Ring radius R_E . Also shown are the locations of the lensing objects, and the trajectory of the source through the caustic structure.

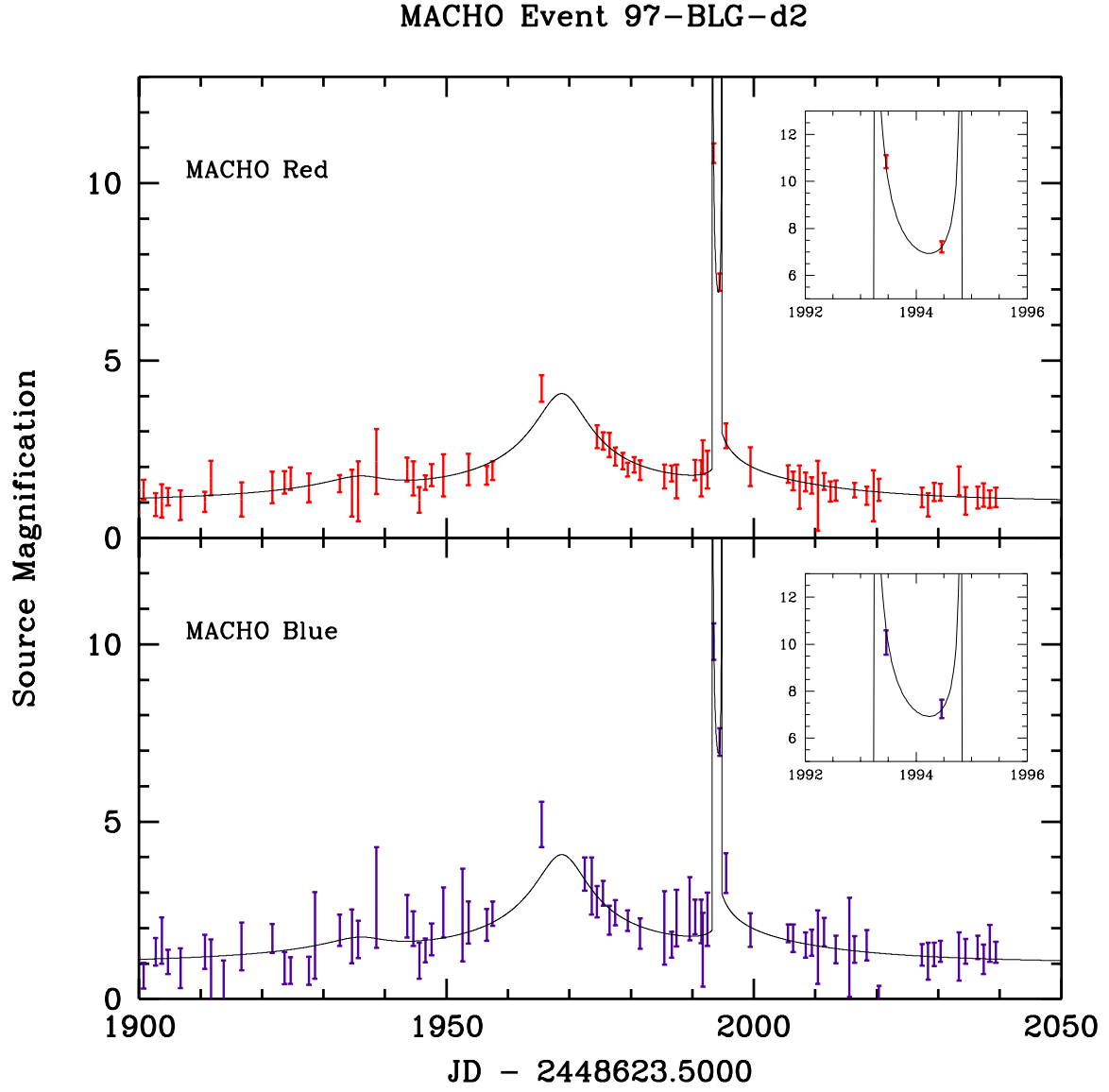


Fig. 39.— Lightcurve of MACHO event 97-BLG-d2, including our fit to binary microlensing.

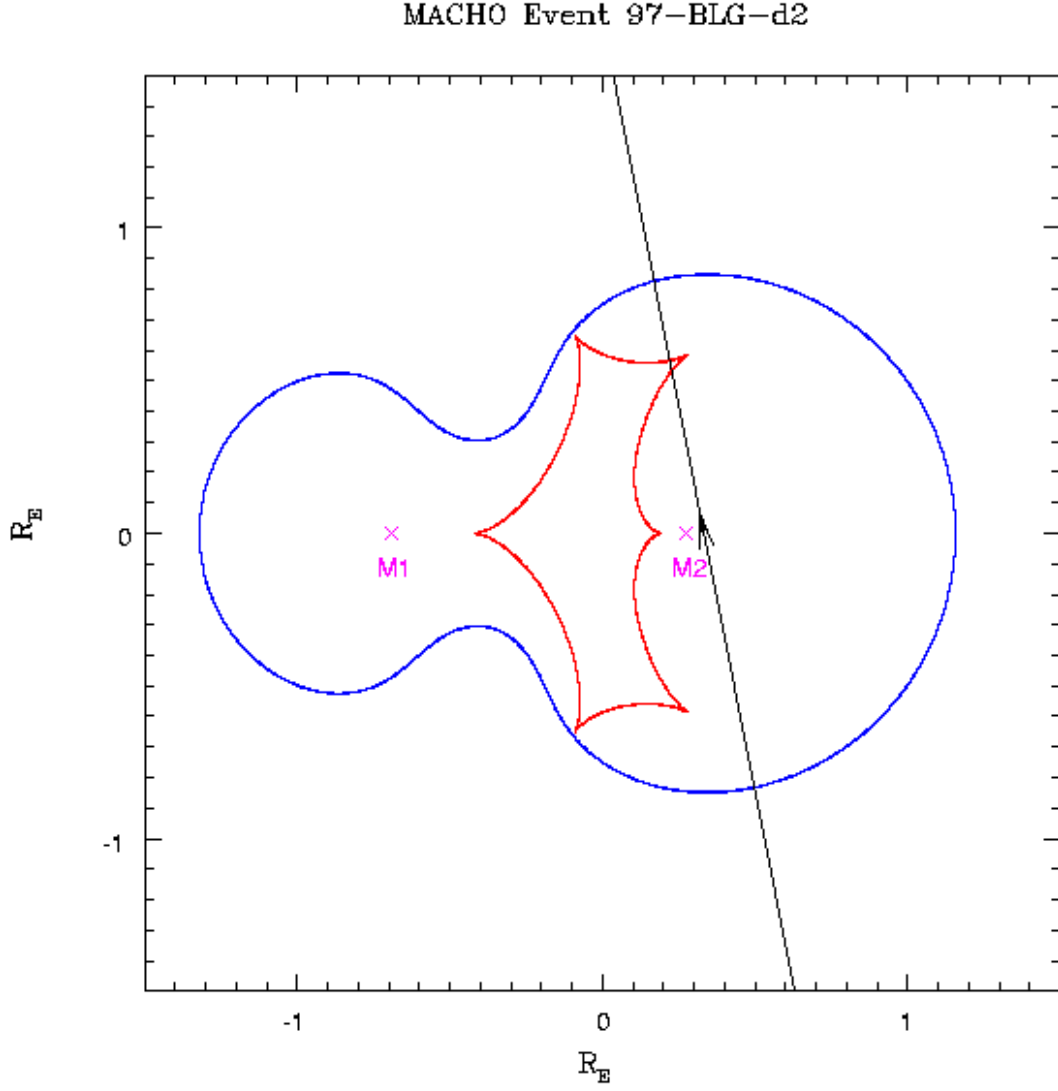


Fig. 40.— Location of the (red) caustic and (blue) critical curves for the 97-BLG-d2 binary lens fit presented in Fig. 39. The coordinate system, whose origin is at the center of mass, indicates distance in units of the system’s Einstein Ring radius R_E . Also shown are the locations of the lensing objects, and the trajectory of the source through the caustic structure.

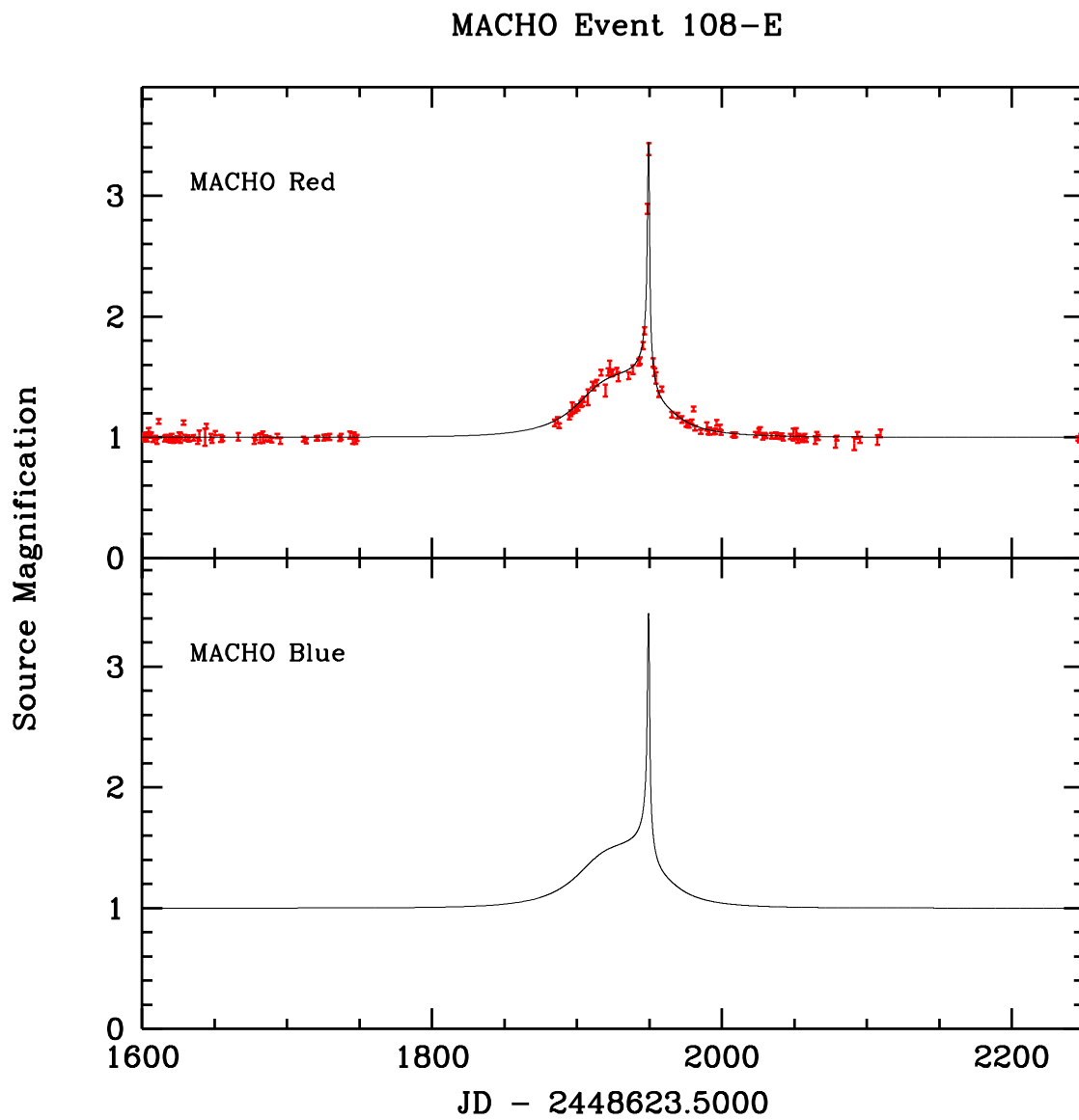


Fig. 41.— Lightcurve of MACHO event 108-E, including our fit to binary microlensing.

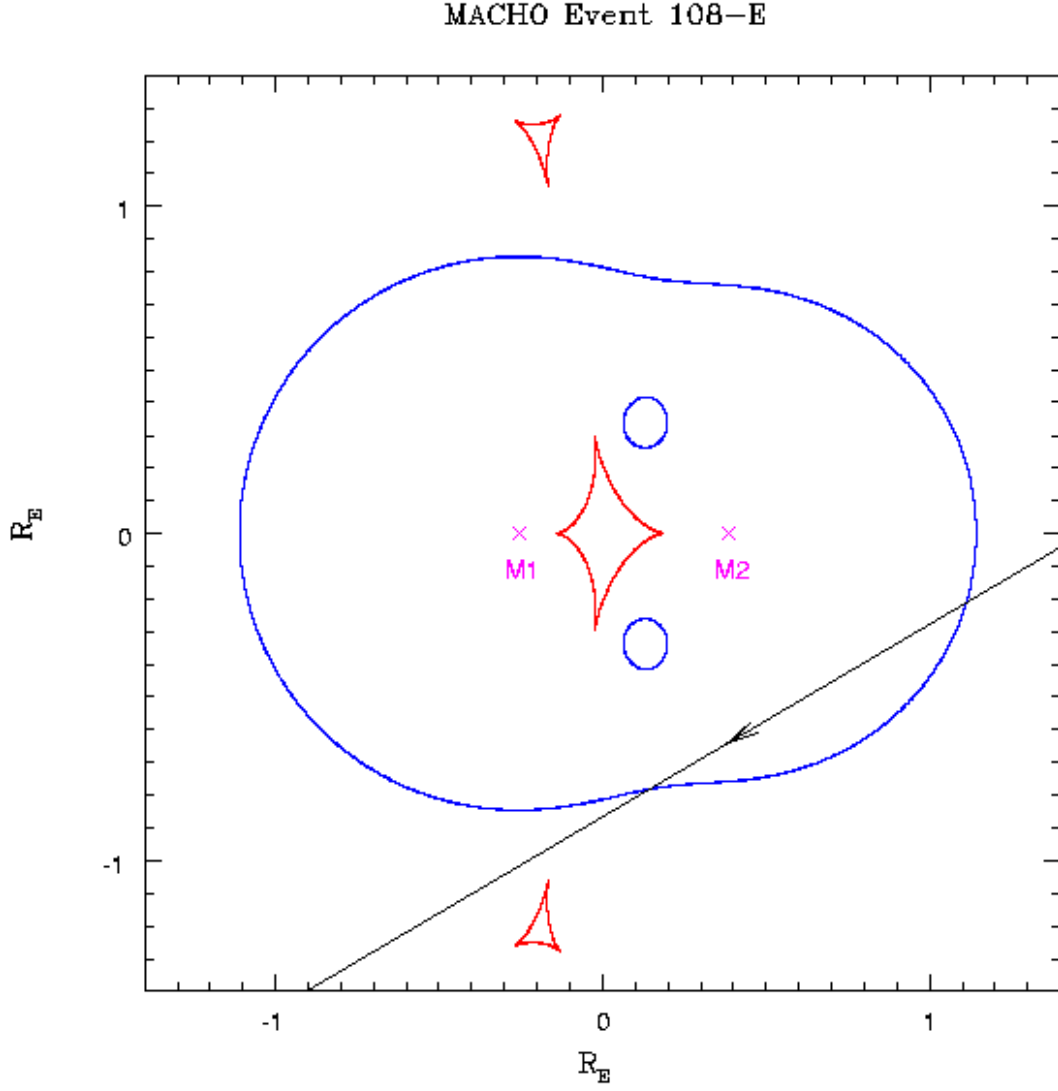


Fig. 42.— Location of the (red) caustic and (blue) critical curves for the 108-E binary lens fit presented in Fig. 41. The coordinate system, whose origin is at the center of mass, indicates distance in units of the system’s Einstein Ring radius R_E . Also shown are the locations of the lensing objects, and the trajectory of the source through the caustic structure.

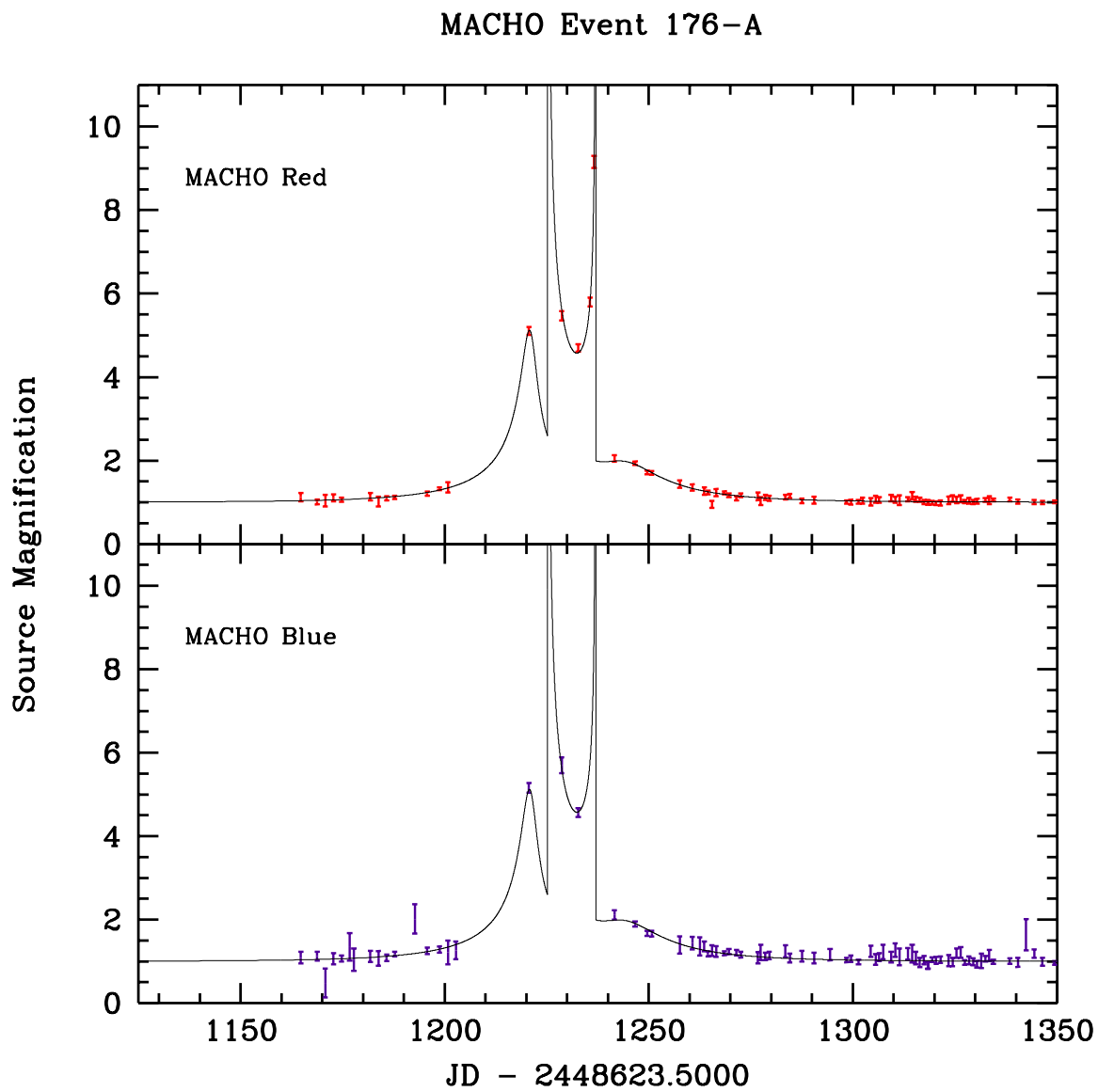


Fig. 43.— Lightcurve of MACHO event 176-A, including our fit to binary microlensing.

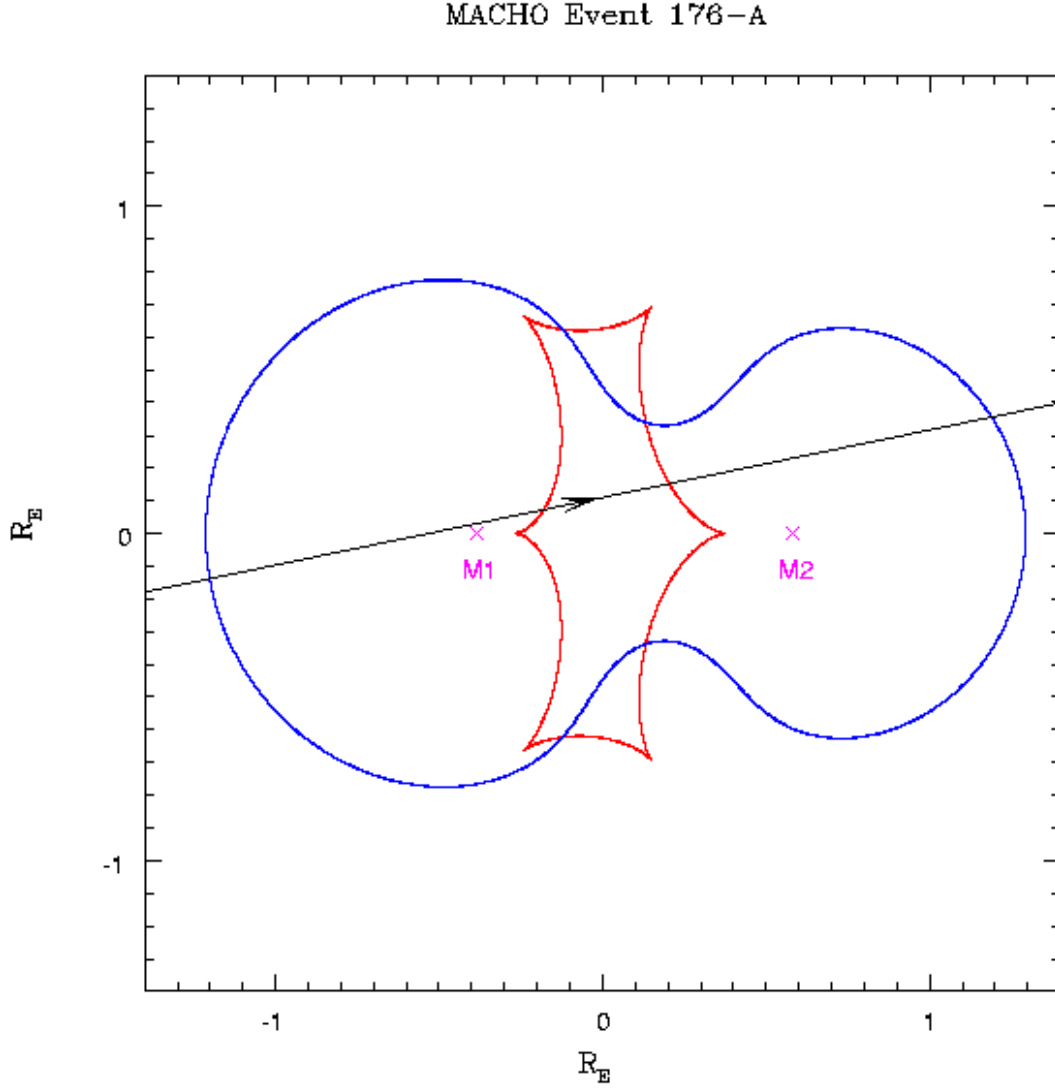


Fig. 44.— Location of the (red) caustic and (blue) critical curves for the 176-A binary lens fit presented in Fig. 43. The coordinate system, whose origin is at the center of mass, indicates distance in units of the system’s Einstein Ring radius R_E . Also shown are the locations of the lensing objects, and the trajectory of the source through the caustic structure.

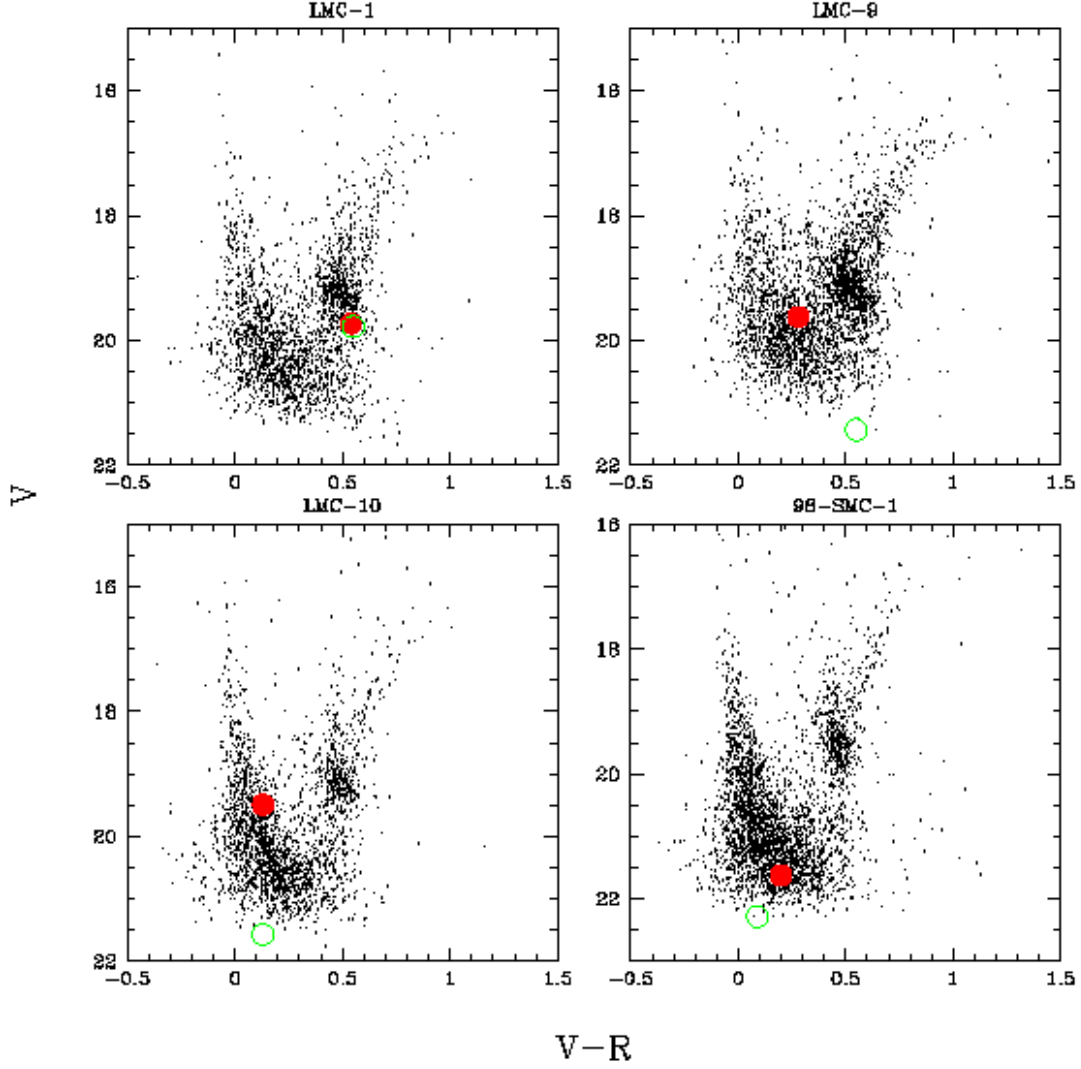


Fig. 45.— Distribution of $V, V - R$ for $\sim 3,000$ stars neighboring the lensed object, indicated with the (red) filled circle, for objects in the Magellanic Clouds. The de-blended source location, determined from blending parameters in the microlensing fit, is indicated with the (green) open circle.

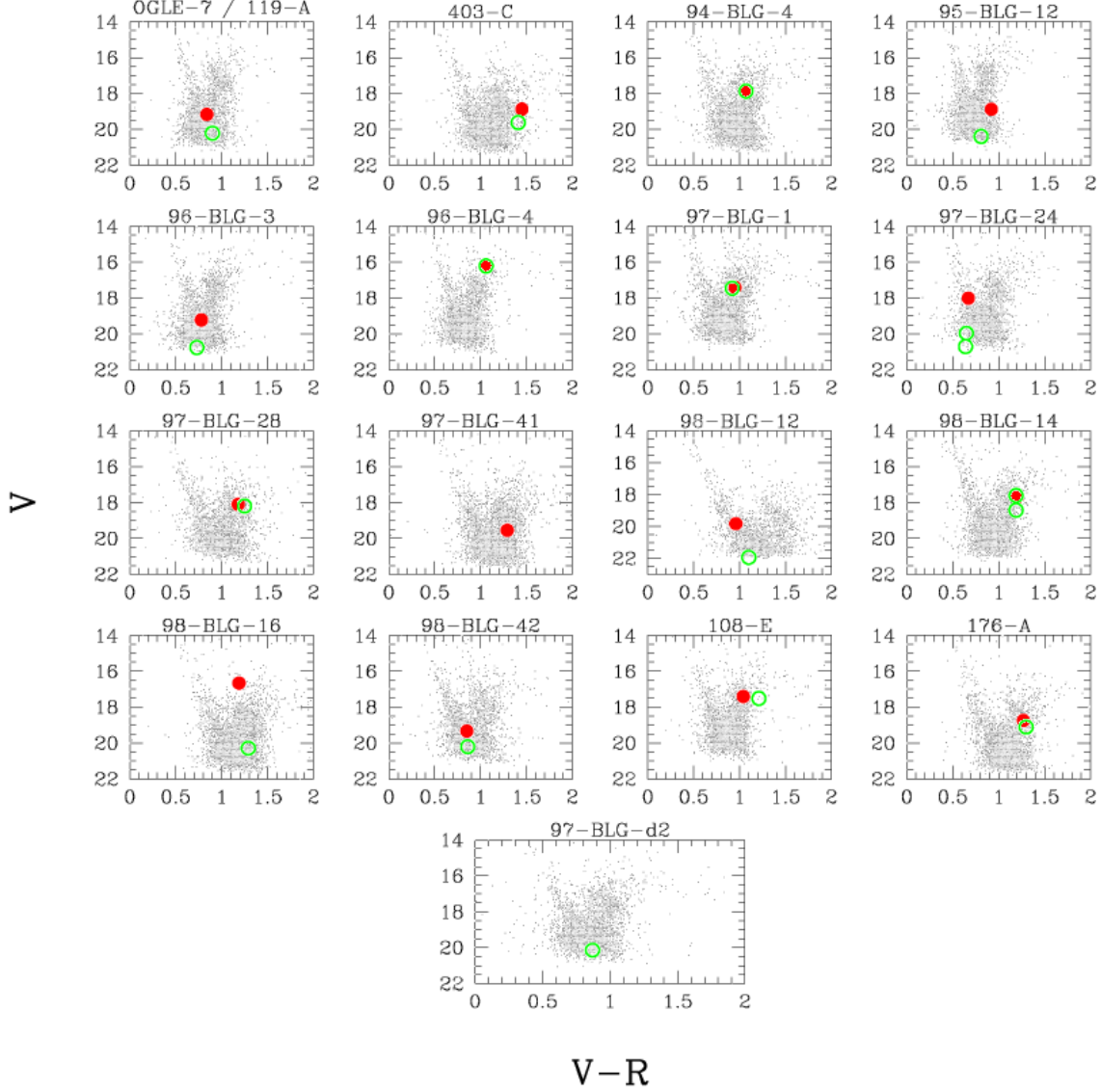


Fig. 46.— Distribution of V , $V - R$ for $\sim 3,000$ stars neighboring the lensed object, indicated with the (red) filled circle, for objects in the Galactic bulge. The de-blended source location, determined from blending parameters in the microlensing fit, is indicated with the (green) open circle. Notable cases: 97-BLG-24, where the brighter source is associated with the low mass ratio fit in Fig. 24; 97-BLG-41, where we have no estimate of the source properties; 98-BLG-14, where the brighter source is associated with the large mass ratio fit in Fig. 32; 97-BLG-d2, where we only have an estimate of the lensed source properties.

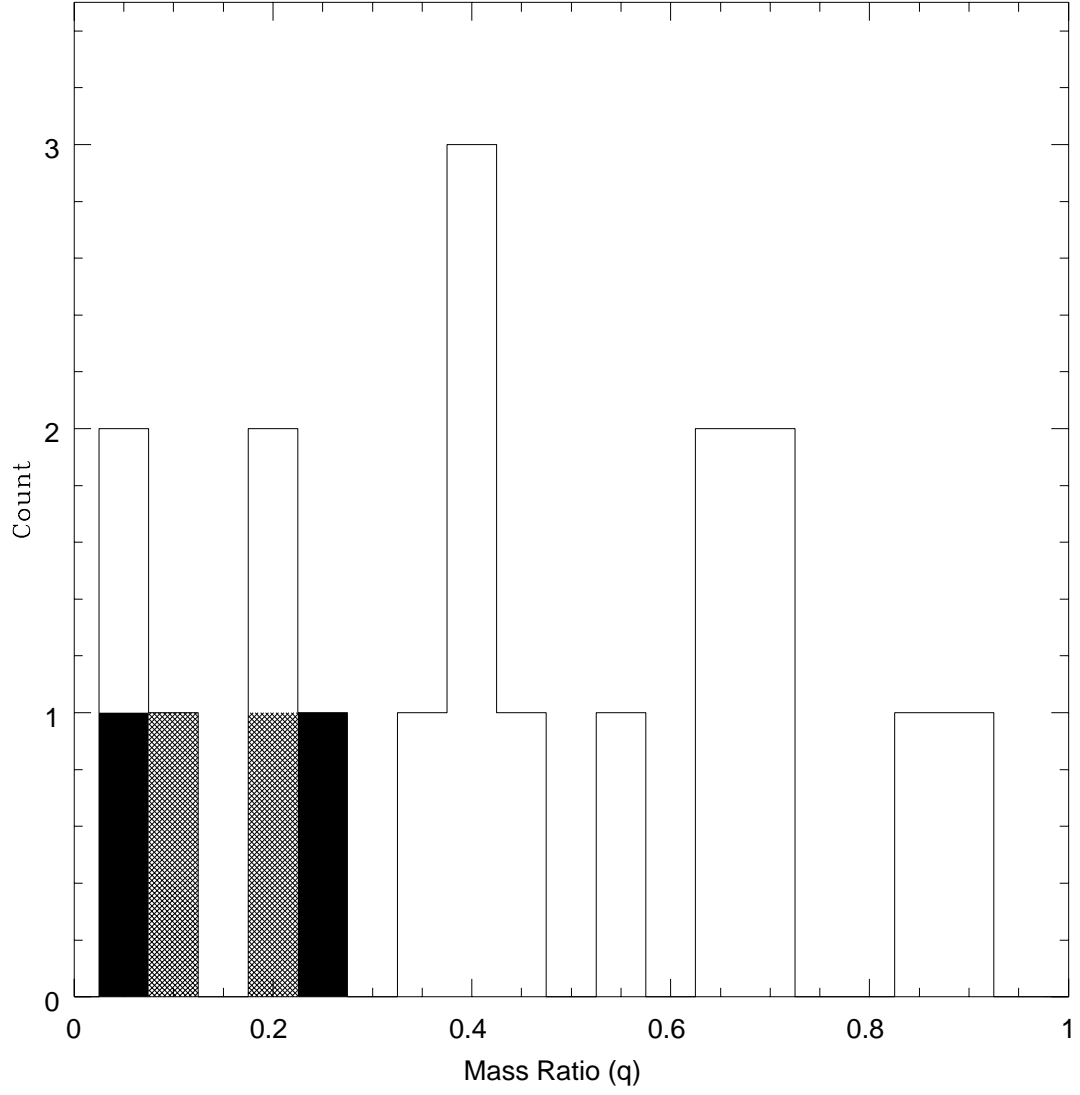


Fig. 47.— The distribution of mass ratios ($q \leq 1$) for our Galactic bulge binary microlensing events. The contribution of our 2 fits each to events 97-BLG-24 and 98-BLG-14 are represented by the dark and light shaded areas, respectively.

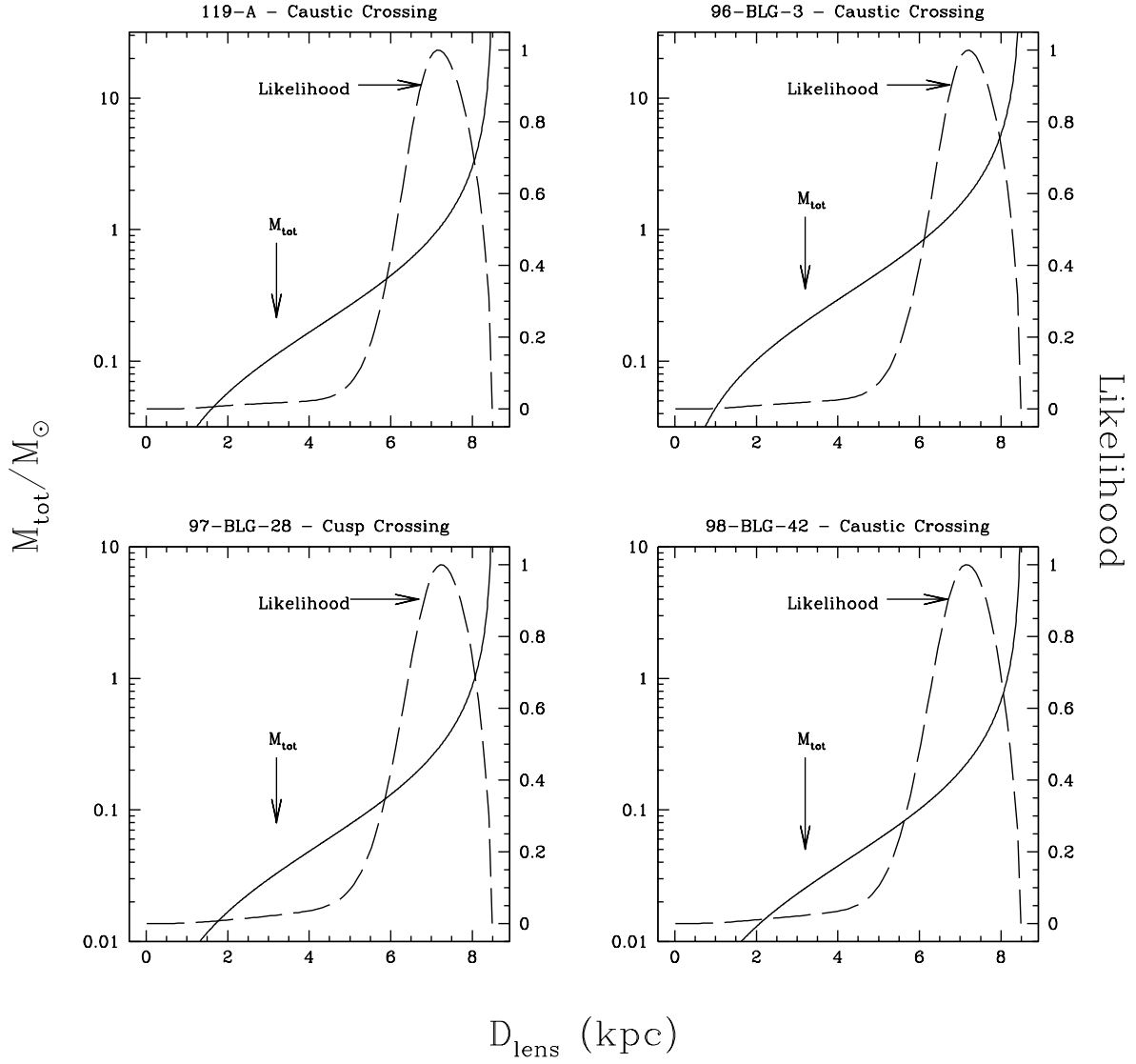


Fig. 48.— The relation between the lens distance, D_{ol} , and the total mass, M_{tot} , is shown for the four lensing events with reliable proper motion determinations. Also shown are the results of a likelihood analysis to estimate the lens parameters. The most likely lens distances and masses are given in Table 5.

Table 1. Candidate Lensed Source Stars

Event	MACHO Id	RA (J2000)	DEC (J2000)	V^a	$V - R$	V^b	$V - R$
LMC-1 (—)	79.5628.1547	05 14 44.5	-68 48 00.1	19.73	0.54	19.75	0.55
LMC-1 (- - -)	19.73	0.54	19.78	0.55
LMC-9	80.6468.2746	05 20 20.2	-69 15 11.8	19.62	0.28	21.43	0.55
LMC-10	18.3324.1765	05 01 16.0	-69 07 33.1	19.49	0.13	21.57	0.13
98-SMC-1	208.15683.4237	00 45 35.2	-72 52 34.1	21.62	0.20	22.28	0.09
OGLE-7 / 119-A	119.20226.2119	18 03 35.7	-29 42 01.2	19.16	0.84	20.21	0.90
403-C	403.47793.2961	17 55 57.9	-29 26 12.1	18.87	1.45	19.62	1.41
94-BLG-4	118.18141.731	17 58 36.7	-30 02 19.2	17.92	1.06	17.87	1.07
95-BLG-12	120.21263.1213	18 06 04.7	-29 52 38.1	18.88	0.92	20.39	0.81
96-BLG-3	119.19444.2055	18 01 45.5	-29 49 46.8	20.00	0.78	21.48	0.73
96-BLG-4	105.21417.101	18 06 11.9	-28 16 52.7	16.25	1.07	16.21	1.06
97-BLG-1	113.18674.756	17 59 53.3	-29 09 07.8	17.41	0.95	17.46	0.92
97-BLG-24 (—)	101.20650.1216	18 04 20.2	-27 24 45.2	18.01	0.67	19.96	0.65
97-BLG-24 (- - -)	18.01	0.67	20.7	0.64
97-BLG-28	108.18951.593	18 00 33.7	-28 01 10.4	18.10	1.18	18.19	1.25
97-BLG-41	402.47862.1576	17 56 20.6	-28 47 41.9	19.54	1.29
98-BLG-12	179.21577.1740	18 06 31.7	-26 16 01.5	18.86	0.96	20.83	1.10
98-BLG-14 (—)	401.48408.649	17 59 08.9	-28 24 54.6	17.70	1.20	18.42	1.19
98-BLG-14 (- - -)	17.70	1.20	17.61	1.19
98-BLG-16	402.47863.110	17 56 18.1	-28 46 04.9	16.66	1.19	20.28	1.29
98-BLG-42	101.21045.2528	18 05 12.6	-27 05 47.1	19.33	0.85	20.20	0.86
97-BLG-d2	108.19073.2291	18 00 39.5	-28 34 43.8	20.14	0.87
108-E	108.19333.1878	18 01 21.1	-28 32 39.4	17.41	1.04	17.52	1.21
176-A	176.19219.978	18 01 04.4	-27 30 41.3	18.74	1.27	19.11	1.30

^a Standard magnitudes and color of the MACHO object that received the lensed flux.

^b Standard magnitudes and color of the actual lensed source star, as determined from the blend fraction in the binary lens fit.

Information on the lensed MACHO objects and de-blended source stars. Events LMC-1, 97-BLG-24, and 98-BLG-14 are each presented with 2 fits of similar significance, but different event parameters. We do not present a binary microlensing fit for event 97-BLG-41, and we only include an estimate of the MACHO object’s baseline flux. Event 97-BLG-d2 was found through difference image analysis (DIA), which uniquely identifies the lensed source.

Table 2. Binary microlensing event parameters

Event	$\chi^2/d.o.f.$	\hat{t}	t_0^a	u_{\min}	a	θ (rad)	M_1 / M_2	t_* (days)
LMC-1 (—)	2794.9/2179	35.54	433.58	0.150	-0.430	-0.488	0.861	0.112
LMC-1 (- - -)	2799.4/2179	34.55	433.58	-0.127	1.217	4.104	108.890	0.122
LMC-9	1476.5/848	143.12	979.59	-0.054	1.657	0.086	1.627	0.651
LMC-10	1672.9/1240	151.05	585.74	0.102	0.823	-3.375	0.034	...
98-SMC-1	1771.9/1583	147.58	2354.93	0.046	0.664	-0.180	0.388	0.116
OGLE-7 / 119-A	1997.6/1407	169.04	550.04	0.077	1.045	-0.940	1.212	0.212
403-C	318.7/342	21.37	1688.75	-0.089	1.227	3.082	0.556	...
94-BLG-4	923.5/1418	10.66	884.13	0.028	-1.068	0.302	18.084	0.096
95-BLG-12	1413.4/1466	307.41	1264.07	0.106	0.421	-0.664	2.148	...
96-BLG-3	1934.8/1542	182.45	1545.66	0.043	-0.436	3.530	0.392	0.086
96-BLG-4	1286.0/1605	162.44	1815.29	0.378	7.454	-0.011	1.140	...
97-BLG-1	1237.7/1305	68.52	1884.02	0.234	0.931	2.583	0.418	0.527
97-BLG-24 (—)	1230.6/943	30.77	1968.38	0.319	2.077	-3.967	4.236	0.050
97-BLG-24 (- - -)	1235.0/943	45.49	1970.82	0.0003	1.752	0.988	0.035	0.197
97-BLG-28	2734.9/1404	52.76	1991.87	0.225	0.707	1.437	0.210	0.760
98-BLG-12	440.5/507	239.92	2321.95	0.163	0.793	11.346	0.681	...
98-BLG-14 (—)	809.4/714	107.65	2322.32	0.214	0.541	3.531	4.504	...
98-BLG-14 (- - -)	814.4/714	74.05	2323.56	0.396	1.213	4.429	0.0857	...
98-BLG-16	461.2/616	69.50	2316.57	0.140	0.758	3.699	1.476	0.163
98-BLG-42	890.4/395	49.19	2422.41	-0.028	1.260	3.328	3.065	0.109
97-BLG-d2	314.1/584	92.65	1971.07	-0.326	0.965	1.766	0.390	...
108-E	934.4/597	71.30	1927.66	0.747	0.637	-2.609	1.514	0.557
176-A	684.0/578	60.02	1230.06	0.108	0.965	0.204	1.514	0.068

^a (JD − 2448623.50).

List of binary microlensing event parameters, as described in Sec. 2, for each of our candidates. Also included are the binary microlensing fit χ^2 , and the degrees of freedom (equal to the number of data points minus 1 for each constraint listed here, and minus 2 for each passband with observations in Tab. 3). Events LMC-1, 97-BLG-24, and 98-BLG-14 are each presented with 2 fits of similar significance, but different event parameters.

Table 3. Binary microlensing event blend parameters

Event	f_{MACHO_R}	f_{MACHO_B}	f_{CTIO_R}	f_{CTIO_B}	f_{MSO30_R}	f_{MSO74_R}	f_{UTSO_R}	f_{UTSO_V}	f_{WISE_R}
LMC-1 (—)	0.99	0.98
LMC-1 (- - -)	0.96	0.95
LMC-9	0.26	0.17
LMC-10	0.15	0.15
98-SMC-1	0.47	0.56	0.79	1.07
OGLE-7 / 119-A	0.41	0.37
403-C	0.48	0.50
94-BLG-4	1.06	1.04
95-BLG-12	0.22	0.26	0.26	0.27	0.26	0.31
96-BLG-3	0.23	0.25	0.35	0.33
96-BLG-4	1.03	1.03	1.05	1.01
97-BLG-1	0.93	0.97	0.87
97-BLG-24 (—)	0.16	0.17	0.15	0.21
97-BLG-24 (- - -)	0.08	0.08	0.08	0.11
97-BLG-28	1.00	0.90	0.97
98-BLG-12	0.17	0.14	0.17	0.16
98-BLG-14 (—)	0.51	0.52	0.52	0.48
98-BLG-14 (- - -)	1.08	1.10	1.07	0.99
98-BLG-16	0.04	0.03	1.10	1.07	0.04
98-BLG-42	0.46	0.45	0.73	0.74
97-BLG-d2	0.30	0.14
108-E	1.10	0.86
176-A	0.74	0.70

List of blending parameters for each of our candidate binary microlensing events. The parameter f represents the fraction of the object’s flux which was lensed in each respective passband. Events LMC-1, 97-BLG-24, and 98-BLG-14 are each presented with 2 fits of similar significance, but different event parameters.

Table 4. Intrinsic Source Properties

Event	# RR Lyrae	$\langle E(V - R) \rangle$	$\langle A_V \rangle$	$(V - R)_0$	V_0	T_{eff} (K)	m_{bol}	θ_* (μas)
119-A	3	0.47 (9)	1.9 (3)	0.43 (9)	18.4 (3)	5350 (500)	18.2 (4)	1.06 (29)
96-BLG-3	6	0.42 (5)	1.7 (2)	0.31 (6)	19.1 (2)	6200 (500)	19.1 (2)	0.53 (11)
97-BLG-28	9	0.67 (4)	2.7 (2)	0.58 (6)	15.5 (2)	4500 (200)	15.0 (2)	6.58 (90)
98-BLG-42	10	0.53 (5)	2.1 (2)	0.33 (7)	18.1 (2)	6050 (500)	18.1 (2)	0.89 (20)

Estimates of the reddening and extinction, as determined from RR Lyrae within $10'$, to each of the 4 sources where we have a well constrained binary lens fit and a reliable measure of t_* . The intrinsic source color $(V - R)_0$ and brightness V_0 are used to determine T_{eff} and m_{bol} , and from these we find the source angular radius θ_* .

Table 5. Properties of the Lensing Systems

Event	μ (mas/yr)	D_{ol} (kpc)	M_{tot}/M_{\odot}	M_1/M_{\odot}	M_2/M_{\odot}
119-A	1.84 (58)	$7.0^{+0.8}_{-0.9}$	$0.89^{+1.25}_{-0.42}$	$0.49^{+0.69}_{-0.23}$	$0.40^{+0.57}_{-0.19}$
96-BLG-3	2.26 (47)	$7.1^{+0.8}_{-0.9}$	$1.61^{+2.25}_{-0.76}$	$0.45^{+0.63}_{-0.21}$	$1.15^{+1.62}_{-0.55}$
97-BLG-28	3.16 (44)	$7.0^{+0.8}_{-1.0}$	$0.26^{+0.36}_{-0.13}$	$0.05^{+0.06}_{-0.02}$	$0.22^{+0.30}_{-0.11}$
98-BLG-42	2.98 (78)	$7.0^{+0.8}_{-1.0}$	$0.19^{+0.26}_{-0.09}$	$0.14^{+0.20}_{-0.07}$	$0.05^{+0.06}_{-0.02}$

The lens proper motion measurements, $\mu = \theta_*/t_*$, have been used in the likelihood analysis detailed in Sec. 5.2.3 to produce the most likely lens distance and mass estimates given here. The errors quoted are 1σ . We note that the errors in M_1 and M_2 are completely correlated.